

**TECHNISCHE UNIVERSITÄT MÜNCHEN**

**Pankreas-Forschungslabor  
Chirurgische Klinik und Poliklinik  
Klinikum rechts der Isar**

**Identification and characterization of molecular subtypes of  
human pancreatic ductal adenocarcinoma**

**Bo Kong**

Vollständiger Abdruck der von der Fakultät für Medizin der  
Technischen Universität München zur Erlangung des  
akademischen Grades eines Doctor of Philosophy genehmigten  
Dissertation

Vorsitzender: Univ.-Prof. Dr. Florian R. Greten

Prüfer der Dissertation:

1. Univ.-Prof. Dr. Bernhard Holzmann
2. apl. Prof. Dr. Achim Krüger
3. apl. Prof. Dr. Andreas Jung,

Ludwig-Maximilians-Universität

München

Die Dissertation wurden am **05.02.2013** bei der Technischen  
Universität München eingereicht und durch die Fakultät für Medizin  
am **20.03.2013** angenommen.

## TABLE OF CONTENTS

<b>1. INTRODUCTION</b> .....	5
1.1. PANCREATIC CANCER BIOLOGY .....	5
1.2. MOLECULAR SUBTYPES AND TREATMENT RESPONSES IN HUMAN PDAC ...	7
1.3. HNF1A/MIA2 AXIS AND ER STRESS/UPR SYSTEM IN PANCREATIC PHYSIOLOGY AND CANCER BIOLOGY .....	9
1.4. TSC1-TSC2 COMPLEX AND MTORC1 ARE COMMON GATEKEEPERS OF PANCREATIC MALIGNANCY .....	11
<b>2. AIMS OF THIS STUDY</b> .....	17
<b>3. MATERIALS AND METHODS</b> .....	19
3.1. MATERIALS .....	19
3.2. METHODS .....	30
<b>4. RESULTS</b> .....	37
4.1. HNF1A CONTROLS MIA2 EXPRESSION IN PDAC .....	37
4.2. THE MIA2 <sup>I141M</sup> VARIANT IS LINKED WITH A SECRETORY DEFECT AND IS CORRELATED WITH PATIENT SURVIVAL .....	40
4.3. THE MIA2 <sup>I141M</sup> VARIANT INCREASES SENSITIVITY OF PANCREATIC CANCER CELLS TO GEMCITABINE .....	44
4.4. THE MIA2 <sup>I141M</sup> VARIANT IS ASSOCIATED WITH INCREASED EXPRESSION LEVELS OF ERN1/XBP1 IN PDAC TISSUES .....	48
4.5. ERN1 IS RESPONSIBLE FOR INCREASED CHEMOSENSITIVITY IN MIA2 <sup>I141M</sup> CARRIERS.....	53
4.6. TSC1 DEFICIENCY INDUCES DEGENERATION OF THE PANCREAS .....	55
4.7. TSC1 HAPLOINSUFFICIENCY PROMOTES TUMOR FORMATION DRIVEN BY PTEN DEFICIENCY AND EXPRESSION OF KRAS <sup>G12D</sup> .....	60
4.8. KRAS <sup>G12D</sup> /ERK OR PI3K/AKT TOGETHER WITH TSC1 HAPLOINSUFFICIENCY DRIVE HYPERACTIVATION OF MTORC1 IN PANCREATIC CELL .....	63
4.9. KRASG12D/ERK OR PI3K/AKT TOGETHER WITH TSC1 HAPLOINSUFFICIENCY DRIVE HYPERACTIVATION OF MTORC1 IN PANCREATIC CELL .....	66
4.10. KRAS <sup>G12D</sup> ; TSC1 <sup>FL/+</sup> CANCER CELLS ARE DEFECTIVE IN RELEASING VEGFA BECAUSE OF HYPOXIA-INDUCED ER STRESS.....	68
4.11. T CELL IMMUNITY PREVENTS CYSTIC LESIONS FROM MALIGNANT TRANSFORMATION IN PTEN <sup>FL/FL</sup> ; TSC1 <sup>FL/+</sup> MICE .....	76
4.12. TSC1 HAPLOINSUFFICIENCY AND P53 DEFICIENCY PROMOTES THE PANCREATIC MALIGNANCY .....	78
4.13. IDENTIFICATION OF ALDH1A3-POSITIVE SUBTYPE OF HUMAN PDAC .....	83
<b>5. DISCUSSION</b> .....	89
5.1. HNF1A/MIA2 SECRETORY NETWORK INTERACTS WITH ER STRESS/UPR SYSTEM .....	89
5.2. A CENTRAL ROLE OF THE TSC1-TSC2 COMPLEX AND OF MTORC1 IN PANCREATIC EXOCRINE MALIGNANCY IN MICE.....	92

5.3. MOLECULAR SUBTYPES OF HUMAN PDAC.....	97
<b>6. SUMMARY .....</b>	<b>100</b>
<b>7. ABBREVIATIONS .....</b>	<b>103</b>
<b>8. REFERENCES .....</b>	<b>106</b>
<b>9. SUPPLEMENTARY DATA .....</b>	<b>123</b>
<b>10. CURRICULUM VITAE .....</b>	<b>126</b>
<b>11. ACKNOWLEDGEMENTS.....</b>	<b>128</b>

## ABSTRACT

Pancreatic ductal adenocarcinoma (PDAC) is an extremely aggressive disease. Despite enormous advances in understanding molecular tumor biology, the overall survival of PDAC patients has remained unchanged for the last 20 years. This may be partially attributed to the fact that PDAC is a histopathologically-defined tumor entity with great heterogeneity – both on the clinical, the histological and the genetic levels. Here, a variety of molecular subtypes with distinctive tumor biologies seem to exist, but current therapies are applied without taking into account these putative differences. Hence, there is, firstly, a necessity to classify PDACs into clinically-relevant subtypes and, secondly, to make use of this knowledge by applying more personalized therapies. To this end, molecular subtypes with a clinical relevance were identified by the current study.

The HNF1 homeobox A (HNF1A) region is a novel PDAC susceptibility locus and melanoma inhibitory activity 2 (MIA2), a protein facilitating protein secretion, is an HNF1A target. In this study, a common germline variant of MIA2, MIA2<sup>I141M</sup>, that is associated with a secretory defect of the MIA2 protein was identified in PDAC cells. Components of the endoplasmic reticulum (ER) stress and unfolded protein response (UPR) system, which are crucial for the secretory function of the pancreas, were widely expressed by pancreatic cancer cells. The interaction between the MIA2<sup>I141M</sup> variant and the ER stress/UPR system specified a molecular subtype of PDAC, which was associated with high expression of ER stress/UPR genes and cancer cell sensitivity to gemcitabine.

Using a genetically engineered mouse model (GEMM) of pancreatic cancer (determined by pancreas-specific expression of oncogenic Kras), the Tsc1-Tsc2 complex was defined as the common gate-keeper of pancreatic exocrine malignancies. Over-activity of the mammalian target of rapamycin (mTOR) caused by pancreas-specific ablation of tuberous sclerosis 1 (Tsc1) resulted in pancreatic degeneration and concomitant induction of two negative feedback regulators: p53 and phosphatase and tensin homolog (Pten). Inactivation of Pten in the context of Tsc1 haploinsufficiency promoted the formation of pancreatic cystic lesions that rarely progressed into invasive tumors – most likely due to antitumor T cell immunity. Interestingly, inactivation of p53 in the context of Tsc1 haploinsufficiency did not significantly impact on pancreatic morphology; but isolated pancreatic epithelial cells from these animals unanimously displayed epithelial-to-mesenchymal transition (EMT) features and were surprisingly tumorigenic in nude mice. Furthermore, Tsc1 haploinsufficiency and Kras<sup>G12D</sup> expression induced aggressive PDACs characterized by anaplastic growth, large areas of tumor necrosis and wide-spread metastasis. Molecular characterization of isolated cancer cells uncovered that they released high amounts of Vegfa (vascular endothelial growth factor A), a potent angiogenic factor, however, they were not able to further boast their Vegfa secretion under hypoxic conditions due to hypoxia-induced ER stress. By combining the comprehensive phenotypic characterizations of the different mouse models and the expression analysis of isolated cell lines, an ALDH1A3-positive PDAC subtype was identified. Patients

positive for this subtype lived significantly shorter than their negative counterparts and were less likely to benefit from the adjuvant/additive standard chemotherapy. Thus, alternative therapies should be specifically exploited for this particular PDAC subtype.

In conclusion, two major novel subtypes of PDAC were identified. Though both subtypes are associated with different tumor biologies, the underlying mechanisms are completely different.

## 1. INTRODUCTION

### 1.1. Pancreatic cancer biology

#### 1.1.1. The clinical challenge

Despite enormous advances in understanding pancreatic cancer biology in the last years – mostly due to whole exome sequencing, to the development of transgenic mouse models and to refined molecular pathway analyses in human and mouse – the prognosis of patients diagnosed with pancreatic ductal adenocarcinoma (PDAC) remains poor (Siegel et al., 2011). This does not only refer to patients in advanced stages but also to patients with resectable pancreatic cancers whose cancer tissues are widely available for molecular characterization. Here, nearly all patients die eventually from either local recurrence or remote metastasis with a median survival of less than 2 years (Neoptolemos et al., 2004). The unfavourable outcome (or treatment failure) reflects two awkward facts: 1) insufficient understanding of tumor biology; 2) a lack of translation of existing knowledge in tumor biology into clinical practice.

#### 1.1.2. Founder mutations of human PDAC

Characterization of cancer genomes suggested that genes belonging to 12 core pathways and biological processes are altered in established PDAC cells (Jones et al., 2008). In particular, *KRAS* (v-Ki-ras2, Kirsten rat sarcoma viral oncogene homolog), *TP53* (tumor protein p53), *P16/CDK2NA* (cyclin-dependent kinase inhibitor 2A), and *SMAD4* (SMAD family member 4) are the most frequently altered genes, which have been termed as cancer “founder” mutations (Iacobuzio-Donahue et al., 2012; Yachida et al., 2012). Briefly, the oncogenic *KRAS* mutations found in human PDAC result in a protein locked in a constitutively active state, leading to persistent downstream signals such as phosphatidylinositol-4, 5-bisphosphate 3-kinase (PI3K) and RAF-MEK (mitogen-activated protein kinase kinase) - ERK (extracellular signal-regulated kinase) (Iacobuzio-Donahue, 2012). Recently, it has been demonstrated that loss of heterozygosity (LOH) in the wild type (WT) *Kras* allele occurs frequently during metastatic progression of PDAC in mice (likely also in humans), implying a tumor suppressor function of the WT *Kras* allele in pancreatic carcinogenesis (Qiu et al., 2011). P16 encoded by *CDKN2A* is a protein of the cyclin-dependent kinase

inhibitor family which plays a role in regulating the cell cycle. Through multiple mechanisms (mainly through hypermethylation-induced silencing or intragenic mutations), P16 is inactivated in the majority of pancreatic cancers (Yachida et al., 2012). The loss of TP53 tumor-suppressor function is mainly caused by either missense mutations in its DNA-binding domain (resulting in a mutated protein with dominant-negative effects), by other intragenic mutations (e.g. frameshift and nonsense mutations) or by homozygous deletions (Yachida et al., 2012). *SMAD4* is a tumor-suppressor gene which plays a crucial role in mediating growth-inhibiting effects triggered by transforming growth factor  $\beta$  (TGF $\beta$ ) signaling (Kleeff et al., 1999). The loss of SMAD4 function is mainly caused by missense or nonsense mutations and homozygous deletions in human PDAC (Yachida et al., 2012). The importance of these alterations as the founder mutations of human PDACs is reflected by two important facts (also see below): 1) these mutations can be detected in a variety of putative precursor lesions; 2) they are able to initiate murine PDAC.

### **1.1.3. Precursor lesions of pancreatic cancer**

The histological evaluation of resected PDAC has allowed for morphological classification of dysplastic lesions that represent the putative precursors of invasive carcinomas: pancreatic intraepithelial neoplasia (PanIN), intraductal papillary-mucinous neoplasm (IPMN) and mucinous cystic neoplasm (MCN) (Vincent et al., 2011). Among these “precursor lesions”, the PanINs are characterized by a spectrum of morphological changes such as mucin production, graded nuclear atypia and loss of cellular polarity. The earliest precursor lesions, PanIN-1A and-1B, are characterized by elongation of “ductal cells” with enhanced mucin production with a flat or papillary architecture. As PanIN lesions progress, they acquire moderate (PanIN2) and eventually severe nuclear abnormalities (PanIN3) (Schneider et al., 2005). Molecular analyses have shown that PanINs (especially high grade PanINs) carry the above mentioned “core” genetic alterations (e.g. mutations in the *KRAS*, *TP53*, *SMAD4* and/or *P16* genes) of PDAC (Hruban et al., 2000; Maitra et al., 2003). These findings support the notion that PDAC may genetically evolve from cells within PanINs - an assumption that has been widely accepted despite the lack of formal proof. Recently, the concept of a PanIN-PDAC sequence has been challenged and tubular complexes (TC) and atypical flat lesions (AFL: a special type of TC with a high nuclear-cytoplasmic ratio) have been hypothesized to be (additional) precursors of PDAC (Aichler et al., 2012; Esposito et al., 2007; Guerra et al., 2007; Strobel et al., 2010).

### **1.1.4. Development of genetically engineered mouse models of PDAC**

The understanding of the molecular mechanisms responsible for the specification of different cellular compartments of the pancreas together with the development of the Cre-lox system (Orban et al., 1992; Sauer, 1987; Sauer and Henderson, 1988), have enabled the development of spontaneously pancreatic cancer developing mouse models (termed: genetically engineered mouse models (GEMM)). In these models, Cre recombinase, which is expressed in pancreatic epithelial cells under the control of pancreas-specific promoters (e.g. Pdx1 (pancreatic and duodenal homeobox 1) or Ptf1a-p48 (pancreas-specific transcription factor, 1a), recognizes and recombines a pair of targeted sequences

(Lox sequences), which allows for pancreas-specific gene manipulation. Using such systems, the expression of oncogenic Kras (e.g. Kras<sup>G12D</sup>) during embryonic development initiates PDAC in adulthood, albeit at a relatively low frequency and a relatively long latency (more than 1 year) (Collins et al., 2012; Hingorani et al., 2003). Nevertheless, this mouse model faithfully recapitulates the whole spectrum of human PDAC pathologies, from its precursor lesions to locally invasive and metastatic entities. Additional introduction of other founder mutations (e.g. p16, p53 or Smad4) strongly accelerates carcinogenesis and metastatic spread (Aguirre et al., 2003; Bardeesy et al., 2006a; Bardeesy et al., 2006b; Hingorani et al., 2005). However, depending on the make-up of the introduced founder mutations (Kras<sup>G12D</sup>+p53 vs. Kras<sup>G12D</sup>+p16<sup>INK4A</sup> vs. Kras<sup>G12D</sup>+Smad4), the resulting murine PDAC present with distinctive tumor histologies and biologies. Here, the combination of p16 deficiency and oncogenic Kras<sup>G12D</sup> promotes the development of poorly differentiated/anaplastic PDAC (Aguirre et al., 2003). In contrast, loss of p53 together with the expression of oncogenic Kras<sup>G12D</sup> leads to the formation of moderately differentiated types of PDAC (Bardeesy et al., 2006a). Interestingly, mice with an additional loss of Smad4 (together with expression of Kras<sup>G12D</sup>) develop IPMN-like cystic lesions and PDAC (Bardeesy et al., 2006b). These data suggest that these founder mutations play an important role in specifying different subtypes of murine PDAC.

## **1.2. Molecular subtypes and treatment responses in human PDAC**

### **1.2.1. Genetic profiles, molecular subtypes and chemotherapeutic responses**

Although these 4 founder mutations specify subtypes of murine PDAC with completely different tumor biologies, it remains largely unclear whether the genetic status of these 4 genes correlates with clinicopathologic features of human PDAC. In this regard, a recent study has demonstrated that the number of presented founder mutations in a PDAC is associated with the overall survival and the metastatic burden at autopsy. As such, PDAC patients carrying less than 2 genetic alterations (19% of all cases) have a better prognosis and are more differentiated than those with more than 3 genetic alterations (Yachida et al., 2012). In particular, SMAD4 loss seems to be associated with widespread metastasis, underscoring the importance of SMAD4 and TGFβ signaling in the formation of tumor metastasis (Iacobuzio-Donahue et al., 2009). Furthermore, the presence of certain genetic alterations in established pancreatic cancer cell lines predicts chemotherapeutic response to specific chemotherapeutic drugs in vitro (Cui et al., 2012). Here, SMAD4 inactivation was associated with an increased sensitivity to cisplatin (DNA cross-linking agent) and irinotecan (topoisomerase I inhibitor); TP53 inactivation sensitized pancreatic cancer cells to triptolide (a terpenoid) and a PARP1 (poly (ADP-ribose) polymerase 1) inhibitor (Cui et al., 2012). Though these results are still pre-clinical and require clinical validation, they offer an opportunity: genetic profiles of founder mutations can be used to personalize the chemotherapy for human PDAC.

### **1.2.2. Expression profiles, molecular subtypes and treatment response**

Based on transcriptional profiles, three major molecular subtypes consisting of classical, quasi-mesenchymal and exocrine-like pancreatic cancers have been identified (Collisson et al., 2011). Namely, the classical subtype shows high expression of epithelium-associated genes whereas the quasi-mesenchymal subtype has high expression of mesenchyme-associated genes while the exocrine-like subtype expresses relatively high levels of digestive enzymes. Importantly, these three molecular subtypes of PDAC reflect patient groups with completely different clinical outcomes and therapeutic responses. For example, patients with the classical subtype tend to have a better prognosis and are more likely to benefit from targeted therapy (e.g. erlotinib), whereas patients with the quasi-mesenchymal subtype have a worse prognosis but are likely to respond to conventional chemotherapy (e.g. gemcitabine). To date, it remains elusive whether the above mentioned founder mutations may also play a role in specifying these molecular subtypes at the transcriptional level.

### **1.2.3. Therapeutic impact of germline mutations**

Finally, a subset of PDAC patients (around 10%) has a family history of pancreatic cancer (Petersen et al., 2006). Though the hereditary basis responsible for PDAC predisposition cannot be determined in the majority of the affected families, recent studies have identified a set of germline mutations in candidate genes (e.g. ataxia telangiectasia mutated (ATM) and breast cancer 2, early onset (BRCA2)) by sequencing the genome of familial pancreatic cancer (Roberts et al., 2012). In addition, germline mutations of PALB2 (partner and localizer of BRCA2) have recently been identified as novel risk factors for familial pancreatic cancers (Jones et al., 2009; Slater et al., 2010). Though there is currently no evidence that these germline mutations may specify a particular subtype of PDAC with distinctive tumor biology, the presence of certain mutations affects the response towards chemotherapies. Since the PALB2 is functionally involved in repairing damaged DNA, tumors with germline PALB2 mutations were hypothesized to be more sensitive to DNA cross-linking agents, such as mitomycin C. Indeed, long-term survival after mitomycin C treatment in a metastatic PDAC patient carrying a PALB2 gene mutation has been reported (Villarroel et al., 2011).

Taken together, PDAC is a complex, heterogenic disease with large variations in its genetic and transcriptional profiles that affect disease course and response to treatment. However, personalization of treatment will only be possible once substratification (prior to induction of therapy) has been accomplished. Translation of findings from GEMM, from in-vitro assays and from descriptions of human tumor histologies and biologies will be necessary to guide such classification approaches.



## **1.3. The HNF1A/MIA2 axis and the ER stress/UPR system in pancreatic physiology and cancer biology**

### **1.3.1. HNF1A is a novel cancer risk gene locus for human PDAC**

Although previous genome-wide association studies (GWAS) and epidemiological studies have demonstrated the relevance of a set of genetic (e.g. cancer susceptibility loci) and environmental factors (e.g. smoking and diabetes) in the etiology of PDAC (Bosetti et al., 2011; Petersen et al., 2010; Stevens et al., 2007; Wu et al., 2012), the exact mechanisms by which these factors lead to an increased cancer risk remain largely elusive. Notably, recent genome-wide studies have repetitively identified the HNF1 homeobox A (HNF1A) region as a novel susceptibility locus for pancreatic cancer (Li et al., 2012; Pierce and Ahsan, 2011), whereas the closely related gene HNF1B has no such effect (Elliott et al., 2010). These data underscore a specific importance of HNF1A-mediated gene expression in pancreatic carcinogenesis.

### **1.3.2. The HNF1A-mediated secretory pathway in the exocrine and endocrine pancreas**

Interestingly, HNF1A (HNF1 homeobox A) is a critical transcription factor whose mutations have previously been shown to be responsible for an autosomal dominant form of non-insulin-dependent diabetes mellitus, the maturity-onset diabetes of the young 3 (MODY3) (Yamagata et al., 1996). Though Hnf1a-deficient mice develop pancreatic islets without conspicuous defects in either  $\beta$  cell mass or insulin content, they display a compromised insulin secretion upon glucose and arginine stimulation (Pontoglio et al., 1998). Similarly, pancreatic acini isolated from Hnf1a-deficient mice show a significantly impaired amylase release upon treatment with caerulein (an analog of the potent pancreatic secretagogue cholecystokinin) compared to wild-type mice (Molero et al., 2012). In line, a recent study provided evidence that HNF1A controls the expression of a variety of genes involved in cytoskeleton organization, secretion, vesicle transport, endoplasmic reticulum (ER) and Golgi function (Servitja et al., 2009). Taken together, these data collectively demonstrate that HNF1A-mediated gene expression constitutes an essential component of the secretory pathway in both the endocrine and exocrine pancreas.

### **1.3.3. MIA2 is a target gene of the HNF1A-mediated secretory pathway**

One of the HNF1A target molecules is melanoma inhibitory activity 2 (MIA2) (Bosserhoff et al., 2003; Hellerbrand et al., 2008), which belongs to the MIA family of genes, consisting of MIA, MIA2, MIA3/Tango and otoraplin (OTOR). This is a family of secreted proteins that contain a Src-homologous SH3 structure in the N terminus (Bosserhoff et al., 2003; Hellerbrand et al., 2008). In comparison to MIA and OTOR, MIA2 and MIA3 contain a long additional peptide sequence in the C-terminus. In particular, evidence for the involvement of MIA2 and MIA3 in protein secretion is beginning to emerge. A seminal study uncovers that MIA3 anchored specifically at the ER exit site (ERES), with its SH3 (SRC homology 3)

domain binding to collagen VII (cargo) and its PRD domain (proline-rich domain) binding to the Sec23/24 inner layer of coat proteins, thereby loading collagen VII into coat protein complex-II (COPII)-coated transport vesicles from the ER (Gurkan et al., 2006; Saito et al., 2009). A follow-up study demonstrates that MIA3-deficient mice are defective not only for the secretion of collagen VII, but also for a variety of other collagens such as II, III, IV, VII and IX, further boarding the role of MIA3 in protein secretion (Wilson et al., 2011). Similarly, MIA2 has recently been shown to locate at the ERES and to interact with the COPII proteins Sec23/Sec24, as well; therefore, it has been proposed as a novel ER-to-Golgi trafficking protein that regulates cholesterol metabolism in the liver, though the exact cargo proteins of MIA2 remain unidentified until now (Pitman et al., 2011). Hence, it is likely that MIA2 constitutes one component of the HNF1A-mediated secretory pathway.

#### **1.3.4. The ER stress/UPR system and protein secretion in the exocrine pancreas**

The exocrine pancreas is a professional secretory organ producing a huge amount of digestive enzymes. To fulfill this task, pancreatic acinar cells have evolved to possess an extensive endoplasmic reticulum (ER) network in which the protein synthesis/process machinery is controlled by concerted activities of the ER-assisted folding (ERAF), ER-associated degradation (ERAD) and COPII export pathways (Anelli and Sitia, 2008; Oprins et al., 2001; Wiseman et al., 2007). Importantly, ERAF, ERAD and COPII export are coordinated by a regulatory machinery in the ER, the unfolded-protein response (UPR) which serves to sense mis-folded or overloaded proteins in the ER (ER stress). Thereafter, the UPR activates a series of molecular events with the aim of either mitigating ER stress or inducing cell death whenever the stress is irresolvable (Ron and Walter, 2007).

The UPR consists of three arms: endoplasmic reticulum to nucleus signaling 1 (ERN1), PRKR-like endoplasmic reticulum kinase (PERK) and activating transcription factor 6 (ATF6) (Ron and Walter, 2007). ERN1 possesses the activities of both endoribonucleases and serine/threonine kinases. Upon its activation, the endoribonuclease removes a 26-nucleotide sequence from the mRNA of x-box binding protein 1 (XBP1), producing a spliced form of XBP1 (s-XBP1) - an important transcription factor mediating downstream UPR effects. Meanwhile, the kinase activity of ERN1 activates c-Jun N-terminal kinase (JNK) through its interaction with TNF receptor-associated factor 2 (TRAF2) and apoptosis signal-regulating kinase 1 (ASK1), thereby initiating the apoptosis cascade. PERK phosphorylates eukaryotic translation initiation factor 2 $\alpha$  (eIF2 $\alpha$ ) and shuts down protein translation under ER stress. ATF6 is translocated to the Golgi apparatus and is further cleaved by site-1 and site-2 protease. The resulting cytosolic part of ATF6 acts as a transcription factor that mediates wide downstream effects. Notably, the three UPR arms interact with each other and play a concerted role in maintaining ER homeostasis (Ron and Walter, 2007).

The importance of the UPR in maintaining homeostasis of the exocrine pancreas is reflected by recent findings that genetic ablation of almost any component of the UPR in mice (e.g. ERN1, XBP1 or PERK) invariably results in unrecoverable ER

stress that ultimately leads to acinar cell death (Harding et al., 2001; Hess et al., 2011; Iwawaki et al., 2010; Lee et al., 2005; Zhang et al., 2002). Furthermore, the ERN1/XBP1 arm is indispensable for embryonic development of the exocrine pancreas (likely through a crosstalk with developmental pathways) and promotes cell survival upon acinar cell damage (Lee et al., 2005; Lugea et al., 2011).

### **1.3.5. The potential role of the HNF1A/MIA2 secretory axis in PDAC**

Compellingly, studies in hepatocellular carcinoma (HCC) demonstrate the relevance of the HNF1/MIA2 axis in carcinogenesis: MIA2 expression in HCC is down-regulated due to a wide loss of HNF1 expression while over-expression of MIA2 in cell lines inhibits cell growth and invasion (Hellerbrand et al., 2008). Therefore, the HNF1/MIA2 axis has a tumor suppressor function in the context of HCC. However, it remains largely unknown whether the secretory axis of the pancreas might influence the carcinogenic process of PDAC - a malignancy that likely originates from the transformation of (oncogenesis-susceptible) cells in the exocrine pancreas (Kong et al., 2011). Since an exocrine-like subtype of PDAC has been identified and because HNF1A has been identified as a novel cancer risk gene of PDAC (Collisson et al., 2011), it is likely that the HNF1A/MIA2 secretory axis is active in PDACs. However, it is unclear how pancreatic cancer cells “misuse” these secretory pathways to promote carcinogenesis. Furthermore, it is unknown whether and how these secretory pathways crosstalk with the ER stress/UPR system in promoting malignant progression.

## **1.4. The TSC1-TSC2 complex and mTORC1 are common gatekeepers of pancreatic malignancy**

### **1.4.1. General introduction to the mTOR and TSC1-TSC2 complex**

The mammalian target of rapamycin (mTOR) has been initially identified during genetic screening for target genes mediating the toxic effects of rapamycin on yeast (Cafferkey et al., 1993; Kunz et al., 1993). Then, its homologue in mammals has been found (Brown et al., 1994). Belonging to the phosphoinositide 3-kinase (PI3K)-related kinase family, the mTOR is an atypical serine/threonine kinase which interacts with several other proteins (e.g. Raptor or Rictor) to form two major complexes: mTORC1 and mTORC2 (Shaw and Cantley, 2006). mTORC1 is well characterized and it integrates a variety of intracellular and extracellular cues including growth factors, energy stress, amino acids and oxygen (see below). By activating downstream molecules such as S6 kinase 1 (S6K1) and eukaryotic translation initiation factor 4E (eIF4E)-binding protein 1 (4E-BP1) (Huang and Manning, 2008), mTORC1 influences many cellular processes such as protein and lipid synthesis (Laplane and Sabatini, 2012). In contrast, apart from its role in regulating AKT signaling and cytoskeletal organization, the exact functions of mTORC2 remain largely obscure (Laplane and Sabatini, 2012). In this study, mTOR or mTORC1 (unless otherwise stated) only refer to the functions of mTORC1.

The TSC1 (also known as hamartin) and TSC2 (also known as tuberin) genes have been identified as the mutated genetic loci in tuberous sclerosis complex, which is a multi-system genetic disease characterized by benign tumors in multiple organs (e.g. the brain and the kidney) (1993; Kandt et al., 1992; van Slegtenhorst et al., 1997). TSC1 physically associates with TSC2 to form a functional heterodimer: the TSC1-TSC2 complex (Plank et al., 1998; van Slegtenhorst et al., 1998). TSC2 contains a GTPase Activating Protein (GAP) domain at its C-terminus (a region of limited homology to the catalytic domain of the Rap1-GTPase-activating protein), which is of major functional significance to the TSC1-TSC2 complex (Wienecke et al., 1995; Xiao et al., 1997). TSC1 stabilizes TSC2 by preventing its ubiquitin-mediated degradation (Chong-Kopera et al., 2006). Mutations of TSC1 or TSC2 found in human disease frequently affect either the GAP domain of TSC2 or the stability of the TSC1-TSC2 complex (Nellist et al., 2001).

It becomes clear that the tumor suppressor function of the TSC1-TSC2 complex mainly relies on its role as a negative regulator of mTORC1 activity (Huang and Manning, 2008). Here, biochemical studies have demonstrated that the TSC-TSC2 complex directly stimulates the intrinsic GTPase activity of Ras homolog enriched in brain (Rheb) via the GAP domain of TSC2, converting Rheb-GTP into Rheb-GDP (Inoki et al., 2003a; Inoki et al., 2002). Since Rheb-GTP is required for the activation of mTORC1, the TSC1-TSC2 complex negatively regulates mTORC1 activity through its GAP activity (Huang and Manning, 2008). However, the existence of a corresponding guanine-nucleotide exchange factor (GEF) that opposes the GAP activity of the TSC1-TSC2 complex towards Rheb has been controversially discussed (Rehmann et al., 2008). Nevertheless, an apoptosis-associated protein - translationally controlled tumour protein (TCTP) has been proposed as the Rheb GEF (Dong et al., 2009; Hsu et al., 2007). Taken together, the TSC1-TSC2 complex constitutes an important regulator of mTORC1 that plays an important role in different biological contexts.

Besides, additional functions of TSC1 and TSC2 other than within the TSC1-TSC2 complex and mTORC1 have been reported. For example, both TSC1 and TSC2 have been shown to regulate focal adhesion and formation of stress fibers via interactions with the ezrin-radixin-moesin (ERM) family of actin-binding proteins (Astrinidis et al., 2002; Lamb et al., 2000). Certainly, these functions add another layer of complexity to the putative tumour suppressor functions of the TSC1-TSC2 complex.

#### **1.4.2. Oncogenic signals of PDAC converge at the TSC1-TSC2 complex**

Using GEMM models, it has been demonstrated the oncogenic Kras activity is not only essential for cancer inception, but also for maintenance of malignancy (Collins et al., 2012). Recent studies have unequivocally demonstrated the importance of 3 major effector pathways of oncogenic Kras, consisting of Raf/Mek/Erk, PI3K/Akt and Il1 $\alpha$  (interleukin 1  $\alpha$ ) / p62 (also known as sequestosome 1) / NF- $\kappa$ B (nuclear factor of kappa light polypeptide gene enhancer in B cells 1) in pancreatic carcinogenesis. As such, pancreas-specific expression of BRAF<sup>V600E</sup> (a mutated form of RAF observed in human tumors) leads to PanIN lesion formation while a combination of BRAF<sup>V600E</sup> and a p53

gain-of-function mutation initiates PDAC in mice, underscoring the important role of the Raf/Mek/Erk branch in PDAC genesis (Collisson et al., 2012). Furthermore, one third of human PDACs contain genetic alternations (e.g. PTEN deletions or AKT2 amplifications) that increase PI3K/AKT activity, suggesting that the oncogenic KRAS-mediated activation of PI3K/AKT is possibly repressed by unknown mechanisms (Hill et al., 2010; Kennedy et al., 2011; Ying et al., 2011). To reduce the activation threshold by deleting one or two allele(s) of Pten (a negative regulator of PI3k/Akt) serves to “unleash” the transformation effect of the PI3k/Akt pathway and dramatically accelerates PDAC formation in mice driven by oncogenic Kras expression (Hill et al., 2010; Kennedy et al., 2011; Ying et al., 2011). Finally, the current data suggest that oncogenic Kras activates intrinsic NF-κB in pre-neoplastic (e.g. PanIN) lesions and tumor cells which sets into motion the local inflammatory cascade by releasing a set of pro-inflammatory cytokines and chemokines (Ling et al., 2012; Maniati et al., 2011). Among these inflammatory cytokines, oncogenic Kras-induced Il1α is particularly important because it directly activates NF-κB, which, in turn, transcribes more Il1α and p62 (an adaptor protein for the Il1α receptor), forming a positive feedback activation loop for initiating and sustaining inflammation (Ling et al., 2012). In human PDAC, expression of IL1A is associated with an unfavorable prognosis and promotes a metastatic phenotype of human pancreatic cancer cells (Melisi et al., 2009; Niu et al., 2004). Therefore, the inflammatory branch of the oncogenic Kras effectors - Il1α/p62/NF-κB has emerged as a major oncogenic pathway.

Importantly, biochemical studies have demonstrated that these effector pathways converge their oncogenic signals at the TSC1-TSC2 complex. Here, activated ERK and its downstream molecule-RSK (ribosomal protein S6 kinase) phosphorylate TSC2 at multiple sites (e.g. Ser<sup>664</sup> and to a lesser extent Ser<sup>939</sup>) (Ma et al., 2005; Ma et al., 2007; Roux et al., 2004). Similarly, activated AKT phosphorylates TSC2 on multiple residues (e.g. Ser<sup>939</sup> and Thr<sup>1462</sup>), as well (Inoki et al., 2002; Potter et al., 2002). Recently, it has been shown that activated IKK2 (inhibitor of kappaB kinase β) induced by pro-inflammatory cytokines (e.g. IL1A and TNFA) phosphorylates TSC1 at Ser<sup>487</sup> and Ser<sup>511</sup> (Lee et al., 2007b; Ling et al., 2012). Though the underlying molecular mechanisms (e.g. increased GAP activity or decreased stability of the complex) are not completely understood, the collective effect of these phosphorylations on the TSC1-TSC2 complex is the activation of mTORC1. Therefore, the function of the TSC1-TSC2 complex is important to relay putative oncogenic signals of oncogenic KRAS to mTORC1.

#### **1.4.3. The TSC1-TSC2 complex integrates the tumor suppressor pathways of PDAC**

P53 and LKB1 (serine/threonine kinase 11) are important tumor suppressors in pancreatic cancer. As earlier illustrated, p53 is widely mutated in human PDAC and p53 mutations together with oncogenic Kras effectively initiate PDAC in mice with an appearance of the moderate differentiation (Bardeesy et al., 2006a). Although only a fraction (around 4%) of human PDACs contain a complete loss of LKB1, low expression levels of LKB1 in cancer cells are linked with a poor prognosis of PDAC patients, highlighting its essential role (rather in a quantitative manner) in determining human PDAC biology (Su et al., 1999). In line, Lkb1

haploinsufficiency cooperates with oncogenic Kras to drive PDAC development in mice (Morton et al., 2010). However, it remains largely unknown how the oncogenic Kras integrates these signal inputs from the loss of tumor suppressors into a concerted force which effectively promotes pancreatic carcinogenesis.

Notably, two tumor suppressive signals of PDAC regulate the activity of mTORC1 via the TSC1-TSC2 complex. Triggered by energy stress, the AMPK (AMP-activated protein kinase) is activated by LKB1 (Shackelford and Shaw, 2009; Shaw et al., 2004). Activated AMPK phosphorylates TSC2 on several serine sites (e.g. Ser<sup>1387</sup>), whose phosphorylation is required for the subsequent phosphorylation by GSK3 (glycogen synthase kinase 3) (Inoki et al., 2006; Inoki et al., 2003b). Unlike the ERK/RSK and PI3K/AKT-induced TSC2 phosphorylations, the AMPK-induced TSC2 phosphorylations inhibit mTORC1 activity by poorly understood mechanisms (possibly by increasing GAP activity of the TSC1-TSC2 complex towards Rheb) (Huang and Manning, 2008). Activated by DNA damage, P53 activates AMPK together with sestrin 1/2 (Budanov and Karin, 2008). Also, DNA damage directly induces TSC2 transcription in a P53-dependent manner (Feng et al., 2007).

Given the fact that the TSC1-TSC2 complex serves as an important signal integrating point for both oncogenic and tumor suppressor pathways in PDAC, it is not surprising that mTORC1 is active in nearly all human PDACs (Kennedy et al., 2011). Furthermore, the increased mTORC1 activity has been shown to be associated with an unfavorable prognosis of PDAC patients (Kennedy et al., 2011). It is thus likely that the TSC1-TSC2 complex plays a largely underestimated role in pancreatic carcinogenesis. Compellingly, this notion is further substantiated by the recent identification of somatic mutations in TSC2 in human PDACs (Jones et al., 2008).

#### **1.4.5. A signal circle formed by hypoxia, mTORC1 signaling and the ER stress/UPR system**

Similar to other tumor entities, human PDAC is notoriously hypovascular and hypoxic (Koong et al., 2000; Olive et al., 2009). Upon hypoxia, the hypoxia-inducible factor family of genes (HIFs) is induced to initiate a series of adaptive changes to cope with hypoxic environments (Semenza, 2012). However, these adaptive changes simultaneously foster the malignant behavior of pancreatic cancer by various mechanisms: 1) hypoxia promotes the metastatic potential of pancreatic cancer cells (Niizeki et al., 2002); 2) the hypoxic niche facilitates the acquisition of stem cell-like properties in cancer cells that render them more resistant towards treatment (Penchev et al., 2012); 3) the hypovascular structure of PDAC significantly hinders drug delivery (Olive et al., 2009). Furthermore, the extent of hypoxia correlates with the prognosis of PDAC patients (Kitada et al., 2003; Shibaji et al., 2003). However, the exact molecular mechanisms responsible for the formation of tissue hypoxia in PDAC remain largely unclear to date.

Nevertheless, previous studies have demonstrated that the hypoxic signals crosstalk widely with mTORC1 and the ER stress/UPR system in a variety of cancer entities (Wouters and Koritzinsky, 2008). Interestingly, both mTORC1

activity and the ER stress/UPR system are dynamically regulated by hypoxic signals (see below).

As a part of adaptive changes, hypoxia inhibits mTORC1 by a variety of molecular mechanisms (Bertout et al., 2008; Wouters and Koritzinsky, 2008). Firstly, DNA-damage-inducible transcript 4 (REDD1; also known as DDIK4) induced in a HIF-dependent manner activates the TSC1-TSC2 complex by freeing TSC2 from its association with 14-3-3 (induced by growth factors or energy) (DeYoung et al., 2008; Sofer et al., 2005; Wolff et al., 2011). Secondly, the energy stress induced by extended hypoxia shuts down mTORC1 activity by employing AMPK-mediated phosphorylation of TSC2 (DeYoung et al., 2008; Sofer et al., 2005; Wolff et al., 2011). Finally, hypoxia affects the interaction between Rheb and its substrate – mTORC1. For instance, the hypoxia-induced promyelocytic leukaemia tumor suppressor (PML) binds to mTORC1 and sequesters it in nuclear bodies (Bernardi et al., 2006). Also, BCL2/adenovirus E1B interacting protein 3 (BNIP3, induced by hypoxia) regulates the activity of mTORC1 by binding to Rheb (Li et al., 2007). Taken together, this is a conservative program that shuts down energy-expensive anabolic processes in a hypoxic microenvironment.

Since maintenance of the protein folding capacity requires a coordinated collaboration between the protein synthesis, ERAF, ERAD and COPII machineries, the ER stress/UPR system is susceptible to changes in pathways affecting protein synthesis such as mTORC1. Recently, the bidirectional interaction between the ER stress/UPR system and mTORC1 is beginning to emerge. Here, mTORC1 is able to operate both upstream and downstream of the ER stress/UPR system (Appenzeller-Herzog and Hall, 2012); the interaction between mTORC1 and ER stress may have synergistic or antagonistic effects on various biological processes. For example, ER stress and the mTORC1 promote insulin resistance synergistically whereas they have completely opposite functions in regulating protein translation (Ozcan et al., 2008; Rutkowski and Hegde, 2010; Um et al., 2004). mTORC1 initiates cap-independent translation by phosphorylating S6K1 and 4E-BP1 while the UPR after ER stress apparently decreases protein translation via PERK (as illustrated earlier). Importantly, the coordinated function of mTORC1 and ER stress is fundamental for cell health. For example, loss of Tsc1 or Tsc2 leads to constitutive activation of mTORC1, which results in an induction of ER stress/UPR in mouse embryonic fibroblasts (MEFs). The resulting ER stress not only renders them less sensitive towards insulin signals, but also more susceptible to the apoptosis (Ozcan et al., 2008).

Since the ER stress/UPR system is highly susceptible to changes in mTORC1 activity, which is further dynamically regulated by hypoxic signals, it is conceivable that hypoxia would also have an effect on the ER stress/UPR system. Indeed, transient hypoxia activates the PERK/eIF2 $\alpha$  and ERN1/XBP1 branches of the UPR (Bi et al., 2005; Koumenis et al., 2002; Romero-Ramirez et al., 2004). Though it is not entirely clear how these UPR arms are activated by hypoxia (potentially due to deprivation of oxygen), their activation seem to be essential for cell survival in hypoxic environments because inactivation of either PERK or ERN1 significantly reduces cell survival (Bi et al., 2005; Koumenis et al., 2002; Romero-Ramirez et al., 2004).

In summary, the ER stress/UPR system and mTORC1 reciprocally regulate each other and hypoxic signals tend to inhibit mTORC1 activity and to activate ER stress/UPR. Thus, they form a complicated network, which might play an important role in determining tumor biology of PDAC. In particular, the interplay of the ER stress/UPR system and of mTORC1 activity may shape cancer cells' response to hypoxia. However, it is largely unknown how this regulatory network influences pancreatic carcinogenesis.



## 2. AIMS OF THIS STUDY

Although an increased pancreatic cancer risk conferred by genetic variations at the HNF1A locus and of reported genetic alterations within the MIA2 region in the genome of human PDAC has been reported (Jones et al., 2008; Pierce and Ahsan, 2011), it remains largely unknown whether human PDAC contain a functional HNF1A/MIA2-mediated secretory network that interacts with the ER stress/UPR system in determining tumor biology. Since the TSC1-TSC2 complex together with mTORC1 integrates signal inputs from the major oncogenic and tumor suppressor pathways in PDAC, the role of TSC1-TSC2 in the development of PDAC needs to be defined. Together with hypoxic signals and the ER stress/UPR system, the TSC1-TSC2 complex and mTORC1 form a regulatory network with reciprocally counteractive properties, however, the biological significance of this network in PDAC is unclear.

To this end, 3 major hypotheses have been formed (**Fig. 1**):

Hypothesis 1: The HNF1A/MIA2 secretory network crosstalks with the ER stress/UPR system in human PDAC;

Hypothesis 2: The TSC1-TSC2 complex plays an essential role in pancreatic carcinogenesis by integrating signal inputs from major oncogenic and tumor suppressor pathways;

Hypothesis 3: The interplay between mTORC1, hypoxia and ER stress/UPR system specifies the molecular subtypes of human PDAC (with their respective and distinctive tumor biology).

To address these hypotheses, the following questions have been specifically asked (Fig. 1):

Question 1 (Q1): what is the biological and clinical relevance of an interaction between the HNF1A/MIA2-mediated secretory network and the ER stress/UPR system?

Question 2 (Q2): what are the functions of the Tsc1-Tsc2 complex in murine pancreatic carcinogenesis specifically driven by Kras<sup>G12D</sup> or by complete Pten loss, or by a combination of both?

Question 3 (Q3): what is the role of the Tsc1-Tsc2 complex in murine pancreatic malignancy in the context of p53 loss?

Question 4 (Q4): what is the biological significance of the reciprocally regulatory network formed by mTORC1, the ER stress/UPR system and by hypoxic signals in PDAC biology?

Question 5 (Q5): do the above mentioned signal pathways or biological processes play a role in specifying distinctive molecular subtypes of human PDAC?

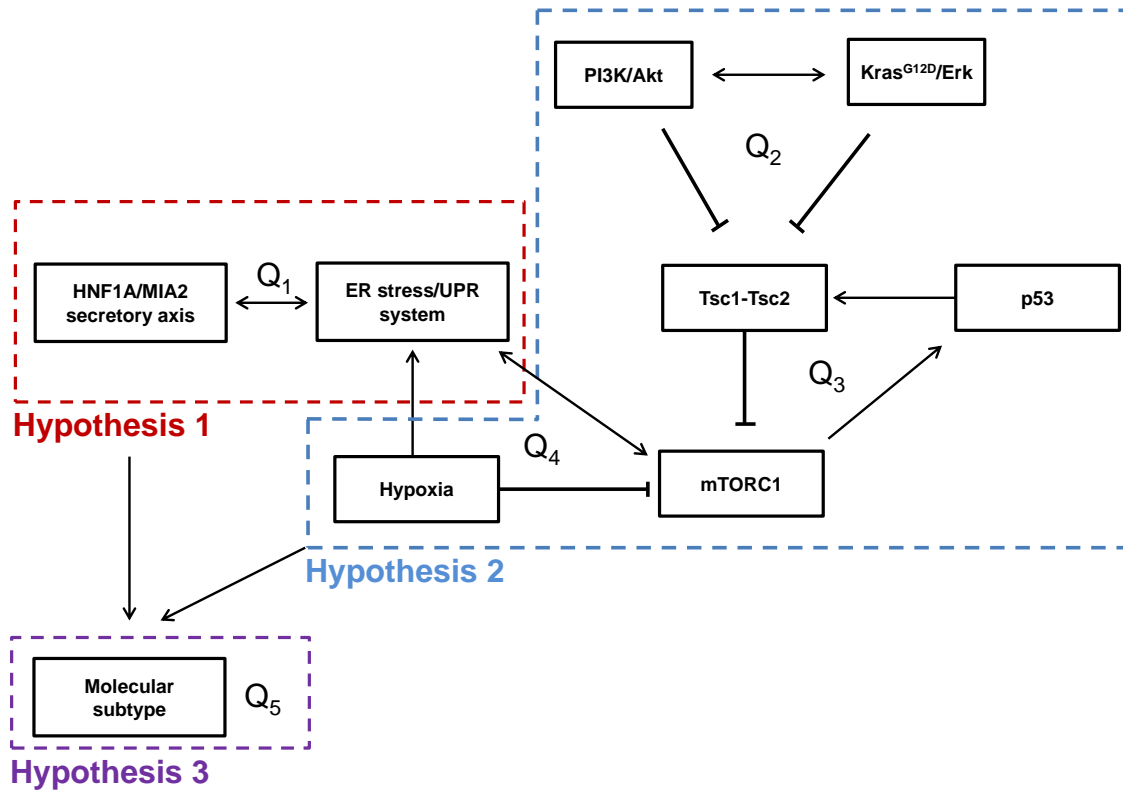


**Figure 1.** Schematic figure illustrating the structure of this study

## 3. MATERIALS AND METHODS

### 3.1. Materials

#### 3.1.1. Patient material and tissue collection

PDAC tissues were obtained from patients on whom pancreatic resections were carried out. The diagnoses of all samples were confirmed histologically. Samples were either snap-frozen in liquid nitrogen or were fixed in paraformaldehyde solution for 24 hours and were then paraffin-embedded for histological analysis. The use of tissue for this study was approved by the local Ethics committee and written informed consent was obtained from the patients prior to surgery (Department of Surgery, Klinikum rechts der Isar, Technical University Munich; resections on PDAC patients have been performed between 2007 and 2010). Detailed clinical and pathological data were obtained from each patient and follow-ups amounted to at least 12 months. Patients with a survival of less than 2 months after surgery were excluded from the survival analysis in order to rule out surgery-related mortality. Tissue collection and patient database maintenance were coordinated by Carsten Jäger and Ivane Abiatari. Genomic DNA used for genotyping analysis was isolated from paraffin-embedded tissues. Donor pancreases were obtained through an organ donor program from previously healthy individuals; pancreases with chronic pancreatitis, pancreatic neuroendocrine tumors (PNET) and PDAC (without detailed clinical data) had previously been collected at Heidelberg University Hospital (written informed consent had been obtained from these patients, as well). Genomic DNA of colorectal cancer tissues and the respective patient data were provided by Dr. Ulrich Nitsche (group of PD Dr. Klaus-Peter Janssen, Molecular Tumor Biology, Department of Surgery, Technical University Munich). Tissues of esophageal cancer were obtained from the Institute of Pathology (Technical University Munich).

#### 3.1.2. Mouse lines

Mice containing a floxed allele of Pten (006440), Tsc1 (005680), p53 (008462) and Loxp-STOP-Loxp-Kras<sup>G12D/+</sup> (LSL-Kras<sup>G12D/+</sup>; 008179) were obtained from Jackson Laboratory (Bar Harbor, USA). The pancreas-specific Cre recombinase line Ptf1a<sup>Cre/+</sup> (also known as p48<sup>Cre/+</sup>) was a generous gift from PD Dr. Jens T. Siveke (Department of Internal Medicine, Technical University of Munich). The exon 17 and 18 of the Tsc1 allele, the exon 5 of Pten and the exons 2-10 of p53 in these animals are flanked by two LoxP sites, respectively, as described previously (Kwiatkowski et al., 2002; Lesche et al., 2002; Marino et al., 2000). The wild type (WT; C57BL/6J) and the immunodeficient mice (BALB/c nude) were obtained from Charles River Laboratory (Sulzfeld, Germany).

#### 3.1.3. Human cell lines

HEK293 cells (a kind gift from PD Dr. Klaus-Peter Janssen, Molecular Tumor Biology, Department of Surgery, Technical University Munich) and eight human

pancreatic cancer cell lines - Aspc-1, Bxpc-3, Capan-1, Colo-357, MiaPaCa-2, Su86.86, Panc-1 and T3M4 (obtained from ATCC, Wesel, Germany) - were used for the experiments.

### 3.1.4. Mouse cell lines

The primary mouse cells 911, 961, 947 were isolated from transgenic p48<sup>Cre/+</sup>; p53<sup>fl/fl</sup>; Tsc1<sup>fl/+</sup> mice, respectively. 946 and 946F were two different clones isolated from the same p48<sup>Cre/+</sup>; p53<sup>fl/fl</sup>; Tsc1<sup>fl/fl</sup> mice. 926, 928 and 952 cells were isolated from transgenic p48<sup>Cre/+</sup>; Pten<sup>fl/fl</sup>; Tsc1<sup>fl/+</sup> mice, respectively. 399, 403, 907, 897, 445Li, 445Pa, 638Li, 908Pa, 908Li and 908Lu cells were isolated from transgenic p48<sup>Cre/+</sup>; LSL-Kras<sup>G12D/+</sup>; Tsc1<sup>fl/+</sup> mice. An overview of the cell lines, mouse numbers, the respective genotypes and histologies is provided in **Table 1**. Two previously described mouse cancer cell lines derived from Pdx1-Cre (another pancreas-specific Cre line); LSL-Kras<sup>G12D</sup>; p53<sup>fl/+</sup> (#T9801 and 944) were obtained from PD Dr. Jens T. Siveke (Dept. of Int. Med., Technical University of Munich).

**Table 1:** List of mouse cell lines

Cell lines	Mouse number	Genotype (With P48 <sup>Cre/+</sup> )	Histology
911	911/3	P53 <sup>fl/fl</sup> ; Tsc1 <sup>fl/+</sup>	Normal
961	961/1	P53 <sup>fl/fl</sup> ; Tsc1 <sup>fl/+</sup>	Normal* (macroscopically)
947	947/1	P53 <sup>fl/fl</sup> ; Tsc1 <sup>fl/+</sup>	Normal
946	946/3	P53 <sup>fl/fl</sup> ; Tsc1 <sup>fl/fl</sup>	Acinar carcinoma
946F	946/3	P53 <sup>fl/fl</sup> ; Tsc1 <sup>fl/fl</sup>	Acinar carcinoma
926	926/3	Pten <sup>fl/fl</sup> ; Tsc1 <sup>fl/+</sup>	Cystic lesions
928	928/3	Pten <sup>fl/fl</sup> ; Tsc1 <sup>fl/+</sup>	Cystic lesions
952	952/3	Pten <sup>fl/fl</sup> ; Tsc1 <sup>fl/+</sup>	Cystic lesions
399	399/3	Kras <sup>G12D</sup> ; Tsc1 <sup>fl/+</sup>	PDAC
403	403/3	Kras <sup>G12D</sup> ; Tsc1 <sup>fl/+</sup>	PDAC
907	907/3	Kras <sup>G12D</sup> ; Tsc1 <sup>fl/+</sup>	PDAC
897	897/3	Kras <sup>G12D</sup> ; Tsc1 <sup>fl/+</sup>	PDAC
638Li	638/MZ	Kras <sup>G12D</sup> ; Tsc1 <sup>fl/+</sup>	PDAC hepatic metastasis
445Pa	445/MZ	Kras <sup>G12D</sup> ; Tsc1 <sup>fl/+</sup>	PDAC
445Li	445/MZ	Kras <sup>G12D</sup> ; Tsc1 <sup>fl/+</sup>	PDAC hepatic metastasis
908Pa	908/3	Kras <sup>G12D</sup> ; Tsc1 <sup>fl/+</sup>	PDAC
908Li	908/3	Kras <sup>G12D</sup> ; Tsc1 <sup>fl/+</sup>	PDAC hepatic metastasis
908lu	908/3	Kras <sup>G12D</sup> ; Tsc1 <sup>fl/+</sup>	PDAC pulmonary metastasis

\*: The whole pancreas of 8-weeks-old mice was used for cell isolation. Gross examination of the pancreas revealed no tumor formation in this mouse.

### 3.1.5. Plasmids, siRNAs and primers

The human MIA2 expression vector (RC224284), the HNF1A expression vector (RC211201) and the HNF1B expression vector (SC122562) were purchased from Origene (VWR International GmbH, Darmstadt, Germany). Human MIA2 siRNA

and ERN1 siRNAs were purchased from Ambion Applied Biosystems (Carlsbad, California, USA) and QIAGEN (Hilden, Germany), respectively. All primers used in this study were synthesized by Metabion (Martinsried, Germany).

Sequences of siRNA used for gene-silencing experiments:

Name	Sense (5'→3')	Antisense (5'→3')
<i>MIA2</i> -siRNA1#	GGAGUAGAAAAUAGCAGUTT	ACUGCUAUUUUUCUACUCCGA
<i>MIA2</i> -siRNA2#	CAGACGAAUCUGAUACUAUTT	AUAGUAUCAGAUUCGUCUGTT
<i>ERN1</i> -siRNA1#	GGACGUGAGCGACAGAAUATT	UAUUCUGUCGCUCACGUCCTG
<i>ERN1</i> -siRNA2#	GCACGGACGUCAAGUUUGATT	UCAAACUUGACGUCCGUGCTG

Sequences of primers used for QRT or RT-PCR analysis of human genes:

Gene Name	Sense (5'→3')	Antisense (5'→3')
<i>MIA2</i>	ATGGCAAATTTGGCGTTC	CCTGCCACAAATCTTCC
<i>ERN1</i>	CGAGGAGGTGGGGGAAGCGA	GCTGCCGGGTGTTGGGGAAA
<i>TSC1</i>	CTGGGAGAGGTTACCCGAGA	GGCCTGGGAAATGATGGTCA
<i>TSC2</i>	CTGCACGCAAATATGGCCTC	AATACCGTCCAAGGCCAGTG
<i>ALDH1A1</i>	CTGTGTTCCAGGAGCCGAAT	AGCATCCATAGTACGCCACG
<i>ALDH1A3</i>	ACTCTGAGTTTGTGAGGCGG	CACTGGCCCCGAAAATCTCCT
<i>XBP1</i> -unspliced	ATGGCTTTGGGCAGTGGCTGG	GGGGATGGATGCCCTGGTTGC
<i>XBP1</i> -spliced	CCTGCACCTGCTGCGGACTCA	GAGTTAAGACAGCGCTTGGG
<i>XBP1</i>	GGTAAGGAACTGGGTCCTT	AGAGAGGCGGGAGAGCCGTG
<i>HNF1B</i>	CCTCCAAAGCCCACGGCCTG	AGCCGTGGGAGAGCAGAGGG
<i>ACTB</i>	CTACGTCGCCCTGGACTTCGAGC	GATGGAGCCGCCGATCCACACGG
<i>HPRT1</i>	GCTTTCCTTGGTCAGGCAGTATAAT	AAGGGCATATCCTACAACAACTG

Sequences of primers used for mutagenesis for generating the *MIA2* variants:

Name	Sense (5'→3')
<i>MIA2</i> -A617G	GTGAATTAACGGTGATTATGGTGAAAATATGATCCTTATGAAGAAGATAAA G
<i>MIA2</i> -G1833 C	ATTTTGAACCCTCATCTTCTAAACATAGTGATGAAAATTCGAACCC

Sequences of primers used for sequencing the human MIA2 cDNA:

Position of MIA2 cDNA	Sequence (5'→3')
Sense-134	CTCTACAACCTGAACAATTGGCTTAA
Sense-751	TATCGGAAGTACCAGTGAATCAAAAG
Sense-1329	ATTTTGGTTTTGCTATACTAGGCTTT
Sense-1237	TAAAGAAGCCACAGTTCCATGTACAG
Sense-1731	GATATTCAAAGTTCATACAGTCTG
Antisense-822	GGAATACGATCCTGTTCCATACTTTC
Antisense-1354	AAAGCCTAGTATAGCAAAACCAAAT
Antisense-1559	ATGGTATAGTATCAGATTCGTCTGTT
Antisense-1769	AGACCATATCTGACAGACTGTATGAA
Antisense-1857	GATGGTTTCGAATTTTCATCACTATC
Antisense-1959	TGAGAAGACAAAGAGTTATCAGTTGA
Antisense-2247	TGACAAAACATTCATATAAAGAGAAA

Sequences of primers used for high-resolution melting curve analysis of the MIA2 variants:

Variant name	Sense (5'→3')	Antisense (5'→3')
<i>MIA2</i> <sup>141M</sup>	AGTGAATTAACGGTGATTATGGTG	CCTCTAATGCTGGAACCTTGGTCT
<i>MIA2</i> <sup>D547H</sup>	AGAGTTACCTACGAGAATTCACGAA	CTATTTAGCAGGGTATTTTCCACG

Sequences of primers used for QRT-PCR analysis of the mouse genes:

Gene Name	Sense (5'→3')	Antisense (5'→3')
<i>Vegfa</i>	ACTCGGATGCCGACACGGGA	CCTGGCCTTGCTTGCTCCCC
<i>Aldh1a3</i>	TCCTGGCTACTCTGGAGACC	TTCCATGGTGTAAATGGCCCC
<i>Aldh1a1</i>	GATGCCGACTTGGACATTGC	CACACTCCAGTTTGGCTCCT
<i>Il1α</i>	AGGGAGTCAACTCATTGGCG	ACTTCTGCCTGACGAGCTTC
<i>B2m</i>	CGGCCTGTATGCTATCCAGAAAACC	TGTGAGGCGGGTGGAACTGTG

### 3.1.6. List of antibodies

#### Primary antibodies

Antibody name	Catalog number	Application* (Reactivity**)	Producer
Rabbit Anti-PDI mAb <sup>#</sup>	3501	WB; IHC (H, M)	Cell Signaling Technology (NEB, Frankfurt/Main, Germany)
Rabbit Anti-BiP mAb <sup>#</sup>	3177	WB; IHC (H, M)	Cell Signaling Technology
Rabbit Anti-Calnexin mAb <sup>#</sup>	2679	IHC (H)	Cell Signaling Technology
Rabbit Anti-PERK mAb <sup>#</sup>	5683	WB; IHC (H)	Cell Signaling Technology
Rabbit Anti-ERN1 mAb <sup>#</sup>	3294	WB (H)	Cell Signaling Technology
Rabbit Anti-Myc-Tag mAb <sup>#</sup>	2278	WB (-)	Cell Signaling Technology
Rabbit Anti-p-Akt <sub>Ser473</sub> mAb <sup>#</sup>	4060	WB; IHC (M)	Cell Signaling Technology
Rabbit Anti-Akt Ab <sup>#</sup>	9272	WB (M)	Cell Signaling Technology
Rabbit Anti-p-Erk1/2 <sub>Thr202/Tyr204</sub> Ab <sup>#</sup>	9101	WB; IHC (M)	Cell Signaling Technology
Rabbit Anti-Erk1/2 Ab <sup>#</sup>	9102	WB (M)	Cell Signaling Technology
Rabbit Anti-p-mTOR <sub>Ser2481</sub> Ab <sup>#</sup>	2974	WB (M)	Cell Signaling Technology
Rabbit Anti-p-mTOR <sub>Ser2448</sub> mAb <sup>#</sup>	5536	WB (M)	Cell Signaling Technology
Rabbit Anti-p-mTOR <sub>Ser2448</sub> mAb <sup>#</sup>	2976	IHC (H, M)	Cell Signaling Technology
Rabbit Anti-Pten mAb <sup>#</sup>	9188	WB; IHC (M)	Cell Signaling Technology
Rabbit Anti-mTOR mAb <sup>#</sup>	2983	WB; IHC (M)	Cell Signaling Technology
Rabbit Anti-p-S6 <sub>Ser235/236</sub> Ab <sup>#</sup>	2211	WB; IHC (M)	Cell Signaling Technology
Rabbit Anti-S6 mAb <sup>#</sup>	2217	WB (M)	Cell Signaling Technology
Rabbit Anti-p-Histone H3 <sub>Ser10</sub> Ab <sup>#</sup>	9701	IHC (M)	Cell Signaling Technology
Rabbit Anti-Cleaved Casp3 mAb <sup>#</sup>	9664	WB; IHC (M)	Cell Signaling Technology
Rabbit Anti-Bnip3 Ab <sup>#</sup>	3769	WB (M)	Cell Signaling Technology
Rabbit Anti-E-cadherin mAb <sup>#</sup>	3195	WB; IHC (M)	Cell Signaling Technology
Rabbit Anti-Hk2 mAb <sup>#</sup>	2867	WB; IHC (M)	Cell Signaling Technology
Rabbit Anti-p-AMPK $\alpha$ <sub>Thr172</sub> mAb <sup>#</sup>	2535	WB (M)	Cell Signaling Technology
Rabbit Anti-Glucagon Ab <sup>#</sup>	2760	IHC; IF (M)	Cell Signaling Technology
Rabbit Anti- $\alpha$ -Amylase	3796	WB; IHC; IF	Cell Signaling Technology

mAb <sup>#</sup>		(M)	
Rabbit Anti-Tsc1 mAb <sup>#</sup>	6935	WB (M)	Cell Signaling Technology
Rabbit Anti-Tsc2 mAb <sup>#</sup>	4308	WB (M)	Cell Signaling Technology
Rabbit Anti-p-Tsc2 <sub>Ser1387</sub> Ab <sup>#</sup>	5584	WB (M)	Cell Signaling Technology
Rabbit Anti-p-Tsc2 <sub>Ser939</sub> Ab <sup>#</sup>	3615	WB (M)	Cell Signaling Technology
Rabbit Anti-p-Tsc2 <sub>Thr1462</sub> mAb <sup>#</sup>	3617	WB (M)	Cell Signaling Technology
Mouse Anti-Hif1 $\alpha$ Ab <sup>#</sup>	NB100-105	WB (M)	Novus Biologicals (Cambridge, UK)
Rabbit Anti-ATF6 pAb <sup>#</sup>	NBP1-41439	WB; IHC (H)	Novus Biologicals
Rabbit Anti-HNF1A pAb <sup>#</sup>	NBP1-33596	WB; IHC (H)	Novus Biologicals
Rabbit Anti-KRT19 Ab <sup>#</sup>	NB100-687	IHC (H)	Novus Biologicals
Rabbit Anti-CAIX Ab <sup>#</sup>	ab15086	IHC (M)	Abcam (Cambridge, UK)
Mouse Anti-Insulin mAb <sup>#</sup>	ab8304	IHC, IF (M)	Abcam
Rabbit Anti-CD3 mAb <sup>#</sup>	ab16669	IHC (M)	Abcam
Rabbit Anti-Pdx1 pAb <sup>#</sup>	ab47267	IF (M)	Abcam
Rat Anti-F4/80 Ab <sup>#</sup>	ab16911	IHC (M)	Abcam
Rabbit Anti-Vimentin mAb <sup>#</sup>	ab92547	IHC, IF (M)	Abcam
Mouse Anti-Vimentin mAb <sup>#</sup>	ab8978	WB (M)	Abcam
Rabbit Anti-Chromogranin A pAb <sup>#</sup>	A0430	IHC (H)	Dako Deutschland GmbH (Hamburg, Germany)
Mouse Anti- $\alpha$ -SMA mAb <sup>#</sup>	M0851	IHC (M)	Dako Deutschland GmbH
Rat Anti-CD31 Ab <sup>#</sup>	DIA-310	IHC (M)	Dianova (Hamburg, Germany)
Rat Anti-Krt19 Ab <sup>#</sup>	TROMA-III	IHC; IF (M)	Developmental Studies Hybridoma Bank (Iowa, USA)
Rat Anti-B220 Ab <sup>#</sup>	MAB1217	IHC (M)	R&D Systems (WIESBADEN, Germany)
Rat Anti-Mouse Neutrophils Ab <sup>#</sup>	CED-CL8993AP	IHC (M)	BIOZOL Diagnostica Vertrieb GmbH (Eching, Germany)
Goat Anti-HNF1B Ab <sup>#</sup>	TA302622	WB (H)	Origene (VWR International GmbH, Darmstadt, Germany)
Rabbit Anti-GAPDH Ab <sup>#</sup>	sc-25778	WB (H, M)	Santa cruz biotechnology (Heidelberg, Germany)
Mouse Anti- $\beta$ actin Ab <sup>#</sup>	sc-69879	WB (H, M)	Santa cruz biotechnology
Rabbit Anti-ERN1 pAb <sup>#</sup>	HPA027730	IHC (H)	Sigma-Aldrich (Munich, Germany)
Rabbit Anti-ALDH1A3 Ab <sup>#</sup>	SAB1300933	IHC; WB (H)	Sigma-Aldrich
Rabbit Anti-ALDH1A3 Ab <sup>#</sup>	HPA046271	IHC; WB (H, M)	Sigma-Aldrich
Rabbit Anti-ALDH1A1 Ab <sup>#</sup>	HPA002123	IHC; WB (H)	Sigma-Aldrich



Rabbit Anti-MIA2 pAb <sup>#</sup>	500-P255	WB; IHC (H)	PeptoTech (Hamburg, Germany)
Rabbit Anti-p-53BP1 <sub>S25</sub> Ab <sup>#</sup>	IHC-00053	IHC (M)	BETHYL Laboratory (Biomol GmbH, Hamburg, Germany)
Rabbit Anti-Sox9 pAb <sup>#</sup>	AB5535	IF (M)	Merck Millipore (Billerica, MA, USA)
Rabbit Anti-REDD1 pAb <sup>#</sup>	10638-1-AP	WB (M)	Proteintech (Manchester, UK)

### Secondary antibodies

Antibody name	Catalog number	Application*	Producer
Rabbit HRP (horseradish peroxidase)-labelled Anti-Rat IgG Ab <sup>#</sup>	P0450	IHC	Dako Deutschland GmbH (Hamburg, Germany)
Goat HRP-Labelled Polymer Anti-Mouse Ab <sup>#</sup>	K4001	IHC	Dako Deutschland GmbH
Goat HRP-Labelled Polymer Anti-Rabbit Ab <sup>#</sup>	K4003	IHC	Dako Deutschland GmbH
Goat Alexa Fluor 488 Anti-Mouse IgG Ab <sup>#</sup>	115-546-062	IF	Dianova (Hamburg, Germany)
Chicken Alexa Fluor 594 Anti-Rabbit IgG Ab <sup>#</sup>	A-21442	IF	Invitrogen (Carlsbad, CA, USA)
Goat Alexa Fluor 594 Anti-Rat IgG Ab <sup>#</sup>	A-11007	IF	Invitrogen
Sheep HRP-labelled Anti-Mouse IgG Ab <sup>#</sup>	NA931	WB	GE Healthcare (Little Chalfont, UK)
Donkey HRP-labelled Anti-Rabbit IgG Ab <sup>#</sup>	NA934	WB	GE Healthcare
Donkey HRP-labelled Anti-Goat IgG Ab <sup>#</sup>	sc-2020	WB	Santa cruz biotechnology

\*Application key: WB = western-blot; IHC = Immunohistochemistry; IF = Immunofluorescence; \*\* Reactivity key: H = human; M = mouse; <sup>#</sup>Ab: antibody

### 3.1.7. Chemicals and Reagents

0.25% trypsin/EDTA	Invitrogen (Carlsbad, CA, USA)
2-Mercaptoethanol	Sigma-Aldrich (St. Louis, MO, USA)
Acetic acid	Merck Biosciences (Darmstadt, Germany)
Acetic anhydride	Sigma-Aldrich
Acrylamide solution	ROTH (Karlsruhe, Germany)

Agarose	ROTH
Ampicillin	Sigma-Aldrich
Ammonium persulfate (APS)	Sigma-Aldrich
Biocoat matrigel invasion unit	BD Biosciences (Franklin Lakes, NJ, USA)
Bovine serum albumin (BSA)	ROTH
Bromophenol blue	Sigma-Aldrich
Calcium chloride	Merck Biosciences
Chloroform	Merck Biosciences
Crystal violet	Merck Biosciences
Dextran	Merck Biosciences
Dextran sulfate	Sigma-Aldrich
Dimethyl sulfoxide	Sigma-Aldrich
Deoxyribonucleotide phosphate	Invitrogen
Dulbecco's MEM	Invitrogen
RPMI 1640 Medium	Invitrogen
ECL detection reagent	Amersham (Little Chalfont, UK)
Ethanol	ROTH
Ethidium bromide	ROTH
Fetal calf serum	PAN Biotech (Aidenbach, Germany)
Formamide	Merck Biosciences
Glycerol	Merck Biosciences
Glycine	Roche diagnostics (Penzberg, Germany)
Haematoxylin	Merck Biosciences
Hydrogen peroxide (30%)	ROTH
Histowax	Leica (Wetzlar, Germany)
Humidified chamber	TeleChem (Sunnyvale, CA, USA)
Isopropyl b-D-thiogalactopyranoside	Sigma-Aldrich
Isopropanol	ROTH

Potassium dihydrogen phosphate	Merck Biosciences
Laurylsulfate (SDS)	Sigma-Aldrich
Liquid nitrogen	Tec-Lab (Taunusstein, Germany)
Liquid DAB & chromogen substrate	Dako Cytomation
Methanol	Merck Biosciences
Molecular weight marker	FERMENTAS/Termo (Waltham, USA)
Dinatrium hydrogenphosphate	Merck Biosciences
Normal goat serum	Dako Cytomation
Nitrocellulose membranes	Bio-Rad (Hercules, CA, USA)
Para-formaldehyde	Apotheke TU München (Munich, Germany)
Phosphate buffered saline (PBS) pH 7.4	Invitrogen
Polyvinylpyrrolidone	Sigma-Aldrich
Potassium chloride (KCl)	Merck Biosciences
Permout	Vector Laboratories (Burlingame, CA, USA)
Protease inhibitor cocktail	Roche diagnostics
Proteinase K	Sigma-Aldrich
RNase DNase-free water	Invitrogen
Sodium borate	Merck Biosciences
Sodium chloride	Merck Biosciences
Sodium citrate	Merck Biosciences
Sodium phosphate	Merck Biosciences
TEMED	Sigma-Aldrich
Toluidine blue	Merck Biosciences
Triethanolamine	Sigma-Aldrich
Tris base	Merck Biosciences
Trypan blue solution	Sigma-Aldrich
Tween 20	Merck Biosciences

PBS powder without Ca <sup>2+</sup> , Mg <sup>2+</sup>	Biochrom AG (Berlin, Germany)
HiPerFect Transfection Reagent	Qiagen (Hilden, Germany)
Gemcitabine hydrochloride	Tocris Bioscience (Wiesbaden-Nordenstadt, Germany)
Rapamycin	Merck Chemicals (Nottingham, UK)

### 3.1.8. Kits

BCA protein assay kit	Thermo Scientific (Waltham, USA)
QIAquick purification kit	Qiagen
QuantiTect Rev. Transcription Kit	Qiagen
RNeasy Mini Kit	Qiagen
QIAquick Gel Extraction Kit	Qiagen
QIAGEN Plasmid Midi Kit	Qiagen
QIAamp DNA Mini Kit	Qiagen
SYBR Green 1 Master kit	Roche diagnostics
Human MIA2 ELISA Development Kit (900-K357)	PEPROTECH (Hamburg, Germany)
Mouse VEGF Quantikine ELISA Kit (MMV00)	R&D Systems (WIESBADEN, Germany)
QuikChange Lightning Multi Site-Directed Mutagenesis Kit	Stratagene/Agilent Technologies (CA, USA)
Active ras pull-down and detection kit	Thermo Scientific

### 3.1.9. Laboratory equipment

Analytic balance	METTLER (Giessen, Germany)
Balance	SCALTEC (Göttingen, Germany)
Biophotometer	Eppendorf (Hamburg, Germany)
Centrifuge	Eppendorf
CO <sub>2</sub> incubator	SANYO (Secausus, NJ, USA)

Computer Hardware	Fujitsu SIEMENS (Tokyo, Japan)
Electrophoresis/Electroblotting equipment/ power supply	Invitrogen
Freezer -20°C	LIEBHERR (Bulle, Switzerland)
Freezer -80 °C	Heraeus (Hanau, Germany)
Microplate Reader	Thermo Scientific
Microscope	LEICA (Wetzlar, Germany)
Microwave oven	SIEMENS (Munich, Germany)
PH-meter	BECKMAN (Washington, D. C., USA)
Power supply	BIOMETRA (Göttingen, Germany)
Refrigerator 4 °C	COMFORT (Buller, Switzerland)
Roller mixer	STUART (Stone, UK)
Scanner	Canon (Tokyo, Japan)
Sterilgard Hood	Thermo Scientific
Thermomixer	Eppendorf
Vortex Mixer	NEOLAB (Heidelberg, Germany)
Water bath	LAUDA (Lauda-Koenigshofen, Germany)
Tissue embedding machine	Leica (Wetzlar, Germany)
Tissue processor	Leica
Glucosemeter (Precision Xceed)	Abbott GmbH (Wiesbaden, Germany)

### 3.1.10. Consumables

Cell scraper	SARSTEDT (Nuembrecht, Germany)
Coverslips	MENZEL (Braunschweig, Germany)
Filter (0.2 µm)	NEOLAB (Heidelberg, Germany)
Hyperfilm	GE Healthcare
Pure Nitrocellulose membrane	BIO-RAD

(0.45 $\mu$ M)	
Sterile needles	BD (Franklin Lakes, NJ, USA)
Tissue culture dishes (60x15 mm; 100x20 mm)	GREINER (Frickenhausen, Germany)
Tissue culture flasks (25 cm <sup>2</sup> ; 75 cm <sup>2</sup> ; 125 cm <sup>2</sup> )	GREINER
Tissue culture plates (6-well; 24-well; 96-well)	GREINER
Tubes (15 ml; 50 ml)	GREINER
Blotting paper	Whatman (Maidstone, Kent, UK)

## 3.2. Methods

### 3.2.1. Immunohistochemistry analysis

Immunohistochemistry was performed using the Dako Envision System (Dako Cytomation GmbH, Hamburg, Germany). Consecutive paraffin-embedded tissue sections (3–5 mm thick) were deparaffinized and rehydrated using routine methods. Antigen retrieval was performed by pretreatment of the slides in citrate buffer (pH 6.0; 10mM Citric Acid, 0.05% Tween 20) in a microwave oven for 10 minutes. Endogenous peroxidase activity was quenched by incubation in deionized water containing 3% hydrogen peroxide at room temperature for 10 minutes. After blocking of nonspecific reactivity with TBS (pH 7.4; 0.1M Tris Base, 1.4M NaCl) containing 3% BSA or goat serum, sections were incubated with the respective antibody at 4°C overnight followed by incubation with horseradish peroxidase-linked goat anti-rabbit or mouse antibodies, followed by a color-reaction with diaminobenzidine and counterstaining with Mayer's hematoxylin.

### 3.2.2. Cell culture

Human or mouse cell lines were cultured in 10 cm dishes either in DMEM or RPMI-1640 cell culture medium supplemented with 10% fetal bovine serum (FBS), 100 u/ml penicillin and 100  $\mu$ g/ml streptomycin at 37°, 5% CO<sub>2</sub>.

### 3.2.3. MRNA and cDNA preparation

All reagents for RNA extraction and cDNA transcription kit were from Qiagen (Hilden, Germany) and were used according to the manufacturer's instructions.

### 3.2.4. Quantitative Real-Time Chain Reaction

Quantitative real time PCR (QRT-PCR) was carried out using the LightCycler™480 system with the SYBR Green 1 Master kit (Roche diagnostics). Expression of the target gene was normalized to human housekeeping genes ACTB ( $\beta$ -actin) and HPRT1 (Hypoxanthine phosphoribosyltransferase 1) or the mouse housekeeping gene B2m ( $\beta$ -2 microglobulin) using the LightCycler™480 software release 1.5, version 1.05.0.39 (Roche diagnostics).

### 3.2.5. Immunoblot analysis

#### *Protein extraction from cells*

Cells were washed twice with ice-cold PBS (pH 7.4; 0.01M PBS). After addition of ice-cold modified RIPA buffer/or cell lysis buffer containing 20 mM Tris-HCl (pH 7.5), 150 mM NaCl, 1 mM Na<sub>2</sub>EDTA, 1 mM EGTA, 1% NP-40, 1% sodium deoxycholate, 2.5 mM sodium pyrophosphate, 1 mM  $\beta$ -glycerolphosphate, 1mM NaVO<sub>4</sub>, 1  $\mu$ g/ml leupeptin and 1 mM PMSF, cells were immediately homogenized by passing them through a G27 syringe needle 10 times. The crude homogenate was then centrifuged at 14,000 g in a pre-cooled centrifuge for 15 minutes. The supernatant was immediately transferred to fresh tubes and was aliquoted. The concentration of the extracted protein was determined using the BCA Protein Assay kit (Pierce, Thermo Scientific, USA) following the manufacturer's instructions. The sample aliquots were stored at -20°C or were used for Western blotting analysis immediately.

#### *Western blotting*

20 to 80  $\mu$ g of the total protein were loaded on 4~12% polyacrylamide gels and were transferred to PVDF membranes. Membranes were blocked in 20 ml Tween-20 (0.05%)-TBS, 3% or 5% skim milk and 0.05% Tween-20 for 1 hour and were incubated with the respective primary antibody overnight at 4°C. Membranes were washed 3 times with 0.05% Tween-20-TBS and were incubated with a horseradish peroxidase (HRP)-conjugated secondary antibody (1:3000) for 1h at room temperature. Signals were detected using the enhanced chemiluminescence system (ECL, Amersham Life Science Ltd., Bucks, UK). Films were scanned with a CanoScan 9900F scanner (Canon, Tokyo, Japan).

### 3.2.6. Cell transfection

#### *Expression vector transfection*

Pancreatic cancer cell lines or HEK293 cells were transfected with different expression vectors in 6-well plates using the Lipofectamine® 2000 transfection reagent (Invitrogen, Carlsbad, CA, USA) according to the manufacturer's instructions. For generation of stable clones, Su86.86 cells were transfected with 20  $\mu$ g of each MIA2 expressing vector or empty vector (as a control) in 10 cm dishes. Selection medium containing G418 (0.5 mg/ml) was applied 24 hours after transfection. After culturing with selection medium for 7 days, cells were reseeded

into 96-well plates at a limited dilution (50, 10, 5, 1 and 0.5 cells per well). 3 days after plating, wells containing a single clone were marked and its clones were further expanded and screened for MIA2 expression by QRT-PCR and by immunoblot analysis. The clones expressing four MIA2 variants at a similar level were sequenced to confirm the genotype of exogenous MIA2 before functional characterization.

#### *siRNA transfection*

Synthetic siRNA oligonucleotides for MIA2, ERN1 and negative control siRNA were prepared and stored according to the manufacturer's instructions. SiRNA transfections were carried out according to the manufacturer's instructions using the HiPerFect Transfection Reagent (QIAGEN, Hilden, Germany). The final concentration of both the control and specific oligonucleotides was 40 nM. The efficacy of the siRNA transfection was ascertained by immunoblot analysis after 72 hours of transfection.

### **3.2.7. ELISA**

Human pancreatic cancer cell lines were cultured with 1 ml of medium in 6-well plates for 96 hours and supernatants were collected for further use. MIA2 concentration was measured using a commercially available kit (Human MIA2 ELISA Development Kit, 900-K357, PEPROTECH, Hamburg, Germany) according to the manufacturer's instructions. For the measurement of Vegfa secretion of mouse cells, cells were cultured with 1 ml of serum-free medium in 6-well plates for 24 hours under normoxic or hypoxic conditions. The Vegfa concentration was determined using a commercially available kit ("Mouse VEGF Quantikine ELISA Kit", MMV00, R&D Systems, WIESBADEN, Germany).

### **3.2.8. High-resolution melting curve analysis**

Reagents and material for the high-resolution melting curve analysis (HRM) were obtained from Roche Applied Science (LightCycler® 480 High Resolution Melting Master, Roche diagnostics). Data were analyzed using the LightCycler™480 software release 1.5, version 1.05.0.39 (Roche diagnostics).

### **3.2.9. Chemotherapy assay**

Determination of the growth inhibition rates of each dose of the used drugs (depicted as growth fold of control) was carried out as described at <http://www.dtp.nci.nih.gov/branches/btb/ivclsp.html>. Briefly, after incubation of the respective cells with different concentrations of gemcitabine, the cell growth was assessed by the 3-(4,5-dimethylthiazole-2-yl)2,5-diphenyltetrazolium bromide (MTT; 5 mg/ml in PBS; Sigma Aldrich, St. Louis, MO, USA) colorimetric growth assay. Growth inhibition was calculated as:  $(Ti - Tz) / (C - Tz)$  [time zero, (Tz), growth of control, (C), and cell growth in the presence of the drug at the different concentration levels (Ti)]. The introduction of Tz in the formula served to reduce the experimental variations resulting from different initial numbers of seeded cells,



thus facilitating interpretation of the data. Growth inhibition of 50% (GI50) was calculated from  $[(Ti-Tz)/(C-Tz)] \times 100 = 50$ . Specifically, gemcitabine was added 24h after seeding of the cells at increasing concentrations. 0.01% PBS was used as a control. After 48 hours, an MTT test was performed to assess cell viability. All experiments were repeated three times.

### **3.2.10. Site-directed mutagenesis**

The site-directed mutagenesis was performed using the “QuikChange Lightning Multi Site-Directed Mutagenesis Kit” purchased from Stratagene (Stratagene, Agilent Technologies, CA, USA) according to the manufacturer’s instructions. Briefly, the pCMV6-Entry vector containing the full-length human MIA2 was used as the backbone to generate the respective MIA2 variant-expressing vector. Newly generated vectors were confirmed by sequencing before transfection.

### **3.2.11. Immunofluorescence**

Paraffin-embedded tissue sections (3  $\mu$ m thick) were deparaffinized and rehydrated using routine methods, were permeabilized with 0.1% Triton X-100, and were incubated with primary antibodies overnight at 4°C. After washing, secondary antibodies and 4,6-diamidino-2-phenylindole (DAPI) were used accordingly.

### **3.2.12. Real-Time PCR array**

Reagents and material for the Real-Time PCR array were obtained from SABiosciences (SABiosciences Corporation, Frederick, USA). The assay was performed according to the manufacturer’s instruction. Human Unfolded Protein Response (PAHS-089F) and Human Extracellular Matrix and Adhesion Molecules (PAHS-013F) arrays were used. In total, 23 RNA samples of PDAC tissues were analyzed (one array per cancer tissue). Data were analyzed using the web-based software from SABiosciences: ([www.sabiosciences.com/pcr/arrayanalysis.php](http://www.sabiosciences.com/pcr/arrayanalysis.php)). Group-wise comparisons were performed using the Student’s t-test.

### **3.2.13. Mouse breeding**

Mouse breeding was performed and husbandry was maintained at the specific pathogen free (SPF) mouse facility at the Technical University of Munich. The compound transgenic mice were maintained on a mixed background. All mouse experiments and procedures were approved by the Institutional Animal Care and Use Committees of the Technical University of Munich. All procedures were in accordance with the Office of Laboratory Animal Welfare and the German Federal Animal Protection Laws.

### **3.2.14. Oral glucose tolerance test (OGTT) in mice**

OGTT was performed as previously described (Ayala et al., 2010). Mice were deprived of food overnight (10 hours) before the test. By amputating the tail tip,

peripheral blood was collected 15, 30, 60, 120 and 180 minutes after the oral administration of glucose (2.5 g/kg body weight) and subjected to glucose measurement using a glucometer (Abbott GmbH, Wiesbaden, Germany).

### **3.2.15. Primary cell isolation**

Freshly dissected sterile tumor tissues were washed twice with ice-cold PBS, were cut into small pieces (approximately 1 mm) and dispensed into 5 ml of complete medium containing collagenase (1.2 mg/ml). The resulting solution (mixed with tissue blocks) was incubated at 37°C for 0.5 hours. After centrifugation at 300 rpm for 5 minutes, small tissue blocks were washed twice with collagenase-free medium, followed by incubation at 37°C with medium containing collagenase for additional 0.5 hours. After passing the undigested tissue blocks through a 100 µm nylon mesh, cell suspensions were obtained. These cell suspensions were washed two times with complete medium and were seeded into a 10 cm<sup>2</sup> dish.

### **3.2.16. Invasion assay**

To assess cell invasion in vitro, 24-well Matrigel invasion chambers with 8-mm pore sizes (BD Biosciences, San Jose, CA) were used and were reconstituted with 600 µl serum-free DMEM medium in both the top and the bottom chambers for 2–4 hours. Cells were trypsinized and seeded into the top chamber at a density of 10<sup>4</sup> cells per well in 500 µl DMEM containing 0.5% fetal calf serum. The lower/bottom chambers contained 0.7 ml of medium (0.5% FBS). According to each experimental set-up, an invasion chamber was placed in normoxic or hypoxic conditions. After incubation at 37°C for 24h, the remaining cells attached to the upper surface of the membrane were carefully removed with cotton swabs, while cells that reached the underside of the chamber were stained with H&E and were counted. All experiments were repeated three times.

### **3.2.17. Hypoxia assay**

Pancreatic cancer cell lines or epithelial cells were incubated in a modular chamber saturated with a hypoxic air mixture (89.25% N<sub>2</sub> + 10% CO<sub>2</sub> + 0.75% O<sub>2</sub>) for 24h or 72h at 37°C. For measurements of Vegfa, serum-free medium was used. The remaining experiments were performed in medium supplemented with 10% FCS. All experiments were repeated three times.

### **3.2.18. Active Ras pull-down assay**

Cells were cultured in serum-free medium for 24 hours followed by treatment with 20% FBS or serum-free medium for 5 minutes. After treatment, active Kras was detected using the Active Ras Pull-Down and Detection Kit (THERMO SCIENTIFIC, Waltham, USA) according to the manufacturer's instruction. 500 µg of total protein were used for the pull-down reaction.

### **3.2.19. Cell transplantation experiment**

For mouse cell transplantation experiments into BALB/c Nude Mouse,  $10^6$  cells were resuspended in 50  $\mu$ l of PBS and were injected into the left lower and right upper flank. Tumor growth was monitored macroscopically every week. Orthotopic implantations of mouse cells were carried out using a published protocol (Pylyayeva-Gupta et al., 2012). Briefly, mice were anesthetized, and a left-lateral incision of the abdomen was made to visualize the tail region of the pancreas.  $10^6$  cells suspended in 50  $\mu$ l of PBS were carefully injected into the pancreatic tail. The abdominal wall and skin were closed using running sutures. All mice were sacrificed for histological evaluation after 4 weeks.

### **3.2.20. Microarray experiment and data analysis**

A whole transcriptome analysis of mouse cell lines (three groups, 11 cell lines) was performed using the Affymetrix GeneChip<sup>®</sup> Mouse Gene 1.0 ST Array according to the manufacturer's instructions in collaboration with the group of PD Dr. Johannes Beckers (Dr. Martin Irmler, Institute of Experimental Genetics, HelmholtzCenter Munich). The experiments were performed in duplicate. The array data were analyzed by Philipp Bruns, M.Sc.. Normalization was performed using the Robust Multichip Average (rma) method provided in the Bioconductor package of R (R Foundation for Statistical Computing, Vienna, Austria). Genes that were expressed at very low levels throughout all samples or those that showed small variation were filtered out using the filtering method nsFilter. In order to identify differentially expressed genes, a linear model was constructed and a one-way ANOVA for pairwise comparison of the three groups was performed. Genes were ranked by p-value (F-test). A principal component analysis (PCA) was performed based on the ten genes with the smallest p-values. In order to identify the gene signature that was specifically upregulated in each group of cell lines, a t-test was used. Here, gene expression levels in one group of cell lines were compared to the levels of the other two groups. Genes were ranked according to the fold of change and the top 20 up-regulated genes were selected for the following clustering analysis. The false discovery rates (FDRs) of selected genes were smaller than 0.001. A heatmap with columnwise clustering was applied to visualize the expression levels of the 60 selected genes. Genes with an FDR less than 0.001 were chosen for further pathway characterization.

### **3.2.21. Statistical analysis**

For statistical analyses, either the GraphPad Prism 5 Software (GraphPad, San Diego, CA, USA) or IBM SPSS 19 Software (Statistical Package for the Social Sciences, IBM, NY, USA) was used. The Chi-square test or Fisher's exact test was used to compare distribution of categorical factors of different groups. All experiments were repeated at least three times. Unless otherwise stated, an unpaired Student's t-test was used for group-wise comparisons of two groups.

The one-way Analysis of Variance (ANOVA) was used for multiple group-wise comparisons (more than 2 groups) and was followed by a post-hoc test (Tukey's test). The level of statistical significance was set at  $p < 0.05$ . Results are expressed as mean  $\pm$  standard deviation (SD) unless indicated otherwise.

## 4. RESULTS

### 4.1. HNF1A controls MIA2 expression in PDAC

Immunohistochemistry (IHC) studies revealed that both HNF1A and MIA2 positivity was mainly detected in the islet cells of the normal pancreas, suggesting that the HNF1A/MIA2 axis belongs to pathways that operate in the endocrine pancreas (**Fig. 2a**). In line with these findings, some pancreatic neuroendocrine tumor (PNET) samples were positive for HNF1A (42%, 18/42) and MIA2 (45%, 19/42) (**Fig. 2b**). These findings implied that the HNF1A/MIA2 axis is active in pancreatic (neuroendocrine) malignancies. Encouraged by these preliminary findings in PNETs and by the reported increased pancreatic cancer risk conferred through changes in the human HNF1A locus, the role of the HNF1A/MIA2 axis was determined in human PDAC. The IHC studies revealed that a significant number of human PDAC tissues were positive for HNF1A (73%, 29/40) and MIA2 (52%, 32/61, **Fig. 2c**). Furthermore, QRT-PCR and Western-blot analyses showed that MIA2 mRNA and protein were detected in three (Aspc-1, Capan-1 and Colo-357) out of eight tested cell lines (Aspc-1, Bxpc-3, Capan-1, Colo-357, Mia-PaCa-2, Panc-1, T3M4 and Su86.86; **Fig. 2d**). Importantly, expression of MIA2 correlated with HNF1A expression in these cells lines; only the three MIA2-positive cells expressed HNF1A at a high level (**Fig. 2e**, upper panel). Accordingly, transient expression of HNF1A (**Fig. 2e**, middle panel) in MIA2-negative cell lines (Panc-1 and Su86.86) induced MIA2 mRNA expression (**Fig. 2e**, lower panel).

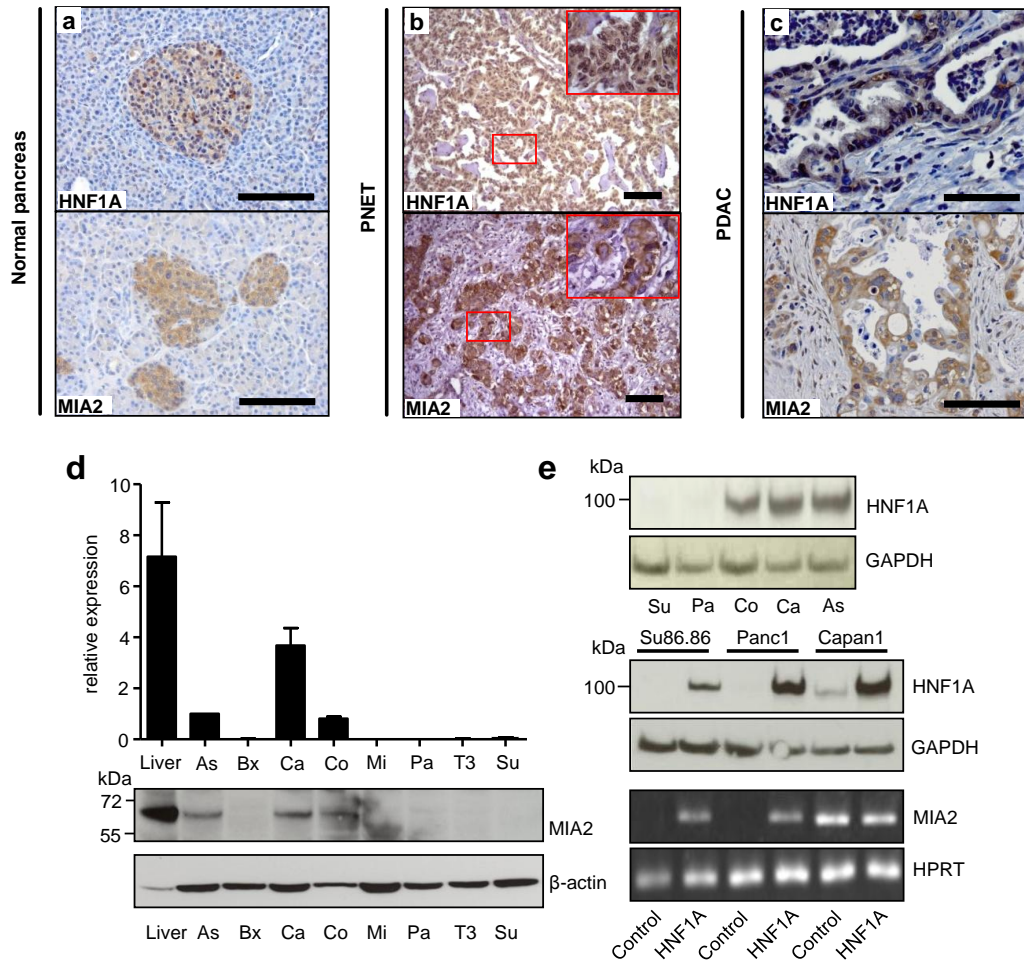


**Figure 2.** (a) Normal pancreatic islet cells are immunopositive for HNF1A and MIA2 (scale bar, 100 μm). (b) Accordingly, 42% and 45% of PNET samples are immunopositive for HNF1A and MIA2 (scale bar, 100 μm). (c) 73% and 52% of PDAC samples are positive for HNF1A and MIA2 staining, respectively (scale bar, 100 μm). (d) MRNA and protein expression analysis of MIA2 in pancreatic cancer cell lines by QRT-PCR and Western-blot. Out of 8 tested cell lines (Aspc-1 (As), Bxpc-3 (Bx), Capan-1 (Ca), Colo357 (Co), Mia-PaCa2 (Mi), Panc-1 (Pa), T3M4 (T3), Su86.86 (Su)), Aspc-1, Capan-1 and Colo-357 express MIA2; endogenous MIA2 is mainly detected at a size of 61 kDa, cell lysates from human liver are used as a positive control; loading control: β-actin. (e) Three MIA2-expressing cell lines (Aspc-1 (As), Capan-1 (Ca) and Colo357 (Co)) also express high levels of HNF1A (upper panel); Western-blot analysis demonstrates transient expression of HNF1A in Su86.86, Panc-1 and Capan-1 cells (middle panel), loading control: GAPDH; One representative immunoblot out of three independent experiments is shown. Semi-quantitative PCR shows that MIA2 mRNA expression is induced by transient expression of HNF1A in Su86.86 and Panc-1 cells, whereas no such effect is observed in Capan-1 cells (lower panel). HPRT1 is used as a housekeeping gene. One of three independent experiments is shown.

However, transient expression of HNF1B had no effect on MIA2 mRNA levels (**Fig. 3**), underscoring a specific role of HNF1A in controlling MIA2 expression in PDAC cancer cell lines.

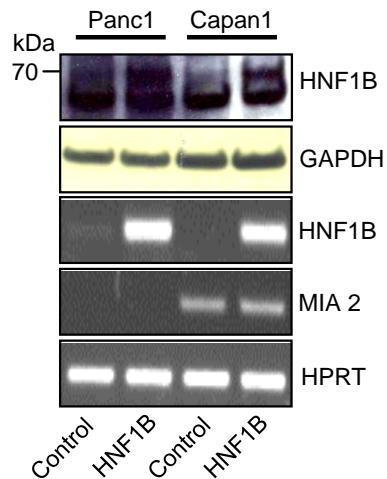


**Figure 3.** Semi-quantitative PCR and Western-blot shows a transient expression of HNF1B in Panc1 and Capan1 cells. A transient expression of HNF1B has no effect on the expression of MIA2 RNA levels, loading control: GAPDH; HPRT1 is used as a housekeeping gene. One of three independent experiments is shown.

Though how and why PDACs acquire “expression features” of endocrine pancreas cells or PNETs is unclear, 29% of PDAC (18/63) samples were also positive for the classical PNET marker Chromogranin A (**Fig. 4**) (Tezel et al., 2000; Ting et al., 2011), suggesting that acquisition of such an expression pattern may have a functional relevance in PDAC.

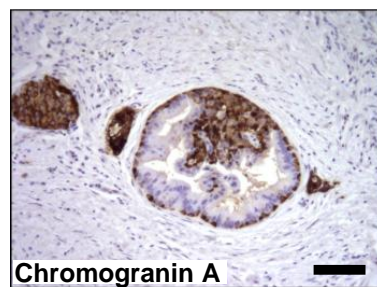


**Figure 4.** 29% of PDAC tissues are immunopositive for Chromogranin A (scale bar, 100  $\mu$ m).

## 4.2. The MIA2<sup>I141M</sup> variant is linked with a secretory defect and is correlated with patient survival

Because MIA2 is a secreted protein and is itself involved in protein secretion, an enzyme-linked immunosorbent assay (ELISA) was used to measure MIA2 concentration in the supernatants of Aspc-1, Capan-1 and Colo-357 PDAC cell lines. MIA2 was detected in the supernatants of Aspc-1 and Capan-1 cells but not in the supernatants of Colo-357 cells (**Fig. 5a**). These data suggested a secretory defect of MIA2 in Colo-357 cells. In order to address the reasons for this hypothesized secretory defect, the MIA2 gene was sequenced in the cell lines. Here, Colo-357 cells carried two common homozygous variants: p.I141M and p.D547H (coding DNA sequence: c.A617G; rs11845046; c.G1833C; rs10134365, **Fig. 5b**).

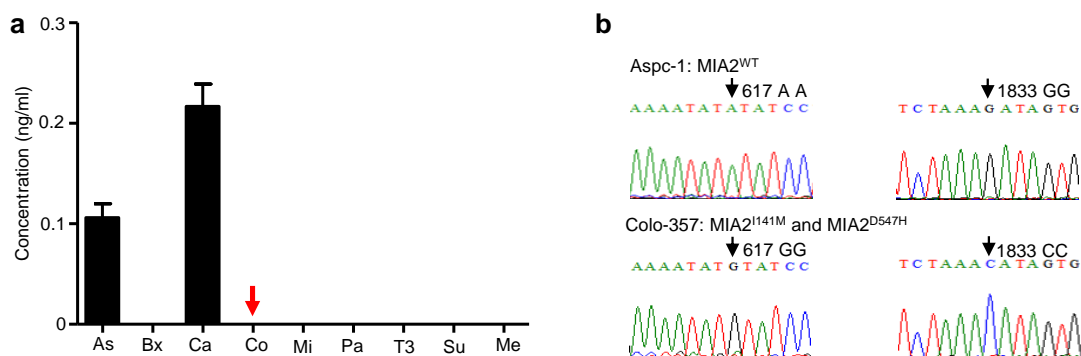


**Figure 5. (a)** MIA2 levels in the supernatants of a panel of pancreatic cancer cell lines (Aspc-1 (As), Bxpc-3(Bx), Capan-1 (Ca), Colo357 (Co), Mia-PaCa2 (Mi), Panc-1 (Pa), T3M4 (T3), Su86.86 (Su)) were determined by ELISA. Aspc-1 and Capan-1 cells showed detectable levels of MIA2 in their supernatants whereas MIA2 in the supernatant of Colo-357 cells was below the detection limit. **(b)** Sequencing analysis revealed that Colo-357 cells carried the MIA2-617A/G (rs11845046) and 1833G/C (rs10134365) variants which induced replacement of 141Ile and 547Asp to 141Met and 547His on its protein sequence.

In an attempt to interrogate the clinical relevance of these two “secretion-associated” polymorphisms, MIA2 genotypes were determined by a high-resolution melting curve analysis (HRM) in tissue samples of 628 subjects consisting of organ donors (26), chronic pancreatitis patients (CP, 18), PNET patients (38), resected PDAC patients (277), colorectal cancer patients (230) and esophageal cancer patients (39), as shown in **Table 2**.



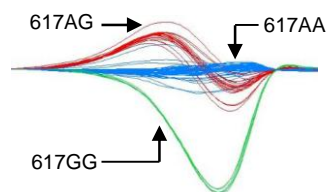
**Table 2.** MIA2<sup>I141M</sup> frequency in organ donors and different disease entities

Samples	rs11845046 (MIA2 <sup>I141M</sup> )			Minor allele frequency (MAF)	In total
	617 AA	617 AG	617 GG		
Donor pancreas	13	13	0	0.50	26
CP	13	5	0	0.28	18
PNET	22	12	4	0.42	38
PDAC	180	80	17	0.35	277
Colorectal cancer	147	71	12	0.36	230
Esophageal adenocarcinoma	26	10	3	0.33	39
In total	401	191	36	0.36	628

CP: chronic pancreatitis, PNET: pancreatic neuroendocrine tumor, PDAC: pancreatic ductal adenocarcinoma.

HRM analysis demonstrated highly distinguishable curve patterns for the SNPs/variants in genomic DNAs from cancer cell lines and patient samples (**Fig. 6a, 6b**).

**a**



**b**

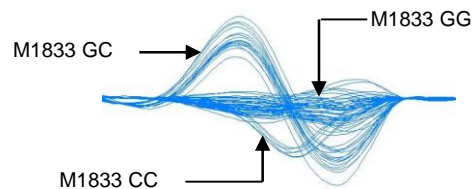


**Figure 6.** (a) HRM analysis of the MIA2<sup>I141M</sup> variant using patient's genomic DNA demonstrated highly different curve patterns for the different MIA2 genotypes; (b) HRM analysis of the MIA2<sup>D547H</sup> variant showed highly different curve patterns for the different MIA2 genotypes.

Randomly chosen samples were sequenced to confirm the results of the HRM analysis (**Fig. 7**).

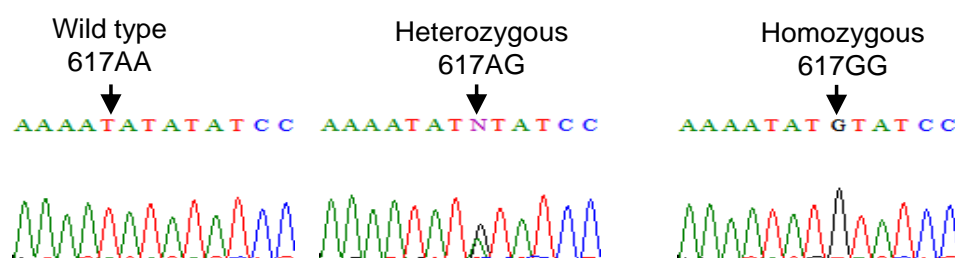


**Figure 7.** Sequencing confirmed MIA2-617A/G hetero- and homozygosity.

The occurrence of the MIA2<sup>I141M</sup> variant strictly correlated with that of the MIA2<sup>D547H</sup> variant in the first tested 262 samples, demonstrating that these are located within the same linkage disequilibrium (LD) block of the human genome. Therefore, for the other samples, only the MIA2<sup>I141M</sup> variant was genotyped. As shown in Table 2, the overall frequency of the MIA2<sup>I141M</sup> (MIA2-617G) variant was 0.36 (ranging from 0.28 to 0.50; 628 samples) and its frequency in PDAC samples was 0.35. For 99 out of 277 PDAC samples, detailed clinical and pathological data were available (**Table 3**).

**Table 3.** Clinical characteristics and comparison between two PDAC cohorts

Variables	PDAC		p-value	total number of patient samples
	MIA2 617 AA	MIA2 617 A/G		
Age (years, median)	66	66	0.92 <sup>1</sup>	-
Gender				
Male	32	19		51
Female	27	21	0.43 <sup>2</sup>	48
Size of tumor (T)				
T1-T2	4	5		9
T3-T4	55	35	0.33 <sup>2</sup>	90
Lymphnode (N)				
N0	17	16		33
N1	42	24	0.25 <sup>2</sup>	66
Metastasis (M)				
M0	53	36		89
M1	6	4	0.98 <sup>2</sup>	10
Grade (G)				
G1				
G2	4	3		7
G3	27	16	0.85 <sup>2</sup>	43

	28	21		49
R status				
R0	31	19		50
R1/R2	20	15		35
unknown	8	6	0.87 <sup>2</sup>	14
Chemotherapy				
Yes	46	34	0.38 <sup>2</sup>	80
No	13	6		19

1: Mann-U-Whitney-Test; 2: Chi<sup>2</sup>-test

Although the distribution of the MIA2<sup>I141M</sup> variant did not correlate with clinical parameters such as T and G (Table 3), Kaplan-Meier analysis revealed that PDAC patients with the MIA2<sup>I141M</sup> variant tended to live longer after surgical resection than patients with WT MIA2 (median survival: 27 vs. 17 months,  $p=0.06$ , **Fig. 8a**). Notably, further analysis demonstrated that the survival benefit of the MIA2<sup>I141M</sup> variant was predominantly derived from patients who received chemotherapy (median survival: 28 vs 18 months,  $p=0.02$ , **Fig. 8b**) because in the non-chemotherapy group, patients with the MIA2<sup>I141M</sup> variant survived relatively shorter after surgical resection (median survival: 10 vs. 17 months,  $p=0.06$ , **Fig. 8c**). This suggests that the MIA2<sup>I141M</sup> variant carriers are more likely to benefit from chemotherapy. However, the MIA2<sup>I141M</sup> variant was not associated with survival in colorectal cancer patients ( $p=0.99$ , **Fig. 8d**).

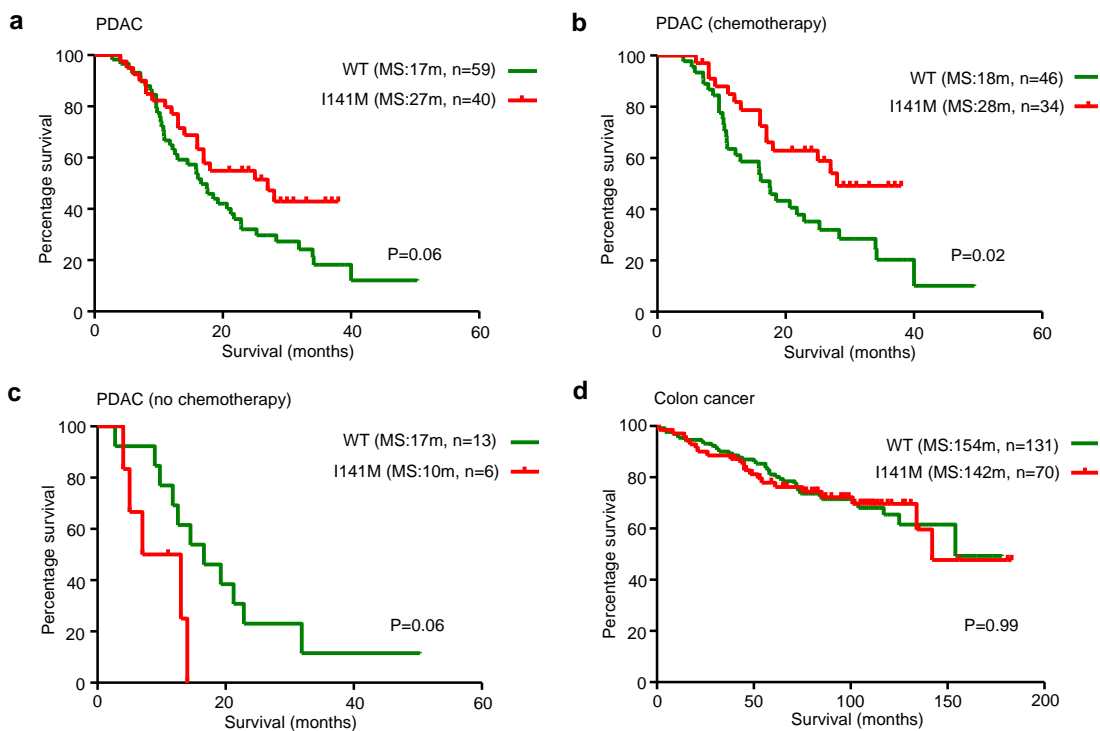


**Figure 8.** (a) PDAC patients carrying the MIA2<sup>I141M</sup> variant tended to live longer than those with wild-type MIA2 (WT; median survival: 27 vs. 17 months, log-rank test:  $p=0.06$ ). (b) The MIA2<sup>I141M</sup> variant carriers who received chemotherapy had a significantly longer postoperative survival (median survival: 28 vs. 18 months, logrank test,  $p=0.02$ ). (c) For patients who did not receive chemotherapy, the MIA2<sup>I141M</sup> variant carriers had a relatively shorter postoperative survival (median survival: 10 vs. 17 months, logrank test:  $p=0.06$ ). (d) The MIA2<sup>I141M</sup> variant did not correlate with patient's survival in colon cancer (UICC stage II, median survival: 154 vs. 142 months, logrank test:  $p=0.99$ ).

### 4.3. The MIA2<sup>I141M</sup> variant increases sensitivity of pancreatic cancer cells to gemcitabine

Because these data in PDAC strongly suggested that the secretion-associated MIA2 polymorphisms were associated with the clinical response to (adjuvant) chemotherapy, it is unknown whether this was reflected in pancreatic cancer cell lines in vitro. Indeed, a chemotherapy assay revealed that Colo-357 cells were extremely sensitive to gemcitabine treatment at a low dose of the drug (10nM), which in contrast only had a marginal effect on the growth of Aspc-1 and Capan-1 cells (**Fig. 9**).

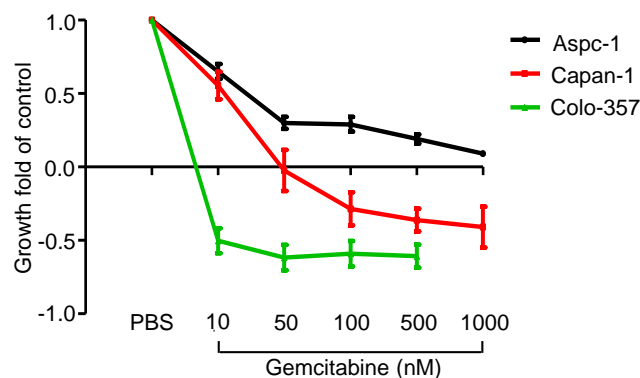


**Figure 9.** A chemotherapy assay revealed that Colo-357 cells were highly sensitive towards gemcitabine. Data from three independent experiments are expressed as mean $\pm$ SD.

Because these three cell lines were also disparate in various aspects other than the MIA2 genotype, it is difficult to directly evaluate the biological effect of the MIA2 variants on the chemoresponse. Hence, using a vector containing the

human full-length MIA2 cDNA sequence (termed as WT) as a backbone (**Fig. 10a**), expression vectors containing either one of the two SNPs (termed I141M and D547H) or both SNPs (termed I141M & D547H) were generated by site-directed mutagenesis. Several clones from each genotype were chosen and sequenced to confirm the introduced mutation (**Fig. 10b, 10c**).

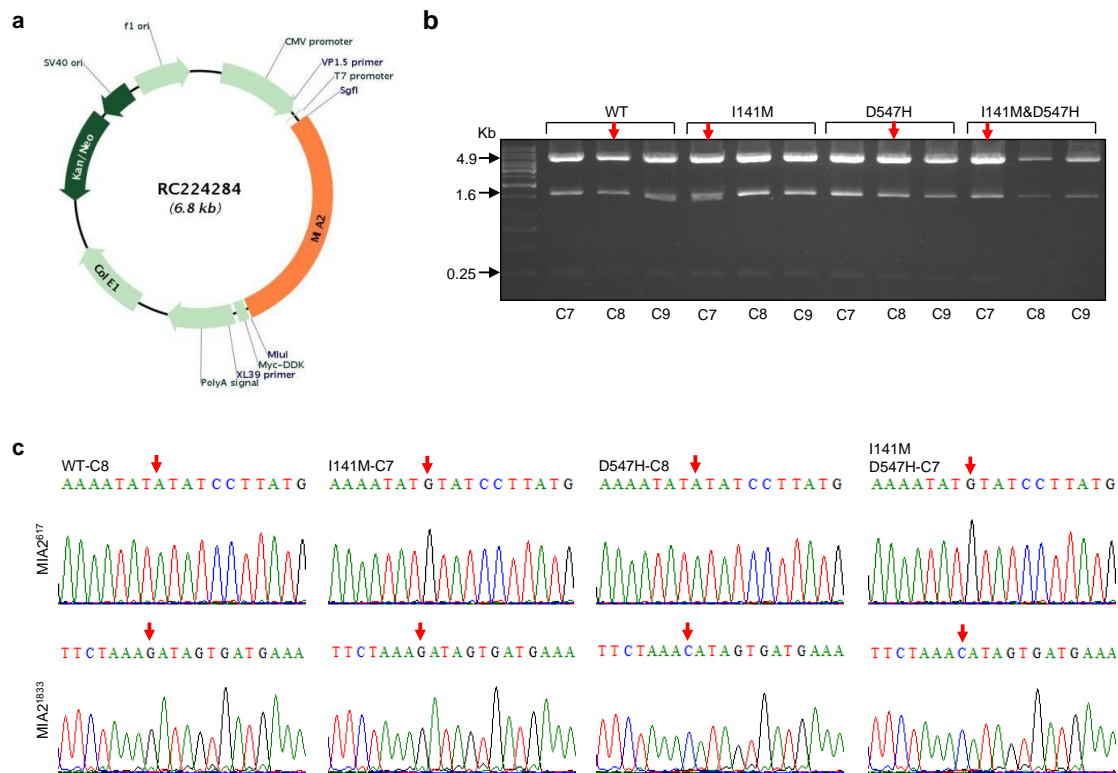


**Figure 10.** (a) Plasmid map of the Myc-tagged open reading frame (ORF) clone of human MIA2 from ORIGENE (<http://www.origene.com>); (b) After site-directed mutagenesis, several clones from each genotype were digested with EcoR1 to confirm the inserted MIA2 fragment. (c) Sequencing confirmed the introduced mutations at the respective positions.

A myc tag was fused to the C-terminus of the exogenous MIA2 protein. Then, HEK293 cells were transiently transfected with the different polymorphism-containing MIA2 vectors. Interestingly, using an antibody recognizing the N-terminal region of MIA2, 5 bands shifting at the size of around 120, 100, 61, 56 and 43 kDa were detected in the HEK293 cell lysates (after transfection) whereas the endogenous MIA2 from human liver lysates was mainly detected at 61 kDa, as previously described (Bossert et al., 2003; Hellerbrand et al., 2008) (**Fig. 11a**). The secreted MIA2 in the supernatants was mainly detected at a size of 43 and 61 kDa (**Fig. 11a**). However, no difference in the secretion of the different MIA2 variants was found; most likely because of

non-physiological expression of MIA2 (driven by the CMV promoter). However, the myc-tag antibody only recognized the 120 kDa band and no signals in the supernatants (**Fig. 11a**). In order to confirm that the detected bands were truly produced due to MIA2-transfection, specific MIA2 siRNAs were co-transfected with the WT-MIA2 vector. These experiments demonstrated that the bands seen at unexpected sizes disappeared following siRNA silencing of MIA2. This data indicates that these different sizes of the MIA2 protein were indeed translated from the MIA2 mRNA (**Fig. 11b**), suggesting that MIA2 undergoes intensive intracellular protein modifications. In this regard, two N-linked glycosylation sites at position 59 (NFT) and 367 (NDS) which are unique features for secretory proteins were found by scanning the protein sequence of MIA2 (Anelli and Sitia, 2008). A deglycosylation assay (using N-Glycosidase F, **Fig. 11c**) demonstrated that treating cell lysates from WT-transfected HEK293 cells with N-Glycosidase F partially lowered the size of the MIA2 proteins. These data provide evidence that MIA2 is a secretory protein that is glycosylated in the ER compartment, which is in accordance with its cellular localization (see below).

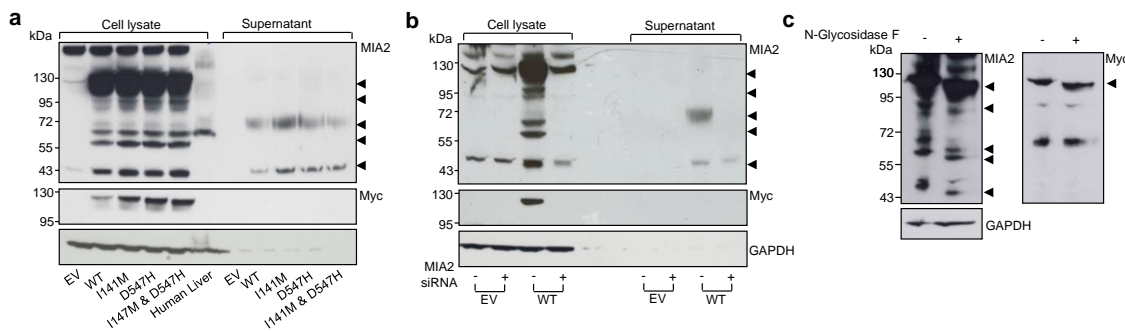


**Figure 11.** (a) Transient expression of WT and MIA2 variants in HEK293 cells gave rise to bands at 120, 100, 61, 56 and 43 kDa (Western-blot analysis of cell lysates) while the secreted forms localized mainly at 43 and 61 kDa when the MIA2 antibody (recognizing the N-terminus of the protein) was used; interestingly, the myc-tag (recognizing the C-terminus) antibody only detected the bands at 120 kDa. (b) These bands at various sizes disappeared upon co-transfection with MIA2-specific siRNA. (c) N-Glycosidase F treatment with cell lysates from WT-transfected HEK293 cells partially reduced the size of the MIA2 proteins. One representative blot out of two independent experiments is shown.

In order to investigate the biological influence of different MIA2 variants on pancreatic cancer biology, Su86.86 cells negative for MIA2 expression were selected to generate pancreatic cancer cell lines expressing WT or different MIA2 variants. To this end, Su86.86 cells were transfected with MIA2 or empty vectors (EV), followed by antibiotics selection (G418). Clones expressing different forms

of MIA2 at a similar level (by Western-blot analysis) or carrying an empty vector were generated and were termed as Su-EV (empty vector), Su-WT, Su-I141M, Su-D547H and Su-I141M & D547H. These were then subjected to further functional characterization (**Fig. 12a**). Additionally, cDNAs from these corresponding clones were sequenced to confirm successful introduction of MIA2 polymorphisms (**Fig. 12b**).

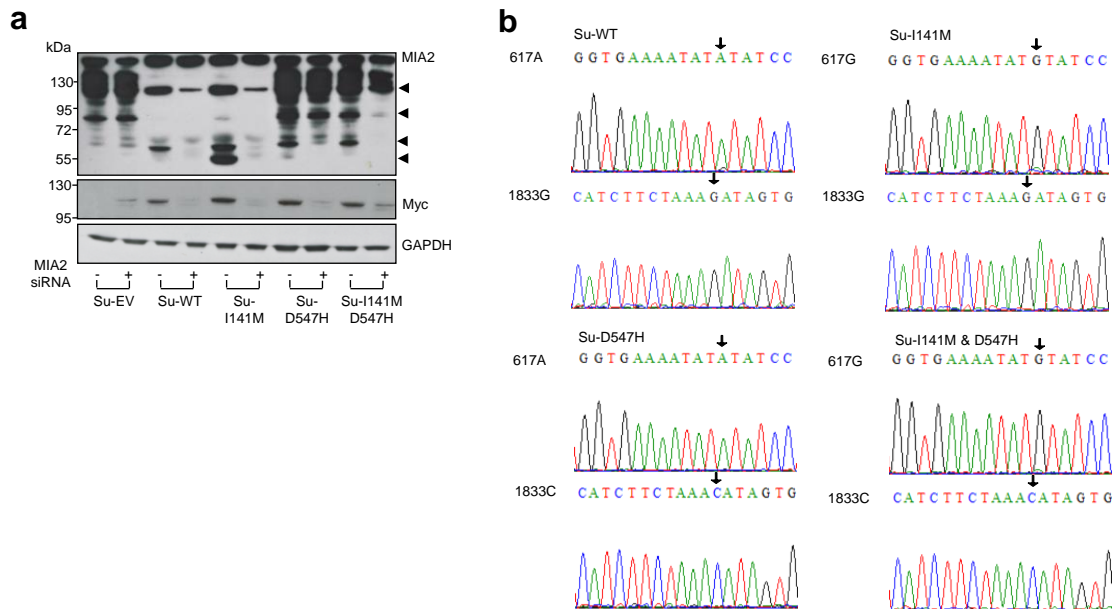


**Figure 12.** (a) Su86.86 cells transfected with different MIA2 expression vectors showed stable and comparable levels of MIA2; empty vector was transfected as a control. Loading control: GAPDH; (b) CDNAs from Su-WT, Su-I141M, Su-D547H and Su-I141M & D547H were sequenced to confirm the introduced SNPs.

Compellingly and in accordance to the results of the chemosensitivity assays, expression of the MIA2<sup>I141M</sup> variant specifically rendered pancreatic cancer cells more susceptible to the effects of gemcitabine (especially at high doses (500 or 1000 nM)) whereas expression of MIA2<sup>WT</sup> or MIA2<sup>D547H</sup> alone had no significant effect (**Fig. 13**). Collectively, these data demonstrate the importance of the MIA2<sup>I141M</sup> variant in mediating chemosensitivity of pancreatic cancer cell lines in vitro.

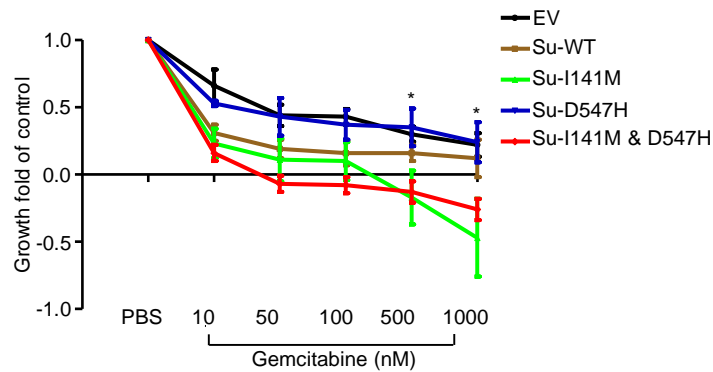


**Figure 13.** A chemotherapy assay demonstrates that introduction of the MIA2<sup>I141M</sup> variant rather than MIA2<sup>WT</sup> or the MIA2<sup>D547H</sup> variant significantly increases sensitivity towards gemcitabine treatment compared to empty vector (EV)-transfected cells in vitro. A t-test was performed; \*: p<0.05. Data from three independent experiments are expressed as mean±SD.

#### 4.4. The MIA2<sup>I141M</sup> variant is associated with increased expression levels of ERN1/XBP1 in PDAC tissues

Because MIA2 is functionally related to protein secretion (Pitman et al., 2011) and because the unfolded protein response (UPR), activated by ER stress, couples the secretory network to cell survival in the adult pancreas (Harding et al., 2001; Hess et al., 2011; Iwawaki et al., 2010; Lee et al., 2005; Zhang et al., 2002), it is likely that the MIA2<sup>I141M</sup> variant influences ER homeostasis and UPR in pancreatic cancer cells. To this end, a real-time PCR array of a large number of genes belonging to the UPR network was performed on PDAC samples from patients with the MIA2<sup>I141M</sup> variant and the MIA2<sup>WT</sup>. Because MIA3 has been shown to be involved in the secretion of extracellular matrix proteins (ECM), ECM and adhesion molecule genes were also analyzed using a PCR array (Gurkan et al., 2006; Saito et al., 2009). In total, 23 samples were analyzed, of which 11 were MIA2 wild type and 12 carried the MIA2<sup>I141M</sup> variant(s) (heterozygous (9), homozygous (3)). As shown in the volcano plot (**Fig. 14a**), many genes involved in UPR were up-regulated in cancer tissues with the MIA2<sup>I141M</sup> variant; 18% (15/84) of these were found to be statistically significantly up-regulated (p<0.05, **Table 4, Fig. 14a**). In the ECM/adhesion molecule arrays, expression of only 4 genes (ITGA2, LAMA1, MMP12 and ICAM1) was significantly different and three of these were down-regulated (**Fig. 14b; Table 4, Table 5**).



**Table 4.** Differentially expressed genes related to UPR in PDAC tissues with the MIA2<sup>I141M</sup> variant or the MIA1<sup>WT</sup>

	Symbol	Description	Fold Change	P value	Function
NM_001675	ATF4	Activating transcription factor 4 (tax-responsive enhancer element B67)	1.3	0.012	Transcription Factor
NM_007348	ATF6	Activating transcription factor 6	1.3	0.018	Transcription Factor
NM_018981	DNAJC10	DnaJ (Hsp40) homolog, subfamily C, member 10	1.4	0.018	Unfolded Protein Binding, Protein Folding, Protein Disulfide Isomerization, Heat Shock Protein
NM_006260	DNAJC3	DnaJ (Hsp40) homolog, subfamily C, member 3	1.2	0.042	Heat Shock Protein Unfolded Protein Binding, Protein Folding,
NM_005528	DNAJC4	DnaJ (Hsp40) homolog, subfamily C, member 4	1.5	0.014	Heat Shock Protein ER Protein Folding, Quality Control,
NM_014674	EDEM1	ER degradation enhancer, mannosidase $\alpha$ -like 1	1.2	0.013	ERAD ER Protein Folding, Quality Control,
NM_025191	EDEM3	ER degradation enhancer, mannosidase $\alpha$ -like 3	1.4	0.046	Ubiquitination
NM_032025	eIF2A	Eukaryotic translation initiation factor 2A, 65kDa	1.3	0.013	Regulation of Translation
NM_001433	ERN1	Endoplasmic reticulum to nucleus signaling 1	1.5	0.044	Transcription Factor, Apoptosis
NM_014685	HERPUD1	Homocysteine-inducible, endoplasmic reticulum stress-inducible, ubiquitin-like domain member 1	1.5	0.019	ERAD, Ubiquitination
NM_005527	HSPA1L	Heat shock 70kDa protein 1-like	1.5	0.004	Heat Shock Protein

NM_003791	MBTPS1	Membrane-bound transcription factor peptidase, site 1	1.3	0.043	Regulation of Cholesterol Metabolism, ERAD, Transcription Factor
NM_021130	PPIA	Peptidylprolyl isomerase A (cyclophilin A)	1.5	0.000	Unfolded Protein Binding, Protein Folding
NM_003262	SEC62	SEC62 homolog (S. cerevisiae)	1.3	0.022	ERAD, Ubiquitination
NM_005080	XBP1	X-box binding protein 1	1.6	0.041	Transcription Factor

ERAD: ER-Associated Degradation

**Table 5.** Differentially expressed genes related to ECM and adhesion in PDAC tissues with the MIA2<sup>I141M</sup> variant or the MIA1<sup>WT</sup>.

	Symbol	Description	Fold Change	P value	Function
NM_002203	ITGA2	Integrin, $\alpha$ 2 (CD49B, $\alpha$ 2 subunit of VLA-2 receptor)	1.9	0.045	Cell-Matrix Adhesion, Transmembrane Molecule
NM_005559	LAMA1	Laminin, $\alpha$ 1	0.4	0.008	Basement Membrane Constituent, Adhesion Molecule
NM_000201	ICAM1	Intercellular adhesion molecule 1	0.7	0.038	Transmembrane Molecule, Cell-Cell Adhesion
NM_002426	MMP12	Matrix metalloproteinase 12 (macrophage elastase)	0.4	0.045	ECM Protease

In particular, genes with a fold change (FC) of more than 50% were plotted (**Fig. 14c**). Among the three UPR arms (ERN1/XBP1, PERK/p-eIF2 $\alpha$  and ATF6/nATF6 $\alpha$ ), the ERN1/XBP1 arm seemed to be particularly affected by the respective MIA2 genotype (**Fig. 14c**), because ERN1 and XBP1 were significantly up-regulated in the MIA2<sup>I141M</sup> variant carriers; in addition, proteins involved in protein folding and unfolding (DNAJC4 and PPIA), in ER-associated degradation (HERPUD1) and in the heat shock response (HSPA1L) were increased (**Fig. 14c**).

Then, changes in ERN1 and unspliced-XBP1 expression were verified by independent QRT-PCR assays with a larger sample size (**Fig. 14d**). Similarly, the densitometry analysis of Western-blot film from 20 randomly selected cancer tissues (10 MIA2<sup>WT</sup> and 10 MIA2<sup>I141M</sup>) revealed that the signal intensity from ERN1 in samples carrying MIA2<sup>I141M</sup> variant were stronger than those carrying MIA2<sup>WT</sup> though such difference does not reach statistical significance (p=0.19). However, there was no such tendency for BiP within the same Western-blot film (**Fig. 14e**).

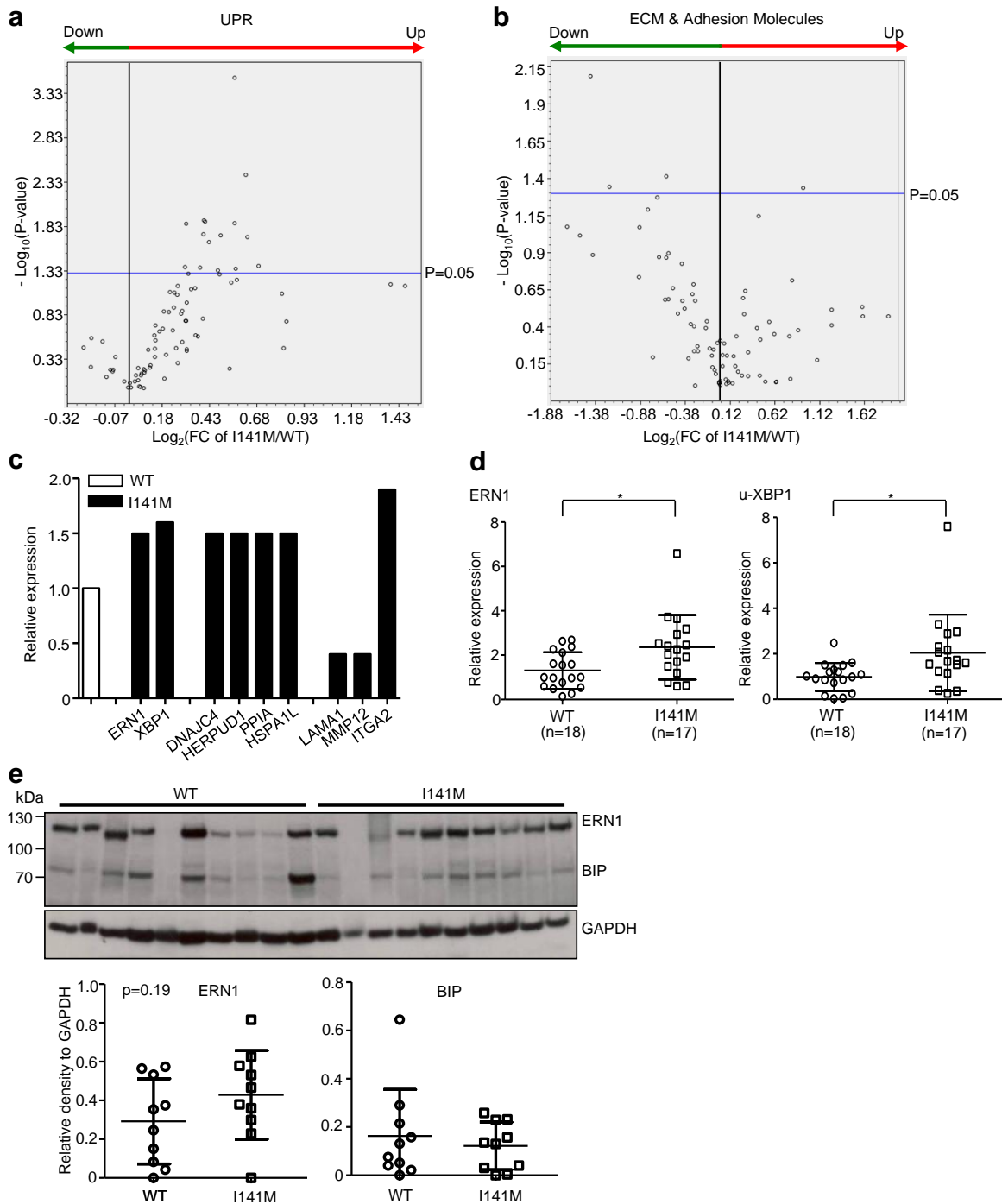


**Figure 14.** (a) A real-time PCR-based array was performed on 23 PDAC tissues (11 MIA2<sup>WT</sup> and 12 MIA2<sup>I141M</sup> variants). Compared to MIA2<sup>WT</sup> samples, 18%

(15/84) of the UPR genes were up-regulated in the MIA2<sup>I141M</sup> variant carrying PDAC tissues; **(b)** However, only four ECM and adhesion molecules (ITGA2, LAMA1, MMP12 and ICAM1) were differentially expressed; **(c)** In particular, among the three UPR arms, ERN1/XBP1 and a number of downstream molecules of the UPR (DNAJC4, HERPUD1, PPIA and HSPA1L) were increased by more than 50% in the MIA2<sup>I141M</sup> samples whereas 2 of the 3 ECM and adhesion molecules were decreased (LAMA1 and MMP12) and one (ITGA2) was up-regulated; **(d)** Up-regulation of ERN1 and the un-spliced XBP1 isoform (u-XBP1) was confirmed by QRT-PCR. Data are presented as relative expression (normalized to the median expression of ERN1 and u-XBP1 in WT samples); \*: p<0.05; unpaired t-test; **(e)** Western-blot analysis using randomly selected 20 cancer tissue lysates (MIA2<sup>WT</sup>: n=10; MIA2<sup>I141M</sup> variant: n=10) shows the expressions of ERN1 and BiP (upper panel); densitometry analysis revealed a tendency that ERN1 expression was higher in MIA2<sup>I141M</sup> samples than in MIA2<sup>WT</sup> samples; p=0.19; unpaired t-test; but, no such tendency was observed for BiP expression.

Furthermore, there was no difference in the expression of the spliced form of XBP1 (**Fig. 15**), suggesting that increased expression of ERN1 and XBP1 does not seem to cause an elevated activity of the XBP1 arm in vivo.

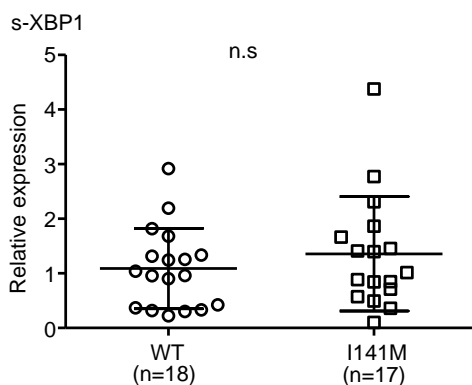


**Figure 15.** There was no difference in the expression of s-XBP1 by QRT-PCR. Data are presented as relative expression (normalized to the median expression of s-XBP1 in WT samples); n.s: not significant; an unpaired t-test was performed.

Since the biological significance of ER stress and the UPR in PDAC remain largely unexplored and because the MIA2 variant seems to be particularly involved in these pathways, a comprehensive descriptive analysis of UPR genes was performed in PDAC tissues. PDAC samples were stained for the general ER stress marker BiP, the three proximal UPR sensors (ERN1, PERK and ATF6) and two targets of the UPR (PDI and Calnexin). This analysis revealed that 64% (39/61) of the tested samples were positive for BiP, underscoring the biological relevance of ER stress in a majority of PDAC cancer cells (**Fig. 16a**). Consistently, 41% (25/61), 48% (32/67) and 35% (21/60) of the samples were positive for each proximal UPR sensor: ERN1, PERK and ATF6, respectively (**Fig. 16b**).

Accordingly, a significant proportion of PDAC samples were also positive for the UPR targets PDI (63%, 39/67) and Calnexin (46%, 31/68, **Fig. 16c**). Importantly, using these ER stress and UPR markers, cancer cells (rather than stroma cells) were the major cell types expressing these molecules.

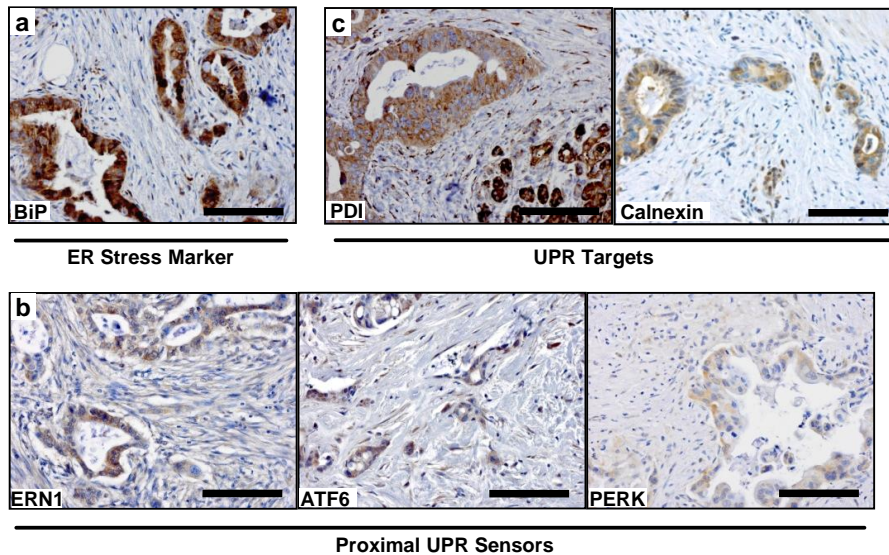


**Figure 16.** (a) 64% (39/61) of the PDAC samples stained positively for the general ER stress marker BiP; (b) 41% (25/61), 35% (21/60) and 48% (32/67) of the samples were positive for the three proximal UPR sensors: ERN1, ATF6 and PERK, respectively; (c) 63% (39/67) and 46% (31/68) of the PDAC samples were positive for the UPR targets PDI and Calnexin, respectively, (scale bar: 100 $\mu$ m).

Collectively, these data suggest a biological significance of ER stress and the associated UPR in pancreatic cancer biology. However, it remained unclear whether increased expression of UPR genes in MIA2<sup>I141M</sup> cancer samples (particularly genes of the ERN1/XBP1 arm) was molecularly “responsible” for the observed differential clinical chemoresponse.

## 4.5. ERN1 is responsible for increased chemosensitivity in MIA2<sup>I141M</sup> carriers

To assess whether the MIA2<sup>I141M</sup> variant affects expression of UPR network genes, pancreatic cancer cell lines (endogenously or exogenously) expressing the MIA2<sup>WT</sup> or the MIA2<sup>I141M</sup> variant were screened for expression of BiP and the initiators of each UPR arm. This analysis revealed that pancreatic cancer cell lines expressing the MIA2<sup>I141M</sup> variant (Su-I141M, Su-I141M & D547H and Colo-357) expressed relatively higher levels of ERN1 compared to other cell lines. No such effect was found regarding the other tested proteins (BiP, ATF6 and PERK, **Fig.**

**17a).** This observation is highly consistent with the results obtained in the patient samples. To demonstrate that increased expression of ERN1 is molecularly “responsible” for increased chemosensitivity to gemcitabine induced by the MIA2<sup>I141M</sup> variant, ERN1 expression in Su-I141M and Su-I141M & D547H cells was silenced by siRNA transfection (**Fig. 17b**). These cells were then subjected to chemotherapy assays (**Fig. 17c**). Notably, ERN1 silencing reversed the chemo-sensitive phenotype of these two cell lines, providing the molecular link between the MIA2<sup>I141M</sup> variant and pancreatic cancer cell chemoresponse.

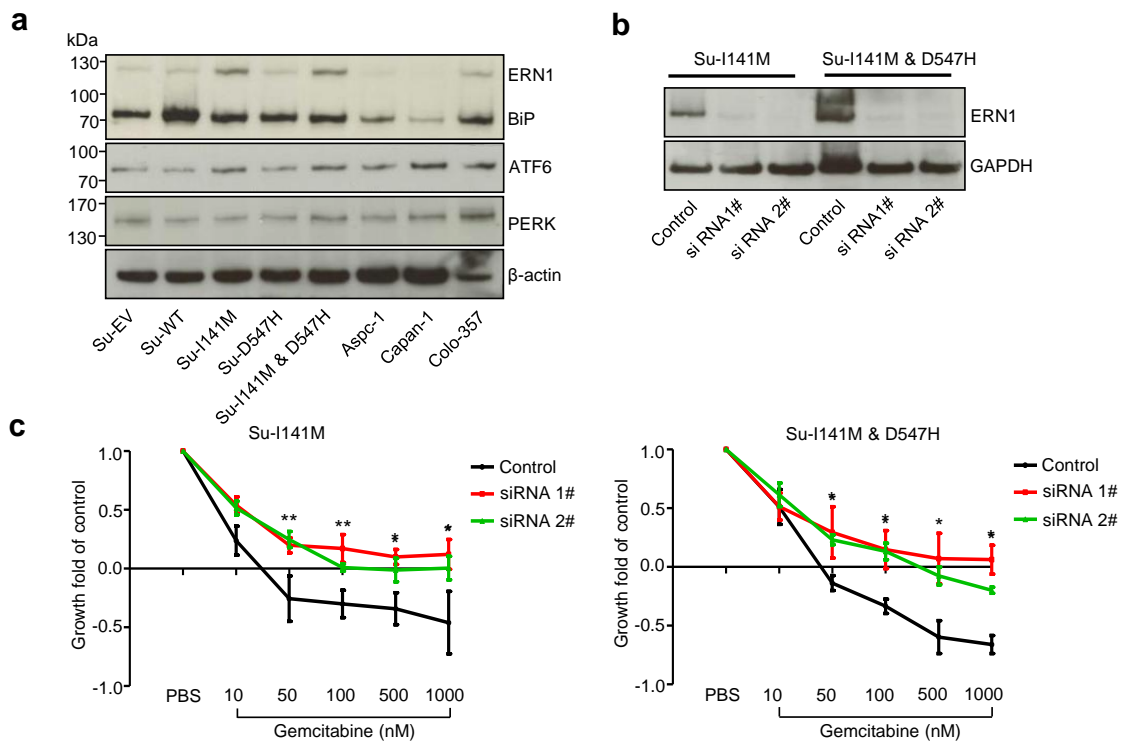


**Figure 17.** (a) Western-blot analysis revealed that pancreatic cancer cell lines expressing the MIA2<sup>I141M</sup> variant (Su-I141M, Su-I141M & D547H and Colo-357) also expressed ERN1 at higher levels than the other cancer cell lines. No such tendency was seen for the other tested molecules (BiP, ATF6 and PERK). (b) ERN1 silencing with two sets of specific siRNA’s (1# and 2#) or negative control siRNA (control) at 72 h in Su-I141M and Su-I141M & D547H cells. One representative blot out of three independent experiments is shown. (c) ERN1 silencing in Su-I141M and Su-I141M & D547H cells reverses the chemosensitive phenotype caused by expression of the I141M variant. \*: both 1# and 2# are significant. \*\*: only 1# is significant,  $p < 0.05$ . Data from three independent experiments is expressed as mean $\pm$ SD.

## 4.6. Tsc1 deficiency induces degeneration of the pancreas

In order to investigate the role of the Tsc1-Tsc2 complex in pancreatic physiology,  $Tsc1^{fl/fl}$  mice were crossed with the  $p48^{Cre}$  line to generate transgenic  $p48^{Cre}; Tsc1^{fl/+}$  (hereafter:  $Tsc1^{fl/+}$  or Tsc1-haploinsufficient) and  $p48^{Cre}; Tsc1^{fl/fl}$  (hereafter:  $Tsc1^{fl/fl}$  or Tsc1-deficient) mice in which one or two allele(s) of Tsc1 were specifically ablated in the pancreas. All transgenic mice were born at the expected rates. Notably, Tsc1-deficient mice ( $n=3$ ) died between 14 and 19 weeks of age whereas Tsc1-haploinsufficient mice were healthy. Histological examination of pancreases obtained from the Tsc1-deficient mice revealed that the pancreatic parenchyma (50%-80%) was replaced by small ductal structures, while no such changes were observed in any of the examined pancreases from the Tsc1-haploinsufficient ( $n=13$ ) and WT ( $n=5$ ) mice (**Fig. 18a**). IHC and double-IF studies revealed that the amount of acinar cells (labeled by  $\alpha$ -amylase antibodies) in the pancreases of the Tsc1-deficient mice was significantly reduced and that the residual acinar cells formed islet-like structures surrounded by Krt19-expressing ductal cells (Krt19: a marker for pancreatic ducts; **Fig. 18b, 18c, 18d**). Furthermore, cells double-positive for  $\alpha$ -amylase and Krt19 were frequently detected within these islet-like structures (**Fig. 18d**), implying the intermediate status of these cells. In contrast, the ratio of acinar cells to ductal cells in the pancreas of Tsc1-haploinsufficient mice appeared to be normal (**Fig. 18b, 18c, 18d**).

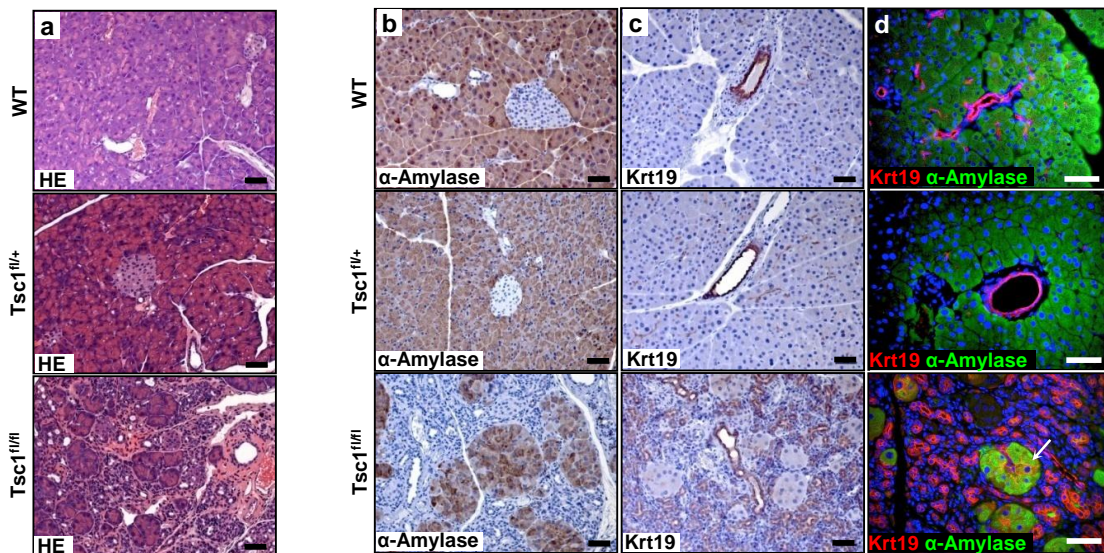


**Figure 18.** (a) Representative H&E-stained sections of the pancreas from WT ( $n=5$ ), Tsc1-haploinsufficient ( $Tsc1^{fl/+}$ ;  $n=13$ ) and Tsc1-deficient ( $Tsc1^{fl/fl}$ ;  $n=3$ ) mice show the enrichment of ductal cells specifically in the pancreases of Tsc1-deficient mice, but not in the pancreases of Tsc1-haploinsufficient or WT mice (scale bar: 50  $\mu$ m); (b-d) Representative IHC and IF pictures display the localization of pancreatic acinar cells (labeled by  $\alpha$ -amylase antibodies) and ductal

cells (labeled by Krt19 antibodies) in the pancreases from WT, Tsc1<sup>fl/+</sup> and Tsc1<sup>fl/fl</sup> mice; arrow: Krt19<sup>+</sup>amylase<sup>+</sup> cells (scale bar: 50µm).

Although the Krt19-expressing ductal cells in the pancreases of Tsc1-deficient mice were co-stained by SRY-box containing gene 9 (Sox9) antibodies (a marker for ductal and centroacinar cells (CACs)), they were largely negative for the pancreatic progenitor marker Pdx1 (**Fig. 19a, 19b**).

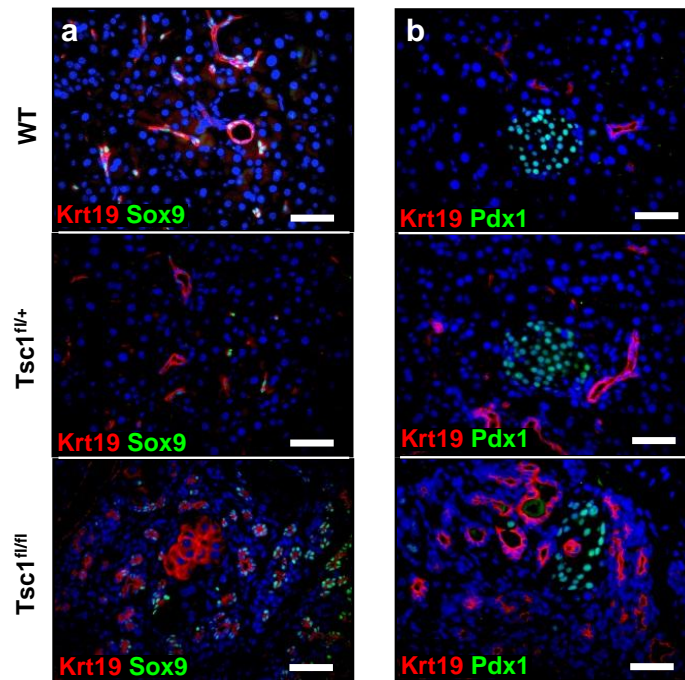


**Figure 19.** (a) Co-immunofluorescence staining for Krt19 and Sox9 in the pancreases of WT, Tsc1-haploinsufficient and Tsc1-deficient mice shows co-localization of Krt19 and Sox9 in ductal structures; (b) Co-immunofluorescence staining for Krt19 and Pdx1 demonstrates that the ductal cells in the pancreases of WT, Tsc1-haploinsufficient and Tsc1-deficient mice are negative for Pdx1 (scale bar: 50 µm).

Since the Tsc1-Tsc2 complex has previously been reported to be essential for the function of the endocrine pancreas (Leibowitz et al., 2008; Shigeyama et al., 2008), it is unknown whether the endocrine function of the pancreas was affected by Tsc1 deficiency. IHC and double-IF studies revealed that the amount of pancreatic  $\beta$  cells (labeled by insulin antibodies) was significantly reduced and that they were dissociated from the  $\alpha$  cells (labeled by glucagon antibodies) in the pancreases of Tsc1-deficient mice (**Fig. 20a, 20b, 20c**). These data suggested that these mice may suffer from diabetes. Indeed, hyperglycemic episodes were documented in two Tsc1-deficient mice by random measurements of glucose levels in peripheral blood (370 and 590 mg/dl; respectively; normal range: 160 to 200 mg/dl). In contrast, no significant abnormalities were observed in the



endocrine pancreases of *Tsc1*-haploinsufficient mice (**Fig. 20a, 20b, 20c**) and results of oral glucose tolerance tests (OGTT) in these animals were normal (**Fig. 20d**), indicating that the function of the endocrine pancreas was not affected by *Tsc1* haploinsufficiency.

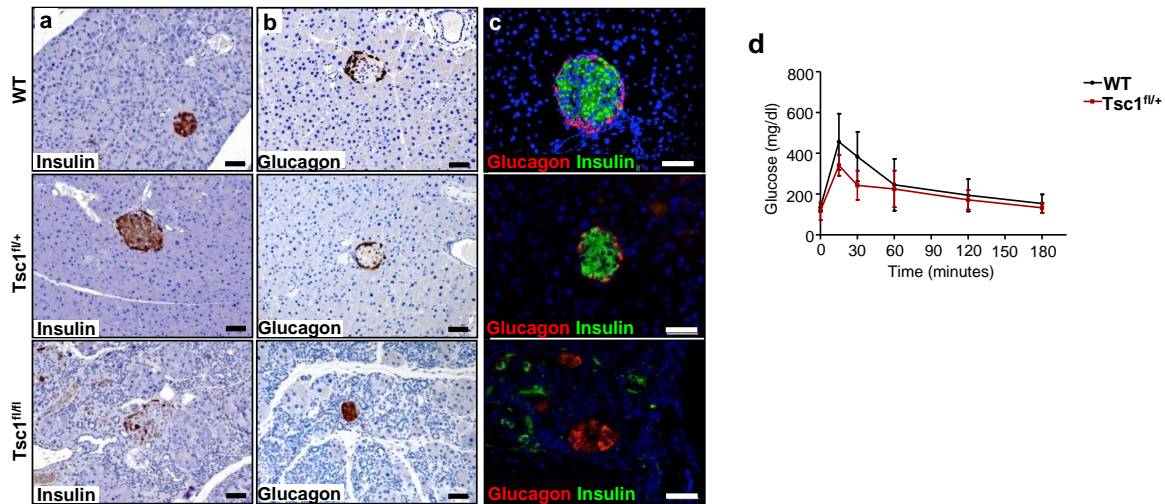


**Figure 20.** (a-c) IHC and double-IF studies for glucagon and insulin demonstrate the amount of pancreatic  $\beta$  cells (labeled by insulin antibodies) and their association to pancreatic  $\alpha$  cells (labeled by glucagon antibodies) in the pancreases of WT, *Tsc1*-haploinsufficient and *Tsc1*-deficient mice (scale bar: 50  $\mu$ m); (d) Blood glucose concentration during OGTT in *Tsc1*-deficient ( $n=3$ ) and WT ( $n=5$ ) mice shows no differences.

Taken together, these data demonstrate that the pancreas in the absence of *Tsc1* undergoes organ degeneration characterized by a progressive loss of pancreatic acinar and  $\beta$  cells. Hence, the molecular mechanisms underlying these degenerative alterations were explored. In order to avoid potential bias derived from analyzing tissues with different cellular compositions, the bulk pancreatic tissue lysates from young *Tsc1*-deficient mice (8 to 12 weeks) for western-blot analysis, in which degenerative alterations had not yet occurred (data not shown). Age-matched *Tsc1*-haploinsufficient and WT mice were used as controls. Here, western-blot analysis confirmed that levels of *Tsc1* and *Tsc2* expression were significantly lower in the pancreases of *Tsc1*-deficient mice in comparison to those of *Tsc1*-haploinsufficient and WT mice (**Fig. 21a**, upper panel). In line, activities of mTORC1 and its downstream molecule S6 were higher (reflected by phosphorylation levels of p-mTOR<sub>Ser2448</sub>, p-mTOR<sub>Ser2481</sub> and p-S6<sub>Ser235/236</sub>) in the pancreas of *Tsc1*-deficient mice than in the *Tsc1*-haploinsufficient and WT mice (**Fig. 21a**, middle panel). In addition, levels of Pten expression were higher in the *Tsc1*-ablated pancreas; likely due to a feedback response to hyperactivated mTORC1 (**Fig. 21a**, low panel) (Mahimainathan et al., 2009; Stambolic et al., 2001). In contrast, no changes in the expression of these molecules were observed in the pancreases of *Tsc1*-haploinsufficient mice except for lower phosphorylation levels of S6 due to unknown reasons (**Fig. 21a**, middle panel). However, it is unclear whether these molecular changes were persistent in the

degenerative pancreases of Tsc1-deficient mice. Indeed, IHC studies for p-mTOR<sub>Ser2448</sub> and p-S6<sub>Ser235/236</sub> uncovered that the residual acinar cells in these degenerative pancreases were strongly stained, demonstrating that pancreatic acinar cells were indeed highly susceptible to Tsc1 deficiency (**Fig. 21b, 21c**). Consistent with the results of the western-blot analysis, the residual acinar cells with hyperactivated mTORC1 were strongly stained by Pten antibodies (**Fig. 21d**). In comparison, the pancreatic acinar cells of the Tsc1-haploinsufficient and WT mice were only weakly stained using these three antibodies (**Fig. 21b, 21c, 21d**). Due to extremely low numbers of  $\beta$  cells, molecular changes in these cells could not be determined.

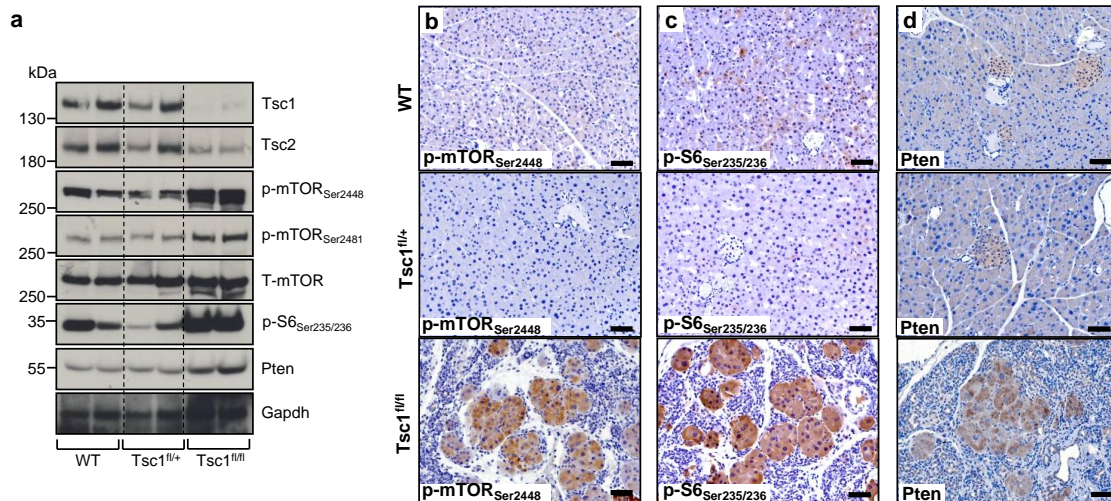


**Figure 21.** (a) Western-blot analysis using bulk pancreatic tissue lysates demonstrates low levels of Tsc1 and Tsc2 expression (upper panel), high phosphorylation levels of mTOR (p-mTOR<sub>Ser2448</sub> and p-mTOR<sub>Ser2481</sub>) and S6 (p-S6<sub>Ser235/236</sub>, middle panel), increased expression of Pten (lower panel) in the pancreases of Tsc1-deficient mice (n=2), but not in the Tsc1-haploinsufficient (n=2) and WT mice (n=2); One representative immunoblot out of three independent experiments is shown. (b-d) IHC studies for p-mTOR<sub>Ser2448</sub>, p-S6<sub>Ser235/236</sub> and Pten show the residual acinar cells with high mTORC1 activity and high Pten expression in the pancreases of Tsc1-deficient mice (n=3), but not in the Tsc1-haploinsufficient (n=3) and WT (n=3) mice.

Next, reasons responsible for the degenerative changes caused by Tsc1 deficiency in the pancreas was defined. Previously, it has been demonstrated in mouse embryonic fibroblasts (MEFs) that Tsc1 deficiency renders them highly susceptible to p53-dependent apoptosis (Lee et al., 2007a). It is likely that such a mechanism might be active in the pancreas, as well. To test this hypothesis, pancreatic tissues from Tsc1-deficient mice, Tsc1-haploinsufficient and WT mice were stained for cleaved-caspase 3 (a marker of apoptosis) and for p53. This analysis revealed that the residual acinar cells in the Tsc1-deficient mice were highly apoptotic and that they were strongly positive for nuclear p53, suggesting activation of the p53 pathways (**Fig. 22a, 22b**). Meanwhile, an increased

proliferation rate was observed in these residual acinar cells (**Fig. 22c**). In contrast, apoptosis, nuclear p53 staining and proliferation were rarely observed in the pancreases of Tsc1-haploinsufficient and WT mice (**Fig. 22a, 22b, 22c**). In line with observations in hematopoietic stem cells (HSCs) in which Tsc1 deficiency leads to increased levels of reactive oxygen species (ROS), the residual acinar cells in the pancreases of Tsc1-deficient mice were strongly stained by malondialdehyde (MDA, a lipid peroxidation adduct) antibodies, indicating excessive ROS accumulation within these cells (**Fig. 22d**) (Chen et al., 2008). Furthermore, a subset of these cells was stained by p-53BP1<sub>Ser25</sub> (a marker for DNA damage) antibodies, suggesting ongoing DNA damage, which was largely in line with excessive ROS accumulation and activation of the p53 pathways (**Fig. 22e**).

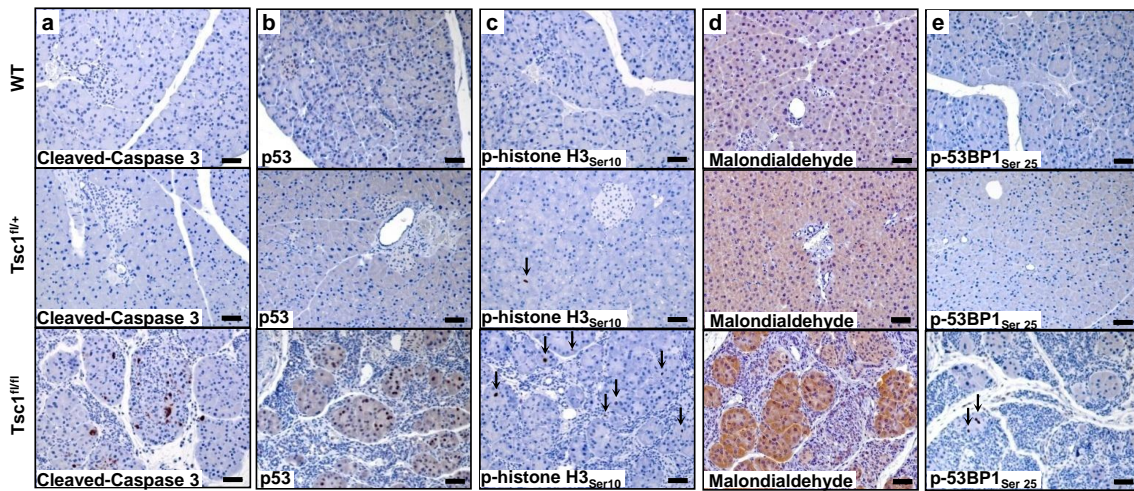


**Figure 22.** (a-b) IHC studies for cleaved-caspase 3 and p53 demonstrate cell apoptosis and nuclear p53 staining in the residual acinar cells of Tsc1-deficient mice, but not in WT and Tsc1-haploinsufficient mice; (c) IHC studies for p-histone H3<sub>Ser10</sub> show increased cell proliferation in the residual acinar cells of the Tsc1-deficient mice, but not in WT and the Tsc1-haploinsufficient mice; (d-e) IHC studies for malondialdehyde and p-53BP1<sub>Ser25</sub> show ROS accumulation and DNA damage in the residual acinar cells of the Tsc1-deficient mice, but not in WT and the Tsc1-haploinsufficient mice (scale bar: 50  $\mu$ m).

Taken together, Tsc1 deficiency induced hyperactivated mTORC1 in the pancreas which in turn triggered a set of feedback responses including activation of p53 and of Pten expression. Continuous activation of mTORC1 eventually resulted in organ degeneration characterized by massive cell death. P53-dependent apoptosis seemed to be involved in this process. However, Tsc1 haploinsufficiency had no significant impact on pancreatic physiology.

## 4.7. Tsc1 haploinsufficiency promotes tumor formation driven by Pten deficiency and expression of Kras<sup>G12D</sup>

Since Tsc1 haploinsufficiency does not have a significant impact on pancreatic physiology, its role in pancreatic carcinogenesis driven by expression of oncogenic Kras<sup>G12D</sup> and by Pten deficiency was defined. To this end, p48<sup>Cre/+</sup>, Pten<sup>fl/fl</sup>, Tsc1<sup>fl/fl</sup> and LSL-Kras<sup>G12D/+</sup> were intercrossed to generate compound transgenic mice with the following genotypes: p48<sup>Cre/+</sup>; Pten<sup>fl/fl</sup>; Tsc1<sup>fl/+</sup> (hereafter: Pten<sup>fl/fl</sup>; Tsc1<sup>fl/+</sup>), p48<sup>Cre/+</sup>; LSL-Kras<sup>G12D/+</sup>; Tsc1<sup>fl/+</sup> (hereafter: Kras<sup>G12D</sup>; Tsc1<sup>fl/+</sup>) and p48<sup>Cre/+</sup>; LSL-Kras<sup>G12D/+</sup>; Pten<sup>fl/+</sup>; Tsc1<sup>fl/+</sup> (hereafter: Kras<sup>G12D</sup>; Pten<sup>fl/+</sup>; Tsc1<sup>fl/+</sup>). Here, the pancreas-specific Tsc1 haploinsufficiency was introduced in the context of an increased activity of either Kras<sup>G12D</sup>/Erk or PI3K/Akt signaling, or both. In parallel, a set of control mice consisting of p48<sup>Cre/+</sup>; LSL-Kras<sup>G12D/+</sup> (hereafter: Kras<sup>G12D</sup>), p48<sup>Cre/+</sup>; Pten<sup>fl/fl</sup> (hereafter: Pten<sup>fl/fl</sup>) were generated. The resulting compound transgenic mice were followed up for 1.5 years, were monitored for pancreatic tumor development and were sacrificed once they showed any signs of disease.

### 4.7.1. Pten loss and Tsc1 haploinsufficiency promote cystic remodeling of the exocrine pancreas

Pten<sup>fl/fl</sup>; Tsc1<sup>fl/+</sup> mice quickly succumbed to pancreatic disease at a median of 132 days (n=18). Homozygous loss of Tsc1 further accelerated the disease course (median survival: 27.5 days; n=4; **Fig. 23c**). Interestingly, all Pten<sup>fl/fl</sup>; Tsc1<sup>fl/+</sup> mice developed macroscopically visible pancreatic cysts by the time of necropsy examination (**Fig. 23b**). However, no visible pancreatic cysts were observed in Pten<sup>fl/fl</sup> mice (n=5) and histological examination revealed only focal cystic lesions (10%), as previously published (**Fig. 23a**) (Stanger et al., 2005). Histological examination of the pancreas revealed that a large proportion of the parenchyma (40-100%) was replaced by large cysts - lined by flat to tall columnar epithelial cells - and by smaller cysts with a cribriform architecture (**Fig. 23d**, middle and right panel). Intracystic and stromal inflammation was observed (**Fig. 23d**, left panel). In particular, the small cysts displayed moderate to high dysplasia with focal invasion in one case (1/18; 6%, **Fig. 23e**, left panel). In addition, the small cystic lesions were surrounded by mesenchymal cells expressing  $\alpha$ -SMA ( $\alpha$ -smooth muscle actin; labels activated fibroblasts) (**Fig. 23e**, right panel). Presumably, most of the mice may have died as a result of severe pancreatic insufficiency and/or complications such as a rupture of the cysts. Thus, together with Pten loss, Tsc1 haploinsufficiency promotes remodeling of the exocrine pancreas by cystic lesions with high-grade dysplasia in smaller cysts; some of the small cystic lesions are able to give rise to invasive carcinoma but only at a low frequency.

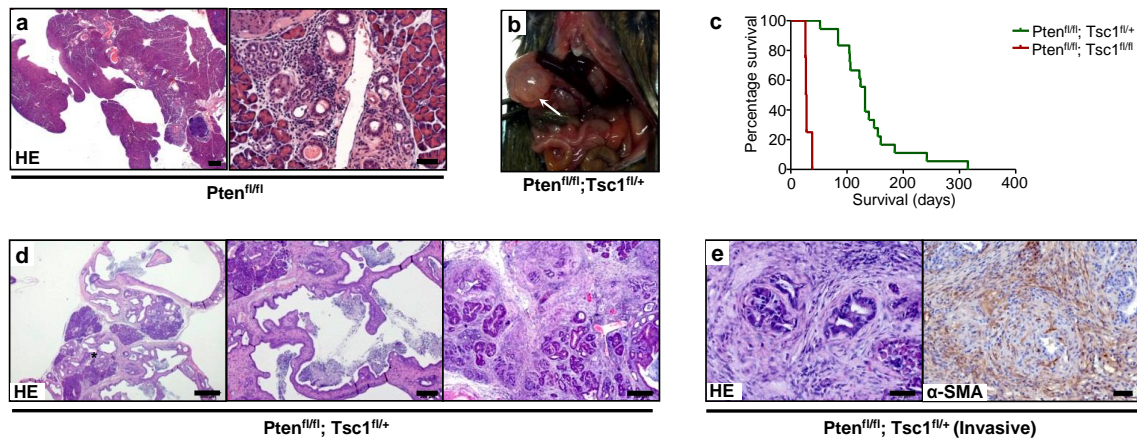


**Figure 23.** (a) Representative H&E-stained sections of  $Pten^{fl/fl}$  mice show localized cystic lesions (left panel, scale bar: 500  $\mu$ m; right panel, scale bar: 50  $\mu$ m); (b) Gross pathology of  $Pten^{fl/fl}; Tsc1^{fl/+}$  mice shows pancreatic cysts at necropsy examination; (c) Kaplan–Meier survival analysis shows survival times of  $Pten^{fl/fl}; Tsc1^{fl/+}$  (median survival: 132 days;  $n=18$ ) and  $Pten^{fl/fl}; Tsc1^{fl/fl}$  (median survival: 28 days;  $n=4$ ) mice; (d) Representative H&E-stained sections of  $Pten^{fl/fl}; Tsc1^{fl/+}$  mice show remodeling of the exocrine pancreas by cystic lesions with high-grade dysplasia in smaller cysts with cribriform architecture (\*: intracystic and stromal inflammatory component; left panel: 500  $\mu$ m; middle panel: 200  $\mu$ m; right panel: 100  $\mu$ m) (e) H&E–stained section shows one case of focal invasion reminiscent of human invasive ductal carcinoma; furthermore, these cells are surrounded by mesenchymal cells expressing  $\alpha$ -SMA (scale bar: 50  $\mu$ m).

#### 4.7.2 $Kras^{G12D}$ and $Tsc1$ haploinsufficiency promote metastatic and necrotic PDAC in mice

To investigate the impact of  $Tsc1$  haploinsufficiency on  $Kras^{G12D}$ -driven pancreatic carcinogenesis, a cohort of  $Kras^{G12D}; Tsc1^{fl/+}$  mice ( $n=12$ ) were followed up for the development of pancreatic diseases. The median survival of this cohort was 272 days, which was significantly shorter than that of  $Kras^{G12D}$  mice (381 days;  $n=18$ , **Fig. 24b**). From all  $Kras^{G12D}; Tsc1^{fl/+}$  mice, detailed histological reports were available for 11 mice. Here, 91% (10/11) of the mice developed invasive PDAC and 73% of those (8/11) developed metastasis in remote organs (**Fig. 24c**) including the liver (8/11, **Fig. 24f**, left panel), the lung (4/11, **Fig. 24f**, middle panel) and the kidney (2/11, **Fig. 24f**, right panel). In contrast, only a fraction of  $Kras^{G12D}$  mice (33%, 5/16) developed PDAC and their metastatic rate is relatively low (13%, 2/16, **Fig. 24d**). Histological analysis of tumors of  $Kras^{G12D}; Tsc1^{fl/+}$  mice revealed invasive PDAC with focal sarcomatoid-like patterns (anaplastic growth) in a majority of the tumors and focal papillary growth patterns in a few cases (**Fig. 24e**, left panel). Compellingly, the majority of tumors displayed diffuse and large necrotic areas - a histological feature which has previously not been described in endogenous PDAC mice (**Fig. 24e**, right panel). No large area of necrosis was observed in tumors of  $Kras^{G12D}$  mice (**Fig. 24a**). These data suggest that cancer cells derived from the  $Kras^{G12D}; Tsc1^{fl/+}$  mice are defective in initiating

angiogenesis. In summary, *Tsc1* haploinsufficiency and *Kras*<sup>G12D</sup> effectively initiate a necrotic and metastatic entity of PDAC with a focal dedifferentiated appearance.

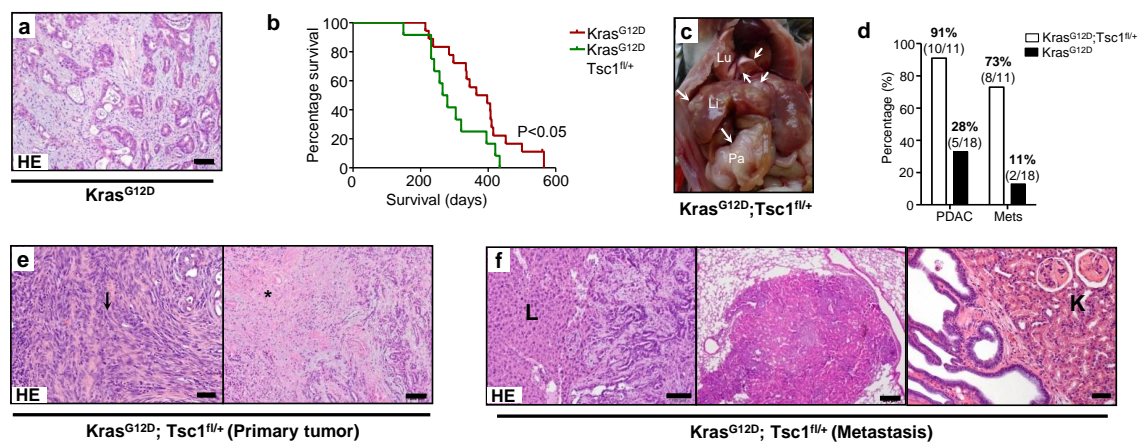


**Figure 24.** (a) An H&E–stained section shows no necrotic areas in tumors developing in *Kras*<sup>G12D</sup> mice; (b) Kaplan–Meier survival analysis shows that the survival times of *Kras*<sup>G12D</sup>; *Tsc1*<sup>fl/+</sup> (median survival: 272 days; n=12) mice are significantly shorter than those of *Kras*<sup>G12D</sup> (median survival: 381 days; n=18) mice, logrank test: p=0.045; (c) Gross pathology of a pancreatic tumor of a *Kras*<sup>G12D</sup>; *Tsc1*<sup>fl/+</sup> mouse shows the primary tumor (Pa), hepatic metastasis (Li) and pulmonary metastasis (Lu); (d) Tumor incidence and the metastatic rate of *Kras*<sup>G12D</sup>; *Tsc1*<sup>fl/+</sup> mice is higher than that of *Kras*<sup>G12D</sup> mice; PDAC: PDAC incidence; Mets: metastasis rate; Tumor incidence: Chi<sup>2</sup>-test, p=0.001; Metastatic rate: Chi<sup>2</sup>-test, p=0.001 (e) Representative H&E-stained sections of *Kras*<sup>G12D</sup>; *Tsc1*<sup>fl/+</sup> mice show invasive PDAC with sarcomatoid features (left panel, arrow: sarcomatoid-like area; scale bar: 50 μm) and large areas of necrosis (right panel, \*: necrosis; scale bar: 200 μm); (f) Representative H&E-stained sections display hepatic metastasis (left panel; scale bar: 100 μm), pulmonary metastasis (middle panel; scale bar: 200 μm) and renal invasion (right panel; scale bar: 100 μm); L: liver; K: Kidney.

#### 4.7.3. *Kras*<sup>G12D</sup> and combined *Pten* and *Tsc1* haploinsufficiency induce invasive carcinomas with IPMN-like lesions

Since no large tumor necrosis was reported in *Kras*<sup>G12D</sup>; *Pten*<sup>fl/+</sup> mice previously (Hill et al., 2010; Kennedy et al., 2011; Ying et al., 2011), an additional loss of one *Pten* allele may alter the necrotic phenotype of the *Kras*<sup>G12D</sup>; *Tsc1*<sup>fl/+</sup> mice. To this end, four *Kras*<sup>G12D</sup>; *Pten*<sup>fl/+</sup>; *Tsc1*<sup>fl/+</sup> mice were generated and were followed up for any signs of pancreatic disease. Notably, these mice succumbed to pancreatic tumors quickly with a median survival of 142 days (131-172 days). Histological examination of these tumors showed an invasive ductal adenocarcinoma with intraductal papillary mucinous neoplasm (IPMN)-like lesions characterized by large cystic lesions lined with prominent papillary epithelium (**Fig. 25**). Alike *Pten*<sup>fl/fl</sup>; *Tsc1*<sup>fl/+</sup> mice, a prominent intraductal inflammatory component was

frequently observed in these IPMN-like lesions (**Fig. 25**). However, no changes such as anaplastic components and/or tumor necrosis were observed in these mice. These data suggest that an additional loss of Pten not only significantly accelerates carcinogenesis, but also alters tumor morphology and biology.

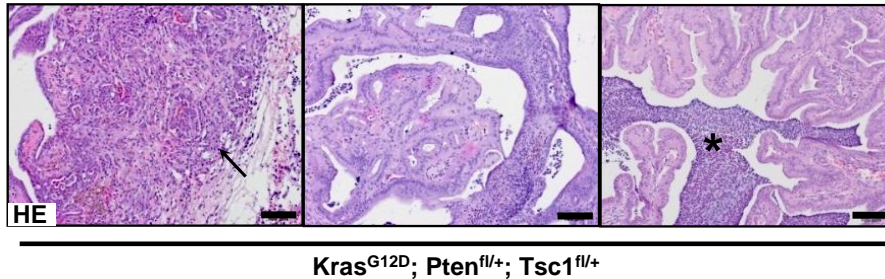


**Figure 25.** Histological examination revealed that  $Kras^{G12D}; Pten^{fl/+}; Tsc1^{fl/+}$  mice developed invasive PDAC (left panel; arrow: invasive part; scale bar: 100  $\mu$ m), featured by IPMN-like lesions (middle panel; scale bar: 100  $\mu$ m) with frequent intraductal inflammatory components (right panel \*: inflammatory component).

#### 4.8. $Kras^{G12D}$ /Erk or PI3K/Akt together with Tsc1 haploinsufficiency drive hyperactivation of mTORC1 in pancreatic cells

In order to characterize signal changes caused by Tsc1 haploinsufficiency in the context of  $Kras^{G12D}$  expression and Pten deficiency, a set of primary cancer cells from the cancer tissues of  $Kras^{G12D}; Tsc1^{fl/+}$  mice and epithelial cells from the cystic lesions of  $Pten^{fl/fl}; Tsc1^{fl/+}$  mice were established. The genotypes of all cell lines were confirmed by PCR analysis (**Supplementary Fig. 1**) and cell lines were used for all experiments at early passages (less than 6 passages). The pancreatic cancer cell lines T9801 and 944 were used as controls. Notably, two  $Pten^{fl/fl}; Tsc1^{fl/+}$  cell lines (926, 928) consisted of small cells and formed typical island-like structures in culture (**Fig. 26a**, left panel) whereas another cell line (952) showed the normal appearance of pancreatic epithelial cells (**Fig. 26a**, right panel). A majority of  $Kras^{G12D}; Tsc1^{fl/+}$  cells displayed a cobble-like appearance (**Fig. 26b**, left panel) with an exception of the 907 cells which displayed a fibroblast-like phenotype (**Fig. 26b**, right panel). As expected, all cells with a Tsc1 haploinsufficiency had lower levels of Tsc1 expression in comparison to the control cell lines (T9801 and 944 cells, **Fig. 26c**, upper panel). Thereafter, the isolated cells were subjected to in vitro pathway characterization by serum stimulation assays. Here, PI3K/Akt signaling (represented by phosphorylation levels of p-Akt<sub>Ser473</sub>) was constitutively active in Pten-deficient cells (926, 928 and

952 cells) which could be augmented by serum treatment. In contrast, the activity of Akt signaling in  $Kras^{G12D}$ -expressing cancer cells relied on the presence of serum. Accordingly, Erk signaling (represented by phosphorylation levels of p-Erk1/2<sub>Thr202/Tyr204</sub>) in  $Kras^{G12D}$ -expressing cancer cells was constantly active and serum treatment only slightly increased Erk phosphorylation. In contrast, the Erk phosphorylation in Pten-deficient cells largely relied on the presence of serum (**Fig. 26c**, middle panel). Nevertheless, mTORC1 signaling (as reflected by phosphorylation levels of p-mTOR<sub>Ser2448</sub> and p-mTOR<sub>Ser2481</sub>) were constantly active in these tested cell lines and could be further elevated by serum treatment in some cases (e.g. 403, 907 cells; **Fig. 26c**, lower panel). These data suggest that mTORC1 signaling in  $Pten^{fl/fl}; Tsc1^{fl/+}$  cells was driven by PI3K/Akt whereas mTORC1 signaling in  $Kras^{G12D}; Tsc1^{fl/+}$  cells was driven by  $Kras^{G12D}$ /Erk. In order to further distinguish these two activation patterns, the conserved Akt sites of Tsc2 were defined in  $Pten^{fl/fl}; Tsc1^{fl/+}$  cells. Indeed, the conserved Akt site of Tsc2 (Ser<sup>939</sup>) in  $Pten^{fl/fl}; Tsc1^{fl/+}$  cells was highly phosphorylated in comparison to that in  $Kras^{G12D}; Tsc1^{fl/+}$  cells (**Fig. 26d**). However, no such difference was observed for AMPK site of Tsc2 (Ser<sup>1837</sup>) between  $Pten^{fl/fl}; Tsc1^{fl/+}$  and  $Kras^{G12D}; Tsc1^{fl/+}$  cells (**Fig. 26d**).

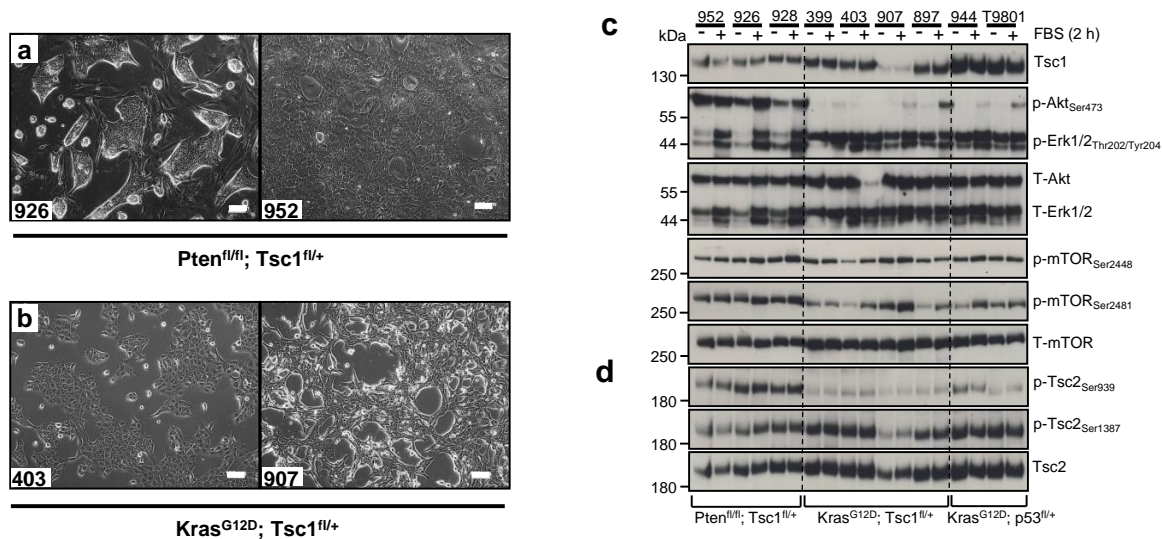


**Figure. 26 (a-b)** Phase contrast images of isolated cells show representative morphologies of isolated cells from cystic lesions of  $Pten^{fl/fl}; Tsc1^{fl/+}$  mice (926 and 952) and cancer tissues of  $Kras^{G12D}; Tsc1^{fl/+}$  mice (403 and 907), scale bar: 100  $\mu$ m; **(c)** Western-blot analysis demonstrates the expression of Tsc1 (upper panel); phosphorylation levels of Akt and Erk (p-Akt<sub>Ser473</sub> and p-Erk1/2<sub>Thr202/Tyr204</sub>; middle panel) and the activity of mTORC1 (p-mTOR<sub>Ser2448</sub> and p-mTOR<sub>Ser2481</sub>; lower panel) in cells isolated from cystic lesions of  $Pten^{fl/fl}; Tsc1^{fl/+}$  (926, 928 and 952) mice and cancer tissues of  $Kras^{G12D}; Tsc1^{fl/+}$  (399, 403, 907 and 897) mice. 9801 and 944 cells ( $Kras^{G12D}; p53^{fl/+}$ ) were used as controls. **(d)** Western-blot analysis shows phosphorylation levels of the Akt site (Tsc2<sub>Ser939</sub>) and the AMPK site



(Tsc2<sup>Ser1387</sup>) on Tsc2 in Pten<sup>fl/fl</sup>; Tsc1<sup>fl/+</sup>, Kras<sup>G12D</sup>; Tsc1<sup>fl/+</sup> and Kras<sup>G12D</sup>; p53<sup>fl/+</sup> cells. FBS: fetal bovine serum; One representative immunoblot out of three independent experiments is shown.

Thereafter, these molecular events were also defined in vivo. A series of markers including p-Akt<sub>Ser473</sub>, p-Erk1/2<sub>Thr202/Tyr204</sub>, p-mTOR<sub>Ser2448</sub> and p-S6<sub>Ser235/236</sub> were used to stain pancreatic tissues from transgenic mice. Indeed, this analysis confirmed the in vitro findings: pancreatic cells within pancreatic cystic lesions of Pten<sup>fl/fl</sup>; Tsc1<sup>fl/+</sup> mice were strongly stained by the p-Akt<sub>Ser473</sub> antibody with a membrane enhancement (a typical pattern for Akt activation) while the cancer cells in the pancreatic cancer tissues of Kras<sup>G12D</sup>; Tsc1<sup>fl/+</sup> mice were generally devoid of p-Akt<sub>Ser473</sub> staining (**Fig. 27a**). Accordingly, nuclear p-Erk1/2<sub>Thr202/Tyr204</sub> staining was widely detected in cancer cells from Kras<sup>G12D</sup>; Tsc1<sup>fl/+</sup> mice, however, it was generally absent in the cystic lesions of Pten<sup>fl/fl</sup>; Tsc1<sup>fl/+</sup> mice except for one invasive case in which the cystic lesions were strongly stained by p-Erk1/2<sub>Thr202/Tyr204</sub> antibodies (**Fig. 27b** and **Fig. 44d**). In line, both p-mTOR<sub>Ser2448</sub> and p-S6<sub>Ser235/236</sub> (a surrogate marker for the activation of mTORC1) antibodies stained cancer cells and small cystic lesions, indicating the in vivo activation of mTORC1 in these animals (**Fig. 27c, 27d**). Taken together, mTORC1 can be predominantly activated either through the Kras<sup>G12D</sup>/Erk or the PI3K/Akt cascade in pancreatic epithelial cells; the different activation patterns are associated with different pathological consequences. Finally, the IPMN-like lesions in Kras<sup>G12D</sup>; Tsc1<sup>fl/+</sup>; Pten<sup>fl/+</sup> mice were positively stained for these markers, exhibiting a dual activation of mTORC1 via the Kras<sup>G12D</sup>/Erk and PI3K/Akt cascades (**Fig. 26a, 26b, 26c, 26d**).

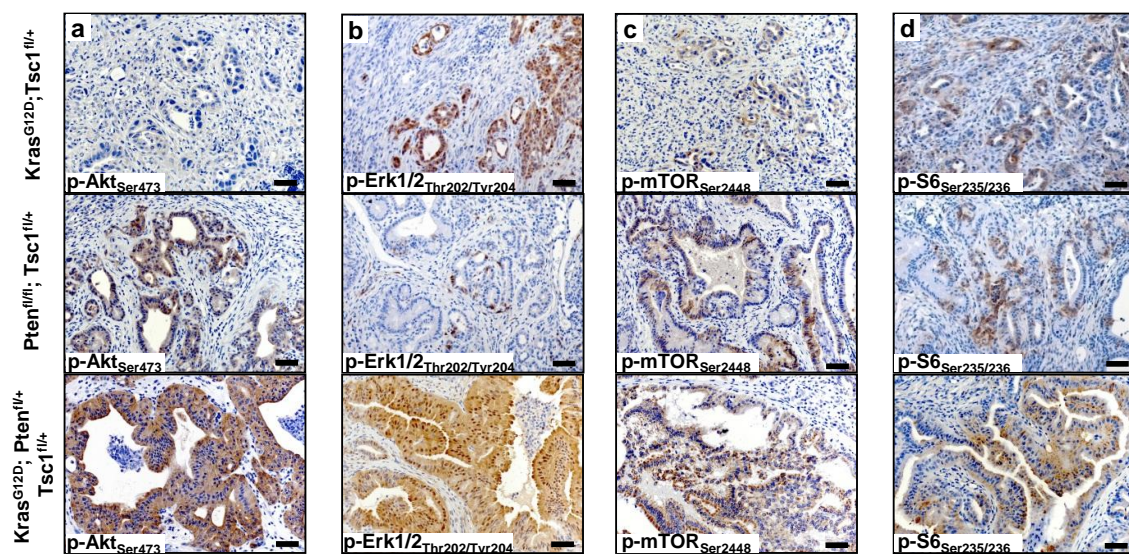


**Figure 27.** (a-d) Representative IHC pictures show distinct activation of Akt (p-Akt<sub>Ser473</sub>), Erk (p-Erk1/2<sub>Thr202/Tyr204</sub>), mTORC1 (p-mTOR<sub>Ser2448</sub>) and S6 (p-S6<sub>Ser235/236</sub>) in pancreatic tissues obtained from Kras<sup>G12D</sup>; Tsc1<sup>fl/+</sup> (upper panel), Pten<sup>fl/fl</sup>; Tsc1<sup>fl/+</sup> (middle panel) and Kras<sup>G12D</sup>; Tsc1<sup>fl/+</sup>; Pten<sup>fl/+</sup> mice (lower panel), scale bar: 50  $\mu$ m.

## 4.9. Hypoxia promotes the metastatic potential of pancreatic cancer cells

Next, the reasons why pancreatic tumors in the Kras<sup>G12D</sup>; Tsc1<sup>fl/+</sup> mice tended to metastasize were defined. A unique feature of these tumors was the large and diffuse tumor necrosis, in which many duct-like structures from pre-existing cancer cells were preserved, resembling an ischemia-induced necrosis. Moreover, the distribution of the necrotic region followed an eccentric pattern. These morphological observations suggested that cancer cells may have certain defects in initiating angiogenesis. To test this hypothesis, vessels were labeled in pancreatic tissues using CD31 antibodies. This analysis revealed that the central necrotic region was surrounded by vascularized tumor tissues (**Fig. 28a**, upper panel); and that there was a transitional zone in which cancer cells were completely devoid of blood supply. No such transitional zone was observed in Pten<sup>fl/fl</sup>; Tsc1<sup>fl/+</sup> mice (**Fig. 28a**, lower panel). Since tumor hypoxia constitutes a driving force for tumor metastasis (Cooke et al., 2012), it remains elusive whether cancer cells within the transitional zone were generally hypoxic. To this end, a hypoxia marker – carbonic anhydrase IX (Caix) – whose expression is induced by exposure to hypoxia, was stained (Hiraoka et al., 2010). This analysis revealed that Caix staining intensity was specifically enhanced in cancer cells in the vicinity of necrotic tissues, building up a hypoxic “zone” between necrotic and vascularized tissues (**Fig. 28b**, upper panel). In Pten<sup>fl/fl</sup>; Tsc1<sup>fl/+</sup> mice, the Caix-expressing cells were scattered between the cystic lesions, probably due to activation of Hif-1 $\alpha$  signaling via the increased mTORC1 activity (**Fig. 28b**, lower panel) (Pore et al., 2006). In addition, apoptotic cells (as labeled by cleaved-caspase 3) specifically accumulated within this hypoxic zone, demonstrating a dynamic “dying” process following an eccentric pattern in these necrotic PDACs (**Fig. 28c**, upper panel); however, apoptotic cells were rarely detected in the cystic lesions of Pten<sup>fl/fl</sup>; Tsc1<sup>fl/+</sup> mice (**Fig. 28c**, lower panel). In order to evaluate the effects of hypoxia on the aggressiveness of cancer cells, an invasion assay was performed using the above mentioned cancer cell lines or epithelial cells isolated from Pten<sup>fl/fl</sup>; Tsc1<sup>fl/+</sup> and Kras<sup>G12D</sup>; Tsc1<sup>fl/+</sup> mice. Although the basal invasive potential of these cell lines varied greatly, hypoxia promoted the invasive potential of all tested cells (**Fig. 28d**). These data demonstrate that

hypoxia constitutes a strong stimulus for a pro-invasive capacity of pancreatic cells irrespective of their genetic background. Though hypoxia for 24 hours only slightly reduced E-Cadherin expression in cells with *Tsc1* haploinsufficiency, E-Cadherin expression in these cells was collectively lower than that of the *Kras*<sup>G12D</sup>; *p53*<sup>fl/+</sup> cell lines (T9801 and 944 cells; **Fig. 28e**). As an internal control, the expression of Hk2 (hexokinase 2) was increased by hypoxia (**Fig. 28e**). Furthermore, these hypoxia-induced molecular changes were also observed in cancer tissues of *Kras*<sup>G12D</sup>; *Tsc1*<sup>fl/+</sup> mice: membrane expression of E-Cadherin in cancer cells located at the “hypoxia zone” was lost in cancer cells with an acquisition of a fibroblastic (e.g. mesenchymal) phenotype (**Fig. 28f**, upper panel); the staining intensities of Hk2 were enhanced within these cells (**Fig. 28f**, lower panel). Although E-Cadherin expression was preserved in *small* cystic lesions, its expression was generally lost in *large* cystic lesions of *Pten*<sup>fl/fl</sup>; *Tsc1*<sup>fl/+</sup> mice (**Fig. 28g**, upper panel). Hk2-expressing cells were scattered within the cystic lesions, exhibiting a similar staining pattern as the Caix-expressing cells (**Fig. 28g**, lower panel).

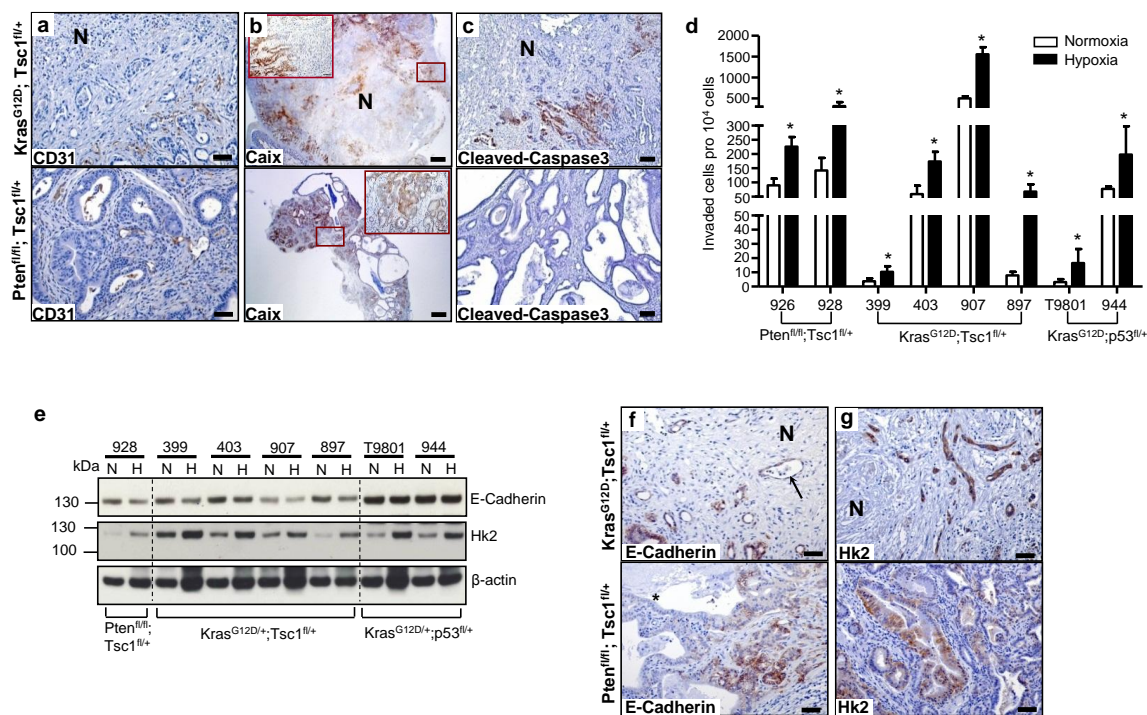


**Figure 28.** (a-c) IHC studies of CD31, Caix and cleaved-caspase 3 as surrogate markers for vessel densities (scale bar: 50 μm), hypoxic zones (scale bar: 500 μm) and apoptotic cells (scale bar: 100 μm) in pancreatic tissues obtained from *Kras*<sup>G12D</sup>; *Tsc1*<sup>fl/+</sup> (upper panel) and *Pten*<sup>fl/fl</sup>; *Tsc1*<sup>fl/+</sup> (lower panel) mice, N: necrosis; (d) In a Matrigel invasion assay, hypoxia triggers the invasion of all tested pancreatic cancer cell lines and epithelial cells; values shown are obtained from at least three independent experiments; \*: p<0.05; (e) Western-blot analysis reveals that the cancer cells or epithelial cells with *Tsc1* haploinsufficiency

collectively have a lower expression level of E-Cadherin; hypoxia only slightly alters E-Cadherin expression in the hypoxic cells with Tsc1 haploinsufficiency; N: normoxia, H: hypoxia; One representative blot out of three independent experiments is shown. **(f-g)** IHC studies for E-Cadherin and Hk2 show the loss of membrane staining of E-Cadherin (arrow) and increased expression of Hk2 in cancer cells in the vicinity of tissue necrosis in cancer tissues of  $Kras^{G12D}; Tsc1^{fl/+}$  mice (upper panel), but not in the cystic lesions of  $Pten^{fl/fl}; Tsc1^{fl/+}$  mice (lower panel), scale bar: 50  $\mu$ m.

#### **4.10. $Kras^{G12D}; Tsc1^{fl/+}$ cancer cells are defective in releasing Vegfa because of hypoxia-induced ER stress**

To understand the molecular mechanisms responsible for the large areas of necrosis observed in the cancer tissues of  $Kras^{G12D}; Tsc1^{fl/+}$  mice, the introduced  $Kras$  mutation in the isolated pancreatic cancer cell lines (399, 403, 907 and 897 cells) was sequenced.  $Pten^{fl/fl}; Tsc1^{fl/+}$  cell lines (926 and 928 cells) were used as controls. As expected, the 926 and 928 cells contained no  $Kras^{G12D}$  mutation; the 399 and 403 cells were heterozygous for  $Kras^{G12D}$ . Compellingly, sequencing data from the 907 and 897 cells only showed a single reading signal of the  $Kras^{G12D}$  allele (**Fig. 29a**), implying either a loss of the (remaining) wild type  $Kras$  allele or a de novo acquisition of an additional  $Kras^{G12D}$  mutation. In order to distinguish these two possibilities, a PCR was performed to amplify the genetic region containing the remaining LoxP site (after the removal of the STOP cassette) of the  $Kras^{G12D}$  allele. In this case, the wild type allele would also be amplified but would give rise to a shorter amplicon (one LoxP site less: 34 bp, **Fig. 29a**, lower panel). This analysis revealed that the wild type  $Kras$  allele had been selectively deleted in the 907 and 897 cells, resulting in a loss of heterozygosity (LOH) of  $Kras^{G12D}$ , as previously reported (Qiu et al., 2011). In order to determine whether  $Kras$  expression and/or  $Kras$  activity were affected by the LOH status of  $Kras^{G12D}$ , western-blot analyses and Ras pull-down assays were performed. This analysis revealed that neither  $Kras$  expression nor the steady-state/ serum-induced  $Kras$  activity (GTP- $Kras$ ; **Fig. 29b**) were affected by the LOH status of  $Kras^{G12D}$ . As a control, expression of WT  $Kras$  in  $Pten^{fl/fl}; Tsc1^{fl/+}$  cells (928) was demonstrated to be significantly lower in comparison to other cell lines and serum treatment significantly induced  $Kras$  activity in these cells (**Fig. 29b**).

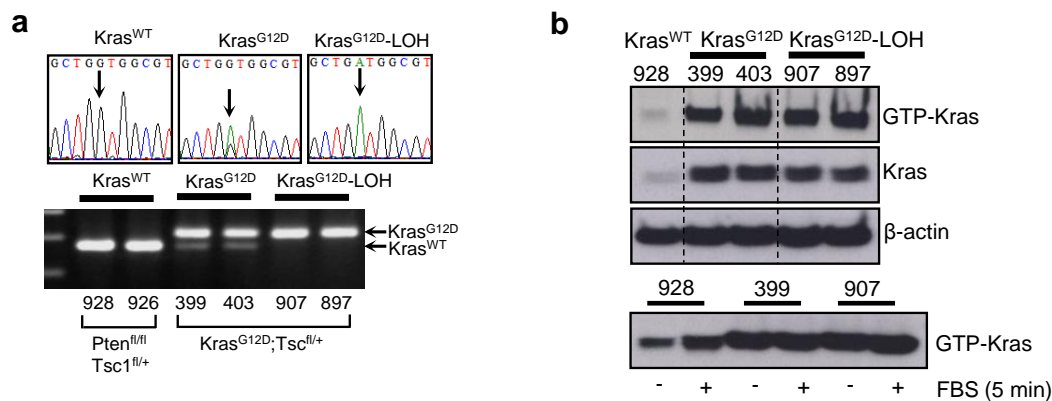


**Figure 29.** (a) Sequencing results and PCR analysis demonstrate a  $Kras^{G12D}$ -LOH in the 907 and 897 cells, but not in the 399 and 403 cells; two  $Pten^{fl/fl}; Tsc1^{fl/+}$  cell lines (928 and 926 cells) contain two wild type  $Kras$  alleles; one representative PCR analysis out of three independent experiments is shown. (b) Ras pull-down assays show that the cancer cells with the  $Kras^{G12D}$ -LOH (907, 897 cells) have a comparable steady-state (upper panel) and serum-stimulated  $Kras$  activity (lower panel) as the cancer cells with  $Kras^{G12D}$ . The 928 cells ( $Pten^{fl/fl}; Tsc1^{fl/+}$  cells) with the wild type  $Kras$  alleles were used as a negative control for these assays. One representative blot out of three independent experiments is shown.

In order to determine whether these cancer cells were able to reproduce the histological features of the respective primary tumors in a transplanted tumor model, these cancer cells were orthotopically implanted into the pancreas of WT mice. 3 cell lines (399, 403 and 907) formed tumors in WT mice with a 100% penetrance while only 1 out of 4 (25%) of the 897 cell-transplanted mice developed tumors with a relatively small size (**Table 6**). An overview of the transplanted cell lines, mouse numbers, and tumor incidences is provided in **Table 6**.

**Table 6.** Tumor formation of  $Kras^{G12D}; Tsc1^{fl/+}$  cancer cells in WT mice

Cell lines	Genotype	Primary tumor	WT mice		BALB/c nude mice	
			Tumor/Total	Rate (%)	Tumor/Total	Rate (%)
399	$Kras^{G12D}; Tsc1^{fl/+}$	PDAC	16/16	100%	-	-
403	$Kras^{G12D}; Tsc1^{fl/+}$	PDAC	12/12	100%	-	-
907	$Kras^{LOH}; Tsc1^{fl/+}$	PDAC	4/4	100%	-	-
897	$Kras^{LOH}; Tsc1^{fl/+}$	PDAC	1/4	25%	-	-

Importantly, a clear heterogeneity and discrepancy in tumor histology were observed in the transplanted tumors: the 399 cells ( $Kras^{G12D}$ ) gave rise to a necrotic form of PDAC featured by large areas of centralized necrosis (**Fig. 30a**, left panel); the 403 cells ( $Kras^{G12D}$ ) formed papillary adenocarcinomas with large cysts and focal necrosis (**Fig. 30a**, right panel); the 907 and 897 cells ( $Kras^{G12D}$ -LOH) developed a solid form of tumors (**Fig. 30b**). Furthermore, histological examinations and IHC studies for E-Cadherin revealed that the tumors formed by cancer cells with  $Kras^{G12D}$ -LOH contained a high proportion of anaplastic/sarcomatoid-like components resembling the histological features of the primary tumors. Furthermore, IHC studies for CD31, Caix and cleaved-caspase 3 revealed that the necrotic form of the transplanted tumors recapitulated the histological features of the respective primary tumors including devascularized tumor regions, hypoxic zones and cell apoptosis within the hypoxic zones (**Fig. 30e, 30f, 30g**). In summary, these data demonstrate that the major features of the primary tumor including necrosis/hypoxia and sarcomatoid/dedifferentiation can be reproduced in a (syngeneic) transplantation mouse model of pancreatic cancer. Moreover, tumor necrosis and dedifferentiation can be distinguished by the LOH status of  $Kras^{G12D}$ .

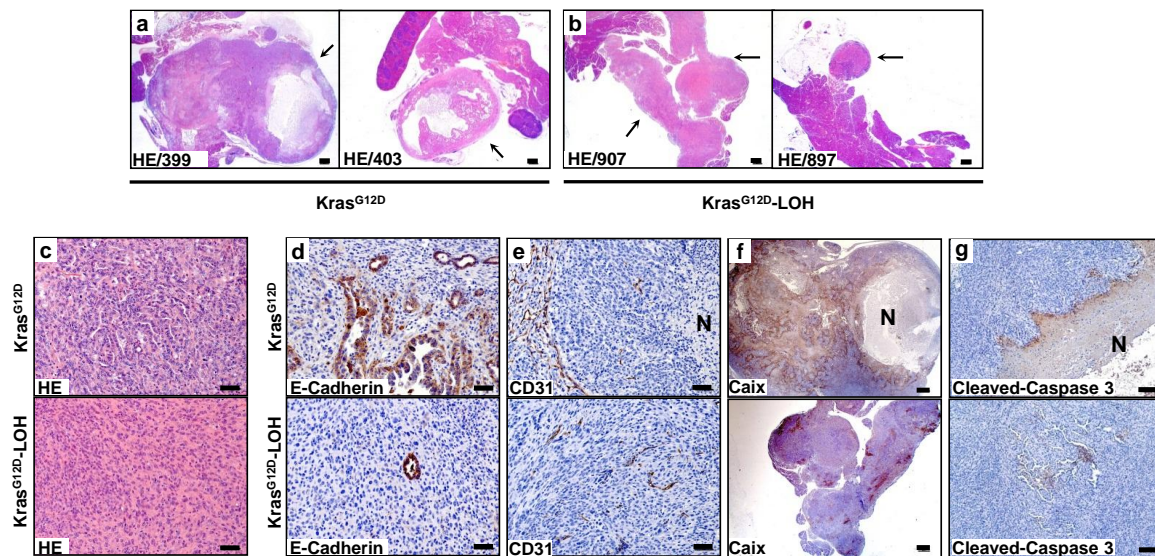


**Figure 30.** (a-b) H&E–stained sections show centrally-necrotic and papillary (with focal necrosis) tumors formed by orthotopic implantation of  $Kras^{G12D}$ ;  $Tsc1^{fl/+}$  cancer cells (399 and 403) and more solid forms of tumors formed by  $Kras^{G12D}$ -LOH;  $Tsc1^{fl/+}$  cells (907 and 897), scale bar: 500  $\mu$ m; arrow; tumor tissues; (c-d) H&E–stained sections and IHC studies for E-Cadherin demonstrate a high proportion of anaplastic components in tumors developed by  $Kras^{G12D}$ -LOH;  $Tsc1^{fl/+}$  cancer cells (upper panel), but not in tumors developed by  $Kras^{G12D}$ ;  $Tsc1^{fl/+}$  cancer cells (lower panel), scale bar: 50  $\mu$ m; (e-h) IHC studies for CD31 (scale bar: 50  $\mu$ m), Caix (scale bar: 500  $\mu$ m) and cleaved-caspase 3 (scale bar: 100  $\mu$ m) show devascularized tumor regions, hypoxic zones and cell

apoptosis in the necrotic forms of transplanted tumors (upper panel), but not in the anaplastic tumors; N: necrosis.

In addition, in order to rule out the possibility that large areas of necrosis in the tumor tissues developed by  $Kras^{G12D}; Tsc1^{fl/+}$  cells were not caused by their increased sensitivity to hypoxia-triggered apoptosis; these cancer cells were exposed to an extended period of hypoxia (72 hours). Here, western-blot analysis revealed that the induction of cleaved-caspase 3 (as a readout for cell apoptosis) was comparable between  $Kras^{G12D}; Tsc1^{fl/+}$  (399 and 403) and  $Kras^{G12D-LOH}; Tsc1^{fl/+}$  (907 and 897) cancer cells (**Fig. 31**).

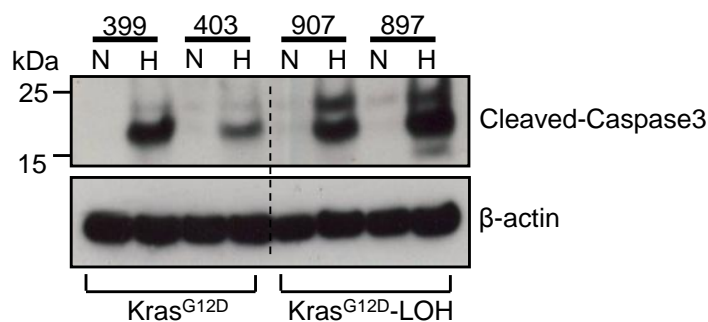


**Figure 31.** Western-blot analysis demonstrates that  $Kras^{G12D}; Tsc1^{fl/+}$  cells and  $Kras^{G12D-LOH}; Tsc1^{fl/+}$  cells exhibit a similar induction of cleaved-caspase 3 in response to extended exposure to hypoxia (72 hours); N: normoxia, H: hypoxia; One representative blot out of three independent experiments is shown.

These data suggested that it was the intrinsic defect of  $Kras^{G12D}; Tsc1^{fl/+}$  cells in initiating angiogenesis that was responsible for tissue hypoxia and necrosis; and that the  $Kras^{G12D-LOH}$  seemed to be able to overcome this defect. To test this hypothesis, the angiogenic potential of these cells under hypoxic conditions was analyzed.  $Kras^{G12D-LOH}; Tsc1^{fl/+}$  cells (907 and 897) which did not give rise to necrotic tumors were used as “syngenic controls” and  $Pten^{fl/fl}; Tsc1^{fl/+}$  (926, 928) cells were used as external controls for these assays. The release of Vegfa into the supernatants was determined by ELISA assays after 24 hours of exposure to hypoxia. As expected, hypoxia increased the concentration of Vegfa in the supernatants obtained from  $Pten^{fl/fl}; Tsc1^{fl/+}$  cells (**Fig. 32**). The  $Kras^{G12D}; Tsc1^{fl/+}$  cell lines, 399 and 403 cells had a relatively high basal level of Vegfa production; however, they did not show an increased Vegfa concentration after exposure to hypoxia. Furthermore, the  $Kras^{G12D-LOH}; Tsc1^{fl/+}$  cell lines (907 and 897) had a rather low level of basal Vegfa release and exhibited a significant increase in

Vegfa concentration after exposure to hypoxia (**Fig. 32**). These data suggest that the  $Kras^{G12D}; Tsc1^{fl/+}$  cells were defective in releasing Vegfa under hypoxic conditions, albeit their high basal Vegfa secretion.

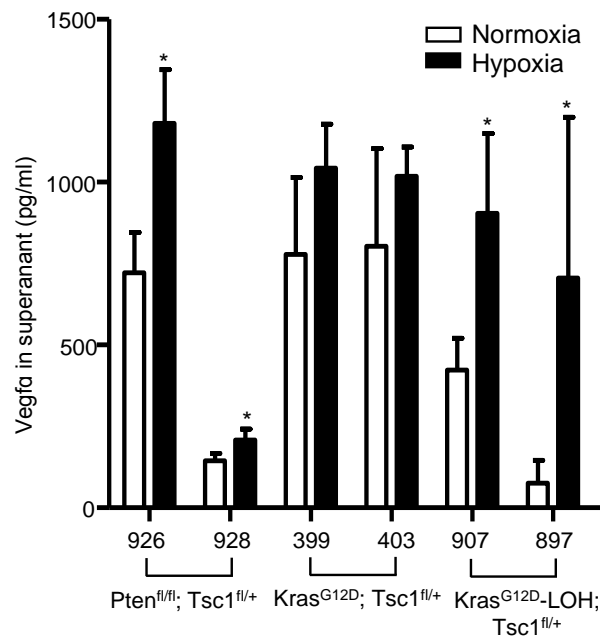


**Figure 32.** ELISA assays show an increased release of Vegfa into the supernatants of pancreatic cancer cell lines or epithelial cells after exposure to hypoxia for 24 hours. values shown are obtained from at least three independent experiments; \*:  $p < 0.05$

Next, the reasons for this defective Vegfa secretion were determined. Since Vegfa is a target gene of Hif-1 $\alpha$ , the possibility that the  $Kras^{G12D}; Tsc1^{fl/+}$  cells were not able to stabilize the Hif-1 $\alpha$  signals was ruled out. In this respect, western-blot analysis revealed that 399 and 403 cells displayed strong nuclear accumulation of Hif-1 $\alpha$  comparable to the other tested cell lines (**Fig. 33a**). In line, QRT-PCR assays revealed that the Vegfa mRNAs were significantly induced in all tested cell lines, indicating that the impaired release of Vegfa in the 399 and 403 cells was not due to altered Vegfa transcription (**Fig. 33b**). Meanwhile, the levels of phospho-S6 (p-S6<sub>Ser235/236</sub>) were reduced, whereas levels of Bnip3, which is important in mediating mitochondrial autophagy under hypoxic conditions (Zhang et al., 2008), were robustly induced. No significant differences were observed between these two cells and the other tested cell lines. These data demonstrated that general metabolic adaptive processes under hypoxic conditions were normal and neither Tsc1 haploinsufficiency nor  $Kras^{G12D-LOH}$  had a significant influence on these adaptive changes. Interestingly, the hypoxia-induced REDD1 (DNA-damage-inducible transcript 4) expression was more pronounced and that



basal levels of AMPK phosphorylation were higher in cancer cells with  $Kras^{G12D}$ -LOH in comparison to others. The exact biological significance and reasons for these observations remain to be defined (**Fig. 33a**).

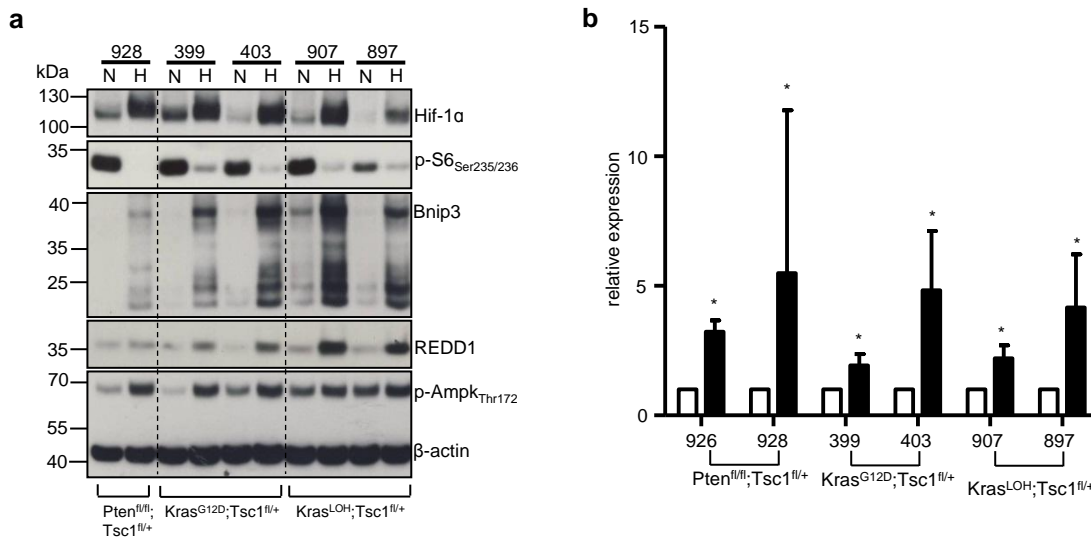


**Figure 33.** (a) Western-blot analysis shows expression of Hif-1 $\alpha$ , p-S6<sub>Ser235/236</sub>, Bnip3, REDD1 and p-Ampk<sub>Thr172</sub> in Tsc1 haploinsufficient cancer cells with  $Kras^{G12D}$  (399, 403) or with  $Kras^{G12D}$ -LOH (907, 897) after exposure to hypoxia for 24 hours; a Pten<sup>fl/fl</sup>; Tsc1<sup>fl/+</sup> cell line (928) was used as the control. N: normoxia, H: hypoxia; one representative blot out of three independent experiments is shown; (b) Vegfa mRNA levels measured by QRT-PCR were induced by hypoxia in all tested cell lines. Data are presented as relative expression (normalized to the median of the respective expression level under normoxia); an unpaired t-test was performed; values shown are obtained from at least three independent experiments; \*: p<0.05.

Since the secretion and folding of Vegfa strictly rely on the formation of a disulfide bond in the ER (Malhotra and Kaufman, 2007; May et al., 2005; Wouters and Koritzinsky, 2008), which is an oxidative reaction (oxygen provides the ultimate oxidative power), it is likely that high-throughput basal secretions of Vegfa rendered the ER homeostasis of these cells more vulnerable to oxygen deprivation. Indeed, Bip, which is a sensitive marker for ER stress, was dramatically induced by hypoxia in  $Kras^{G12D}$ ; Tsc1<sup>fl/+</sup> cells (399 and 403 cells) with relatively high levels of basal Vegfa secretion (**Fig. 34a**). The  $Kras^{G12D}$ -LOH; Tsc1<sup>fl/+</sup> cells and Pten<sup>fl/fl</sup>; Tsc1<sup>fl/+</sup> cells were resistant to hypoxia-induced ER stress. As the internal control, the expression of protein disulfide isomerase (PDI), which is responsible for the disulfide formation, was comparable between these cell lines and remained unchanged under hypoxic conditions (**Fig. 34a**). In line,

the cancer cells within the hypoxic zone of  $Kras^{G12D}; Tsc1^{fl/+}$  mice were specifically positive for Bip, confirming its occurrence *in vivo*. In contrast, no such staining patterns were observed in the cystic lesions of the  $Pten^{fl/fl}; Tsc1^{fl/+}$  mice (**Fig. 34b**). Consistently, there was no difference in the staining intensity of PDI in pancreatic cancer/cystic tissues from  $Kras^{G12D}; Tsc1^{fl/+}$  and  $Pten^{fl/fl}; Tsc1^{fl/+}$  mice (**Fig. 34c**). Furthermore, Bip-positive cells were also detected in the vicinity of tumor necrosis in the transplanted tumors formed by  $Kras^{G12D}; Tsc1^{fl/+}$  cells, however, there was no such pattern in the transplanted tumors formed by  $Kras^{G12D}$ -LOH;  $Tsc1^{fl/+}$  cells (**Fig. 34d**). Again, no difference was found in the staining of PDI between these tumors entities (**Fig. 34e**). In order to confirm the link between ER function and Vegfa secretion, the ER function of the 403 cells was altered by treating them with 4-phenyl butyric acid (PBA) and N-acetyl-cystein (NAC) and Vegfa release was then measured. PBA is a small molecule which increases the folding capacity of ER. Indeed, PBA treatment (5 mM) significantly increased Vegfa production of the cells (**Fig. 34f**). Since the ER is a highly oxidative environment optimized for protein folding (Malhotra and Kaufman, 2007), the maintenance of the oxidative potential is essential for its protein secretion function. NAC interferes with the cellular redox balance, and therefore, high doses of NAC significantly reduce Vegfa release (**Fig. 34f**). These data provide evidence that the ER function is indeed intimately linked with the angiogenic capacity of pancreatic cancer cells with a high-throughput Vegfa secretion under hypoxic conditions. This is particularly relevant to cancer cells with hyperactivated mTORC1.

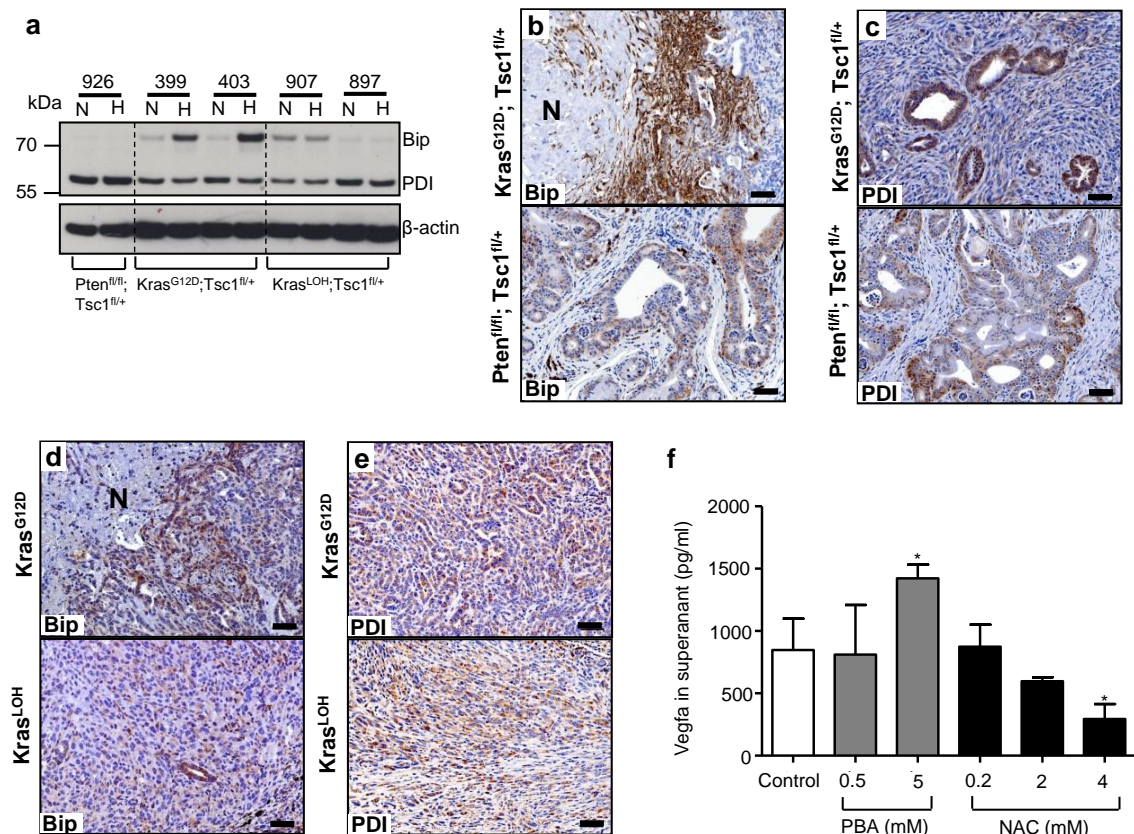


**Figure 34.** (a) Western-blot analysis demonstrates induced expression of Bip and PDI in  $Kras^{G12D}; Tsc1^{fl/+}$  cells (399, 403) and in  $Kras^{G12D}$ -LOH;  $Tsc1^{fl/+}$  cells (907, 897) after exposure to hypoxia for 24 hours; a  $Pten^{fl/fl}; Tsc1^{fl/+}$  cell line (928) was used as the control. N: normoxia, H: hypoxia; one representative blot out of three independent experiments is shown; (b-c) Representative IHC pictures show expression of Bip and PDI in pancreatic tissues obtained from  $Kras^{G12D}; Tsc1^{fl/+}$  and  $Pten^{fl/fl}; Tsc1^{fl/+}$  mice, scale bar: 50  $\mu$ m; (d-e) Representative IHC pictures show expression of Bip and PDI in the transplanted tumor tissues formed by  $Kras^{G12D}; Tsc1^{fl/+}$  and  $Kras^{G12D}$ -LOH;  $Tsc1^{fl/+}$  cells, scale bar: 50  $\mu$ m; (f) ELISA assays show release of Vegfa in 403 cells upon treatment with PBA and NAC for 24 hours; an unpaired t-test was performed by comparing to control-treated samples; values shown are obtained from at least three independent experiments; \*:  $p < 0.05$ ;

In order to investigate its relevance in human PDACs, the expression of BiP by IHC studies in another cohort of human PDACs was determined. Here, 58% (29/50) of the samples were positive for BiP (**Fig. 35a**) and the majority of human PDACs (89%; 39/44) were positive for p-mTOR<sub>ser2448</sub> (**Fig. 35b**), indicating that many human PDACs have ER stress and an active mTORC1 signaling.

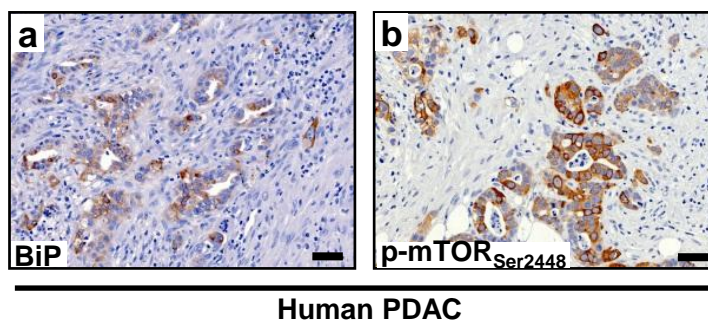


**Figure 35.** (a-b) IHC studies for BiP (ER stress marker) and p-mTOR<sub>ser2448</sub> show that the majority of human PDACs have ER stress and an active mTOR signaling, scale bar: 50  $\mu$ m.

In summary,  $Kras^{G12D}$  and  $Tsc1$  haploinsufficiency lead to hyperactivated mTORC1 in pancreatic cancer cells, which sustain high levels of basal Vegfa secretion. However, this high-throughput Vegfa secretion renders the folding machineries of the ER more susceptible to hypoxic stress. The subtle changes in oxygen cause severe ER stress, leading to impaired Vegfa secretion under hypoxic conditions, which further aggravates local hypoxia. Due to unknown

reasons, pancreatic cancer cells are able to overcome this vicious cycle by deleting the WT Kras allele and simultaneously acquire an anaplastic phenotype.

#### 4.11. T cell immunity prevents cystic lesions from malignant transformation in $Pten^{fl/fl}; Tsc1^{fl/+}$ mice

Since three cell lines (926, 928 and 952 cells) established from  $Pten^{fl/fl}; Tsc1^{fl/+}$  mice had a highly active PI3K/Akt-driven mTORC1 activity and that they were able to proliferate in vitro, it remains unknown why these cystic lesions were unable to further progress into invasive tumors. Recently, it has been shown that antitumor T cell immunity plays a crucial role in the early stages of pancreatic carcinogenesis (Bayne et al., 2012; Pylayeva-Gupta et al., 2012). Hence, it is possible that these cystic lesions were not able to escape T cell immunity. Using a panel of immune cell markers, the immune cell infiltrates within the cystic lesions were profiled. Cancer tissues from  $Kras^{G12D}; Tsc1^{fl/+}$  mice were used as controls. This analysis revealed that the cystic lesions were severely infiltrated by T cells in comparison to tumor tissues from  $Kras^{G12D}; Tsc1^{fl/+}$  mice (**Fig. 36a**). Quantitative evaluation revealed that the number of T cells infiltrating these cystic lesions were 16-fold higher than that in the tumor tissues of  $Kras^{G12D}; Tsc1^{fl/+}$  mice (**Fig. 36b**). However, no significant differences were found regarding the number of B cells, macrophages or neutrophils (**Fig. 36c, 36d, 36e**).

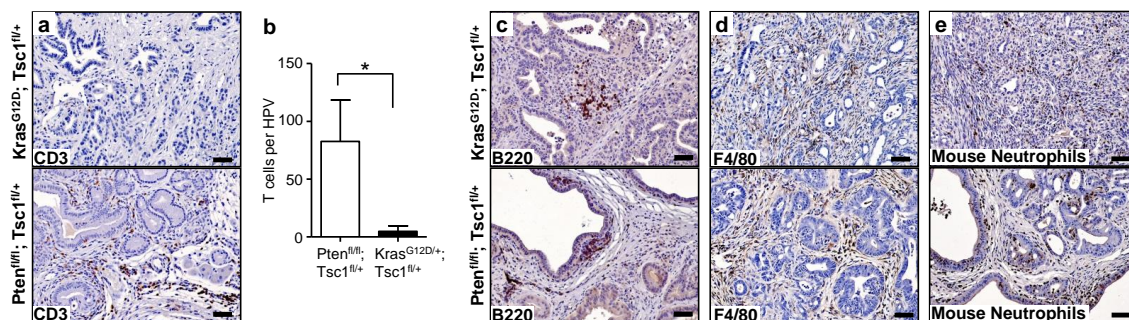


**Figure 36.** (a) IHC studies for CD3 demonstrate a severe T cell infiltration in the cystic lesions of  $Pten^{fl/fl}; Tsc1^{fl/+}$  mice (lower panel), but not in the cancer tissues of  $Kras^{G12D}; Tsc1^{fl/+}$  mice (upper panel), scale bar: 50  $\mu$ m; (b) Quantification of infiltrating T cells shows that the cystic lesions developing in  $Pten^{fl/fl}; Tsc1^{fl/+}$  mice (n=3) contain 16 times more T cells than the tumor tissues developing in  $Kras^{G12D}; Tsc1^{fl/+}$  mice (n=3); unpaired t-test, \*: p<0.05. (c-e) IHC studies using B220, F4/80 and mouse neutrophils antibodies demonstrate no differences in the number of infiltrating B cells, macrophages and neutrophils between cystic lesions in the  $Pten^{fl/fl}; Tsc1^{fl/+}$  mice (lower panel) and cancer tissues of  $Kras^{G12D}; Tsc1^{fl/+}$  mice (upper panel); scale bar: 50  $\mu$ m.

These data suggest that the cystic lesions are highly immunogenic and are able to trigger a strong antitumor T cell immunity that eliminates any cell with an invasive potential. Hence, the tumor-initiating capacities of 3 cell lines (926, 928 and 952: derived from cystic lesions of  $Pten^{fl/fl}; Tsc1^{fl/+}$  mice) were tested in WT mice and in BALB/c nude mice (which lack a functional T cell immunity). Compellingly, none of three cell lines gave rise to tumors in WT mice by orthotopical implantation (**Table 7**). However, they all effectively formed PDAC in BALB/c nude mice at a nearly 100% penetrance by subcutaneous injection (29/30, **Fig. 37a**, **Table 7**). An overview of the transplanted cell lines, mouse numbers, and tumor incidence is provided in **Table 7**.

**Table 7.** Tumor formation of  $Pten^{fl/fl}; Tsc1^{fl/+}$  cells in WT and BALB/c nude mice

Cell lines	Genotype	Primary lesions	WT mice		BALB/c nude mice	
			Tumor/Total	Rate (%)	Tumor/Total	Rate (%)
926	$Pten^{fl/fl}; Tsc1^{fl/+}$	Cystic lesions	0/19	0%	17/18	94%
928	$Pten^{fl/fl}; Tsc1^{fl/+}$	Cystic lesions	0/4	0%	6/6	100%
952	$Pten^{fl/fl}; Tsc1^{fl/+}$	Cystic lesions	0/27	0%	6/6	100%

Depending on the cell lines, histological examination revealed that the tumors contained either large or small cystic lesions, precisely recapitulating the morphologies of the respective primary cystic lesions (**Fig. 37b**). Importantly, focal invasions were observed in these tumors (**Fig. 37b**). IHC studies for descriptive “pathway” analyses of the transplanted tumors revealed that these were strongly positive for p-Akt<sub>Ser473</sub> and p-mTOR<sub>Ser2448</sub>, indicating an activation of the PI3K/Akt-mTORC1 axis within these tumors; however, cells that positively stained for p-Erk1/2<sub>Thr202/Tyr204</sub> were significantly enriched especially within the area between the tumor and the normal tissues. Due to unknown reasons, cells positive for p-S6<sub>Ser235/236</sub> were rarely observed (**Fig. 37c**). Taken together, these data suggest that the T cell immunity constitutes an important barrier for invasive transformation of pancreatic epithelial cells driven by the PI3K/Akt-mTORC1 axis.

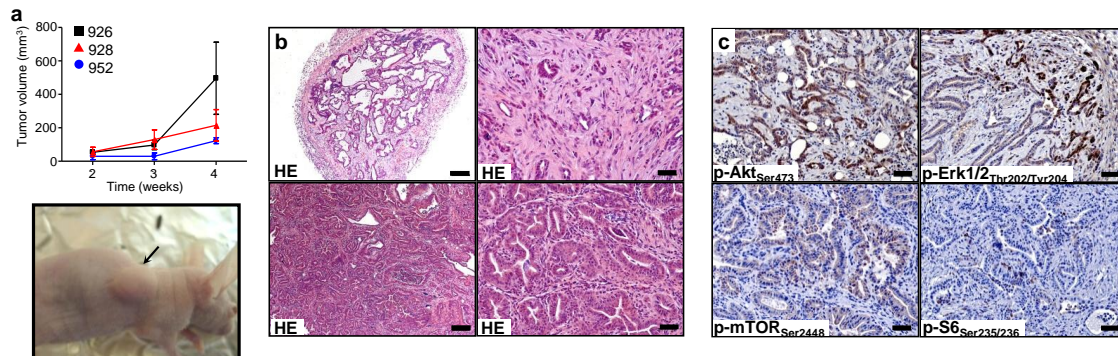


**Figure 37.** (a) The weekly-measured tumor size shows tumor growth of transplanted cancer cells (926, 928 and 952) in BALB/c nude mice; (b)

H&E-stained sections show cystic lesions in the transplanted tumors (left panel; scale bar: 200  $\mu\text{m}$ ) with invasive components (right panel; scale bar: 50  $\mu\text{m}$ ) (c) Representative IHC pictures show activation of Akt (p-Akt<sub>Ser473</sub>), Erk (p-Erk1/2<sub>Thr202/Tyr204</sub>), mTORC1 (p-mTOR<sub>Ser2448</sub>) and S6 (p-S6<sub>Ser235/236</sub>) in the transplanted tumor tissues, scale bar: 50  $\mu\text{m}$ .

## 4.12. Tsc1 haploinsufficiency and p53 deficiency promote pancreatic malignancy

As previously demonstrated, Tsc1 deficiency induced a hyperactivated mTORC1, which eventually resulted in degeneration of the pancreas. Activation of the p53 pathway also seems to be involved in this process. In order to determine the biological relevance of p53 activation, p53 was inactivated in the context of Tsc1 haploinsufficiency and Tsc1 deficiency. Two p48<sup>Cre</sup>; p53<sup>fl/fl</sup>; Tsc1<sup>fl/fl</sup> (hereafter: p53<sup>fl/fl</sup>; Tsc1<sup>fl/fl</sup>) mice were generated and studied. One of them died at the age of 237 days with a large pancreatic tumor (**Fig. 38a**). Histological examination of the tumor revealed that the tumor cells were highly proliferative (**Fig. 38c**) and showed distinctive tumor morphology reminiscent of acinar carcinoma (**Fig. 38b**). The second mouse died at the age of 98 days. Although no tumor was found in the pancreas of this mouse, histological examination showed severe nuclear abnormalities (mainly enlarged nuclei) in acinar cells (**Fig. 38d**). In contrast, the p48<sup>Cre</sup>; p53<sup>fl/fl</sup>; Tsc1<sup>fl/+</sup> (hereafter: p53<sup>fl/fl</sup>; Tsc1<sup>fl/+</sup>) mice were healthy and no tumor or severe nuclear abnormalities were found in their pancreases (n=7). Occasionally, acinar cells with enlarged nuclei were found in the aged animals (**Fig. 38g**). In order to characterize the signal changes caused by Tsc1 and p53 deficiency, a set of cell lines were established from the above mentioned transgenic mice. Briefly, two cell lines (961 and 911) which were Tsc1-haploinsufficient and p53-deficient were established from the p53<sup>fl/fl</sup>; Tsc1<sup>fl/+</sup> mice and two cell clones (946 and 946F) which were deficient for both Tsc1 and p53 were established from the above mentioned tumor mice with p53 and Tsc1 deficiency. The respective genotype of the isolated cell lines was confirmed by PCR analysis (**Supplementary Fig. 1**). In line with the reported observation that p53-deficient mouse pancreatic epithelial cells undergo epithelial-mesenchymal transition (EMT) in culture (Pinho et al., 2011), two p53<sup>fl/fl</sup>; Tsc1<sup>fl/+</sup> cell lines exhibited homogeneous fibroblast-like morphologies in vitro (**Fig. 39h**). Regarding the two cell lines isolated from the tumor mouse, one of them showed a stable epithelial morphology without obvious signs of EMT (946, **Fig. 39e**) while the other one displayed a fibroblast-like phenotype with scattered islands of epithelial cells (946F, **Fig. 39f**), suggesting a dynamic transition between EMT and MET (mesenchymal-epithelial transition).

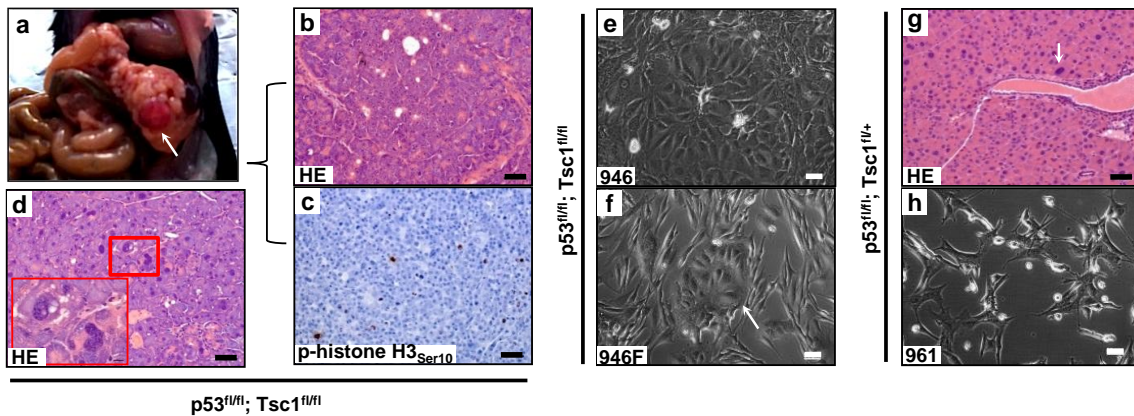


**Figure 38.** (a) Gross pathology of a tumor of a  $p53^{fl/fl}; Tsc1^{fl/fl}$  mouse; (b-c) An H&E–stained section and an IHC of p-histone  $H3_{Ser10}$  show a tumor morphology resembling acinar carcinoma and proliferation of tumor cells, scale bar: 50  $\mu$ m; (d) An H&E–stained section shows nuclear abnormalities in acinar cells, scale bar: 50  $\mu$ m; (e, f, h) Phase contrast images of isolated cells show the fibroblast-like (961, 911 and 946F) and epithelial (946) morphologies of isolated cells from  $p53^{fl/fl}; Tsc1^{fl/+}$  (911 and 961) and  $p53^{fl/fl}; Tsc1^{fl/fl}$  (946 and 946F) mice, scale bar: 50  $\mu$ m, arrow: epithelial island; (g) An H&E–stained section shows acinar cells with an enlarged nucleus in the pancreas of  $p53^{fl/fl}; Tsc1^{fl/+}$  mice, scale bar: 50  $\mu$ m, arrow: cells with enlarged nucleus.

Western-blot analysis confirmed that the cell lines with EMT features (911, 961 and 946F) expressed low levels of E-Cadherin but high levels of Vimentin, compared to those (946, 926, 928 and 952) without EMT features in culture. In addition, Tsc1 expression in the Tsc1-deficient cell lines (946 and 946F) was not detectable even after extended exposure (**Fig. 39a**). These data demonstrated that the fibroblast-like cells (EMT cells) were unlikely to be derived from the pancreas-resident fibroblasts which would still maintain expression of Tsc1. Thereafter, using these isolated cell lines, the signal changes caused by Tsc1 and p53 deficiency in pancreatic epithelial cells were characterized by serum stimulation assays. Unlike  $Pten^{fl/fl}$ ,  $Tsc1^{fl/+}$  or  $Kras^{G12D}$ ,  $Tsc1^{fl/+}$  cells, no constitutively active Akt and Erk signaling was observed but serum treatment induced pronounced Akt and Erk phosphorylation in these cells; though to a much lesser extent in the Tsc1-deficient cells (946 and 946F) than that in Tsc1-haploinsufficient cells (911 and 961). This observation was consistent with reported results showing that Tsc1 mutant cells displayed an impaired activation of PI3K/Akt signaling (Harrington et al., 2004) (**Fig. 39b**, upper panel). All tested cells have high levels of mTORC1 which can be further activated by serum treatment in the 911 and 961 cells. MTORC1 in the Tsc1-deficient cells (946 and 946F) was constantly active and serum treatment only had marginal effects (**Fig. 39b**, lower panel).

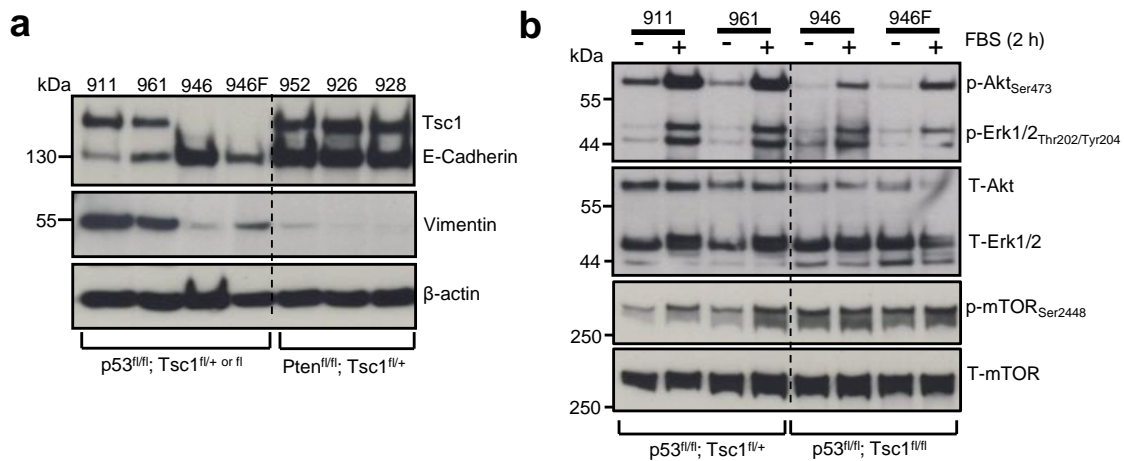


**Figure 39.** (a) Western-blot analysis demonstrates expression of Tsc1 and E-Cadherin in cells with Tsc1 deficiency or haploinsufficiency; the cells with a fibroblast-like morphology have lower levels of E-Cadherin but higher levels of Vimentin than those with epithelial morphologies; cells isolated from the cystic lesions of Pten<sup>fl/fl</sup>; Tsc1<sup>fl/+</sup> mice (926 and 928) were used as external controls. (b) Western-blot analysis demonstrates the steady-state and serum (FBS)-stimulated phosphorylation of Akt (p-Akt<sub>Ser473</sub>), Erk (p-Erk1/2<sub>Thr202/Tyr204</sub>), mTORC1 (p-mTOR<sub>Ser2448</sub>) in cells with p53 and Tsc1 deficiency (or haploinsufficiency). One representative immunoblot out of three independent experiments is shown.

These signal events in vivo were analyzed by IHC studies. This analysis confirmed the in vitro findings: pancreatic epithelial cells in p53<sup>fl/fl</sup>; Tsc1<sup>fl/+</sup> mice and tumor cells (and acinar cells) in p53<sup>fl/fl</sup>; Tsc1<sup>fl/fl</sup> mice were generally devoid of p-Akt<sub>Ser473</sub> and p-Erk1/2<sub>Thr202/Tyr204</sub> stainings (**Fig. 40a, 40b**); pancreatic acinar cells of p53<sup>fl/fl</sup>; Tsc1<sup>fl/+</sup> mice had detectable phosphorylation levels of p-mTOR<sub>Ser2448</sub> and p-S6<sub>Ser235/236</sub>, however, the staining intensities in the cancer cells (or acinar cells) of p53<sup>fl/fl</sup>; Tsc1<sup>fl/fl</sup> mice were more pronounced (**Fig. 40c, 40d**). Taken together, p53- and Tsc1-deficiency (or haploinsufficiency) triggered autonomous mTORC1 signaling independent of Kras<sup>G12D</sup>/Erk and PI3K/Akt signaling in the pancreas.



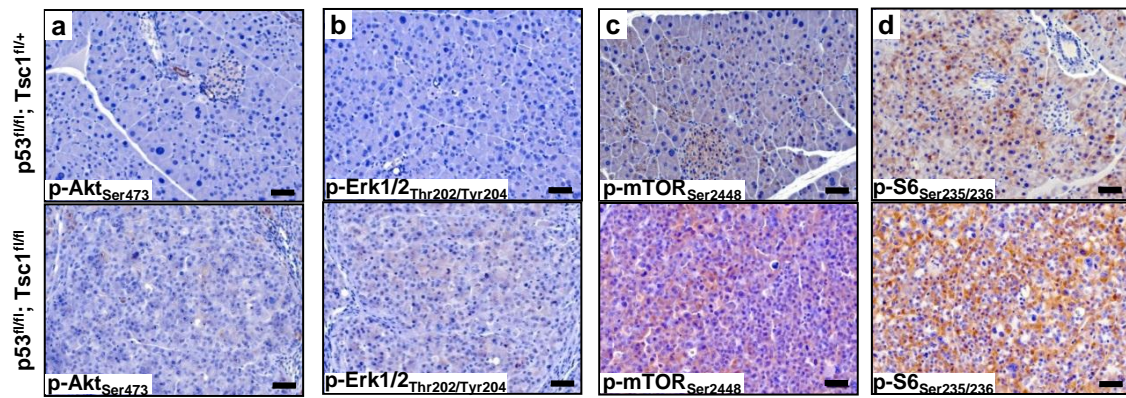


**Figure 40.** (a-d) Representative IHC pictures show phosphorylation levels of Akt (p-Akt<sub>Ser473</sub>), Erk (p-Erk1/2<sub>Thr202/Tyr204</sub>), mTORC1 (p-mTOR<sub>Ser2448</sub>) and S6 (p-S6<sub>Ser235/236</sub>) in pancreatic tissues obtained from p53<sup>fl/fl</sup>; Tsc1<sup>fl/+</sup> (upper panel) and p53<sup>fl/fl</sup>; Tsc1<sup>fl/fl</sup> (lower panel) mice, scale bar: 50  $\mu$ m.

Since the combination of Tsc1 and p53 deficiency was able to initiate pancreatic carcinogenesis in mice, the tumorigenicities of these cells lines were tested through orthotopical implantation into WT mice and subcutaneous injection into BALB/c nude mice. As such, none of the tested cells lines were able to form tumors in WT mice (n=24; **Table 8**). However, 67% of the sites (16/24) injected with cells with EMT features (cell lines 911, 961 and 946F) formed tumors while none of the sites (0/3) injected with the cells without EMT features (946) gave rise to tumors in BALB/c nude mice (**Table 8**). An overview of the transplanted cells, mouse numbers and tumor formation is provided in **Table 8**.

**Table 8.** Tumor formation of p53<sup>fl/fl</sup>; Tsc1<sup>fl/+ or fl</sup> cells in WT and BALB/c nude mice

Cell lines	Genotype	Primary lesions	WT mice		BALB/c nude mice	
			Tumor/Total	Rate (%)	Tumor/Total	Rate (%)
911	p53 <sup>fl/fl</sup> ; Tsc1 <sup>fl/+</sup>	Normal	0/4	0%	4/6	67%
961	p53 <sup>fl/fl</sup> ; Tsc1 <sup>fl/+</sup>	Normal	0/4	0%	5/6	83%
946	p53 <sup>fl/fl</sup> ; Tsc1 <sup>fl/fl</sup>	Acinar carcinoma	0/8	0%	0/3	0%
946F	p53 <sup>fl/fl</sup> ; Tsc1 <sup>fl/fl</sup>	Acinar carcinoma	0/8	0%	7/9	78%

Histological characterization of the tumor tissues revealed that tumors developed from p53<sup>fl/fl</sup>; Tsc1<sup>fl/+</sup> cells (911, 961) were solid/anaplastic adenocarcinomas with few ducts and contained a high proportion of stroma components whereas tumors

developed from  $p53^{fl/fl}; Tsc1^{fl/fl}$  cells (946F) were more cellular and exhibited anaplastic appearances with less pronounced stroma components (**Fig. 41a, 41b**). IHC demonstrated that the tumor cells forming ducts were positively stained by E-Cadherin antibodies whereas the anaplastic components were largely negative in both tumor entities (**Fig. 41c**).

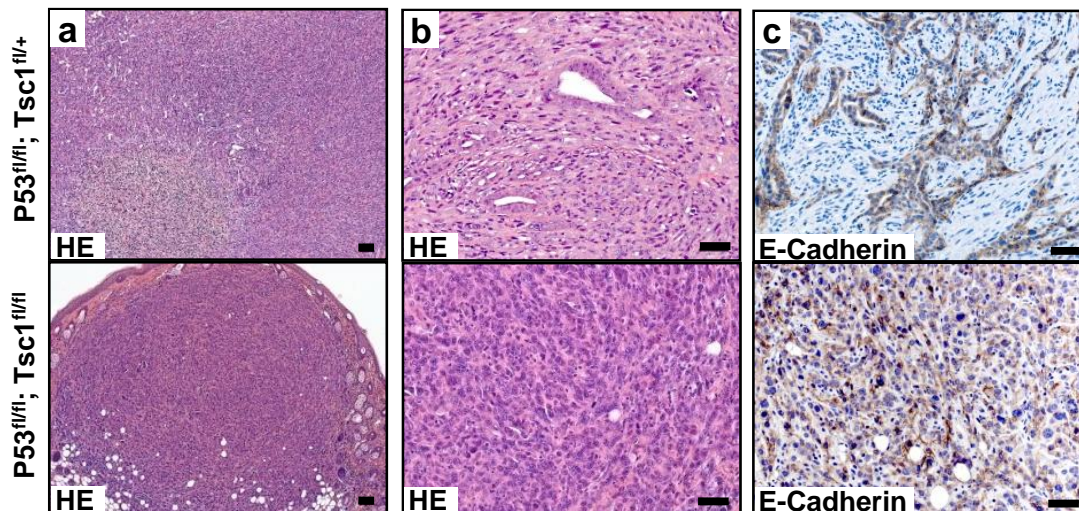


**Figure 41.** (a-b) H&E–stained sections demonstrate the histologies of the tumors developed from  $p53^{fl/fl}; Tsc1^{fl/+}$  (911 and 961 cells, upper panel) and  $p53^{fl/fl}; Tsc1^{fl/fl}$  (946F cells, lower panel) cells in BALB/c nude mice, left panel; scale bar: 100  $\mu\text{m}$ , right panel; scale bar: 50  $\mu\text{m}$ ; (c) IHC studies for E-cadherin demonstrate positively stained ductal structures in both tumor entities, scale bar: 50  $\mu\text{m}$ .

In order to determine whether the EMT process actively took place in these tumors, a double-staining for Krt19 and Vimentin was performed. This analysis revealed that a majority of cancer cells including those forming ducts and showing an anaplastic appearance were positive for Vimentin and that a subset of cancer cells were double-positive for Krt19 and Vimentin, indicating an ongoing EMT process of these cells (**Fig. 42a, 42b**). In particular, Vimentin-negative cancer cells were observed in tumors derived from  $p53^{fl/fl}; Tsc1^{fl/+}$  cells, implying their intrinsic resistance towards EMT (**Fig. 42b**). However, cancer cells that had undergone EMT were largely negative for another mesenchymal marker,  $\alpha$ -SMA ( $\alpha$ -smooth muscle actin), that usually labels activated fibroblasts (**Fig. 42c, 42d**).

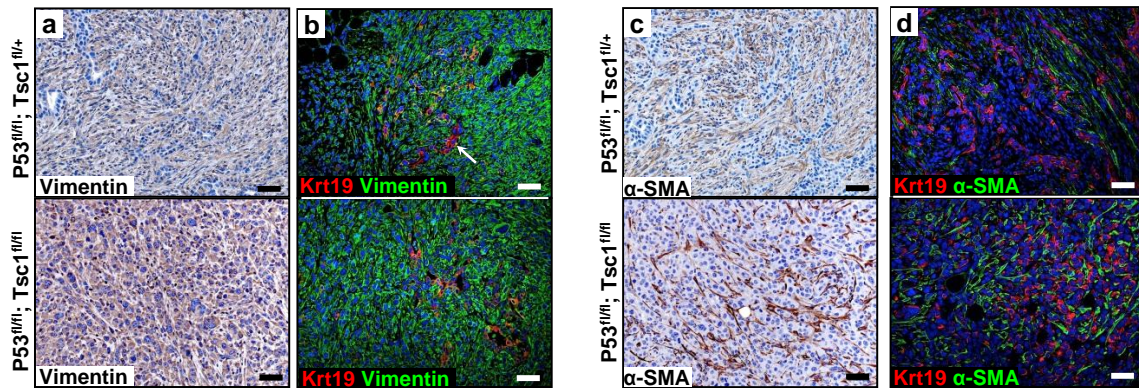


**Figure 42.** (a-b) IHC studies for Vimentin and double-IF studies for Krt19 and Vimentin demonstrate an active EMT process in tumor tissues formed by  $p53^{fl/fl}$ ;  $Tsc1^{fl/+}$  and  $p53^{fl/fl}$ ;  $Tsc1^{fl/fl}$  cells in BALB/c nude mice, scale bar: 50  $\mu\text{m}$ ; arrow: cancer cells without EMT; (c-d) IHC studies for  $\alpha$ -SMA and double-IF studies for Krt19 and  $\alpha$ -SMA show that “EMT cells” are negative for  $\alpha$ -SMA, scale bar: 50  $\mu\text{m}$ .

Taken together, disruption of the Tsc/mTORC1/p53 signal loop in the pancreas serves to decrease resistance towards malignant transformation. One of the potential reasons lies in a facilitated EMT process triggered by p53 deficiency and Tsc1 dysfunction in pancreatic epithelial cells.

#### 4.13. Identification of an ALDH1A3-positive subtype of human PDAC

Although inactivation of the Tsc/mTORC1/Pten or the Tsc/mTORC1/p53 signal loop exposed the exocrine pancreas to a risk of malignant transformation, only the combination of  $Kras^{G12D}$  and Tsc1 haploinsufficiency was effective in initiating metastatic PDACs in mice. In order to determine whether this tumor entity also existed in humans, microarray analyses on the representative cell lines (399, 403, 907 and 897) were performed to search for subtype-specific markers. The closely related cell lines in which mTORC1 is either activated by Pten deficiency and Tsc1 haploinsufficiency (926, 928 and 952) or by p53 deficiency and Tsc1 deficiency or haploinsufficiency (911, 961, 946 and 946F) were used as controls to filter out those genes which may generally contribute to tumor progression but not to the aggressive nature of this particular subtype. Using 0.001 as the statistical cut-off for the false discovery rate (FDR), 4234 genes were differentially expressed genes between three groups (which represent 20.4% of all genes on the array; the top 100 genes are listed in **Supplementary Table 1**). Based on the expression of the top-10 genes with the smallest p-values (Trp53, Hspb8, Fam84a, Aldh1a3, Eml2, Cadps, 1700007K13Rik, Ano3, Unc13a, Wfdc2), 3 groups of cell lines were clearly separated from each other by principal

component analysis (PCA, **Fig. 43a**), underscoring the group distinctiveness of these cell lines. By merging two groups of cells lines, the top 20 up-regulated genes (as compared to the merged group) with the largest fold changes in the third group were then identified (as described in the methods part). For example, the 20 genes that were specifically up-regulated in the  $Kras^{G12D}; Tsc1^{fl/+}$  cell lines were deemed as the “ $Kras^{G12D}/Erk-mTOR$  signature”. As such, the “ $Pten/Akt-mTOR$  signature” and the “ $p53-mTOR$  signature” were identified for  $Pten^{fl/fl}; Tsc1^{fl/+}$  cells and  $p53^{fl/fl}; Tsc1^{fl/+ \text{ or } fl}$  cell lines, respectively. The resulting 60 genes are visualized in **Fig. 43b**. Among these 60 genes, *Cdh17* (liver-intestine cadherin), *Wfdc2* (also known as HE4, WAP four-disulfide core domain 2) and *Gabrp* ( $\gamma$ -aminobutyric acid A receptor, pi) were shared by the  $Kras^{G12D}/Erk-mTOR$  and  $Pten/Akt-mTOR$  signatures. These genes have previously been reported to be expressed by human PDAC tissues and cell lines, indicating the general representation of these mouse cell lines in the human disease (**Fig. 43b**) (Galgano et al., 2006; Panarelli et al., 2012; Su et al., 2008; Takehara et al., 2007). As for the  $Kras^{G12D}/Erk-mTOR$  signature, two genes on top of the list, *Tns4* (also known as *Cten*) and *Il1 $\alpha$* , which are target genes of  $Kras^{G12D}$ , have been reported to be linked with cell motility and metastasis of PDAC (**Fig. 43b**) (Al-Ghamdi et al., 2011; Al-Ghamdi et al., 2013; Ling et al., 2012). In particular, the gene with the lowest p value is *Aldh1a3* (aldehyde dehydrogenase 1 family, member A3) which is considered to be a marker for cancer stem cells (CSCs) in a variety of cancer entities (Marcato et al., 2011a; Marcato et al., 2011b). Though ALDH1 expression is associated with mesenchymal features of PDAC and its expression is an unfavourable factor for patient survival (Kahlert et al., 2011; Rasheed et al., 2010), it is largely unclear which isoform (mainly ALDH1A1 vs. ALDH1A3) actually contributes to the unfavourable biology of the tumors. Therefore, the expressions of 20 Aldh family members were analyzed in the cell lines. This analysis revealed that expression of *Aldh1a3* was associated with the  $Kras^{G12D}/Erk-mTOR$  signature while expression of *Aldh1a1* was rather associated with the  $Pten/Akt-mTOR$  and  $p53-mTOR$  signatures (**Fig. 43c**).

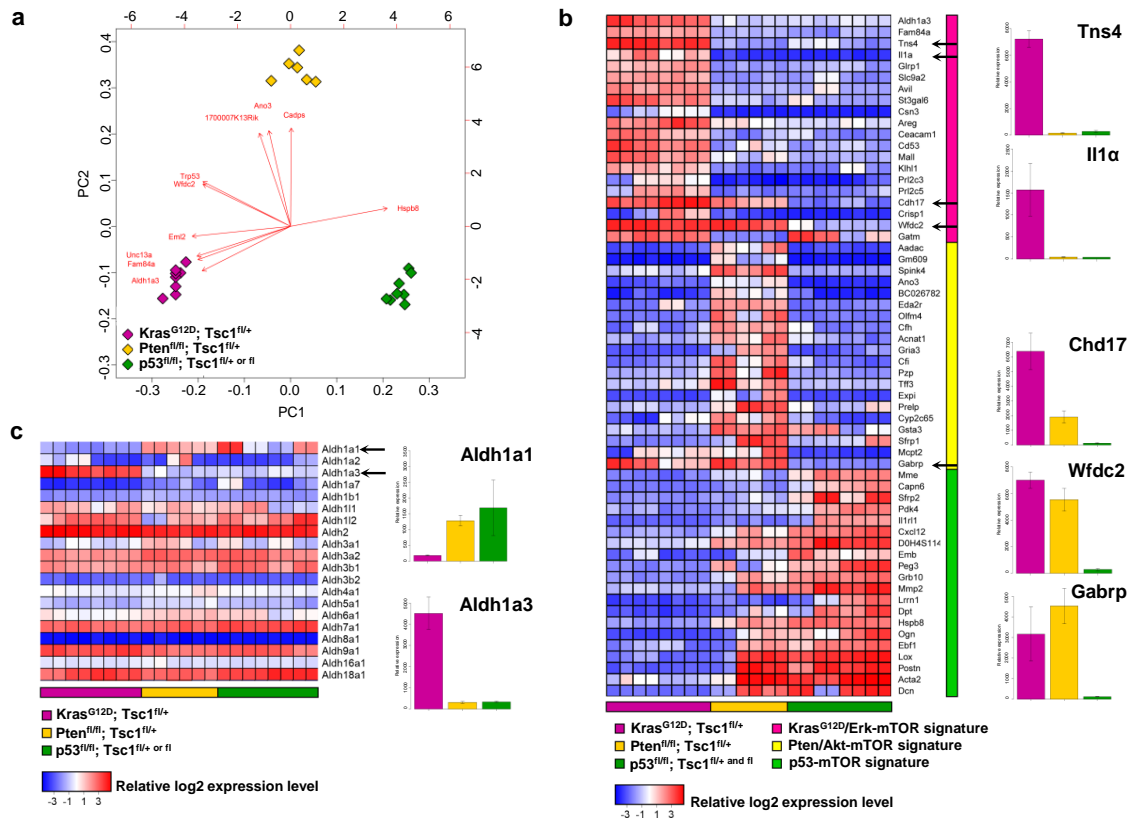


**Figure 43.** (a) PCA analysis demonstrates the group distinctiveness of the analyzed cell lines; (b) The heatmap shows the 20-gene signature that represents different groups of cell lines; *Cdh17*, *Wfdc2* and *Gabrp* are highly expressed by both  $Kras^{G12D}; Tsc1^{fl/+}$  and  $Pten^{fl/fl}; Tsc1^{fl/+}$  cells; however, *Tns4* and *Il1a* are only expressed by the  $Kras^{G12D}; Tsc1^{fl/+}$  cells. (c) The heatmap demonstrates expressions of 20 Aldh members in the three groups of cell lines; *Aldh1a3* is highly expressed by  $Kras^{G12D}; Tsc1^{fl/+}$  cells whereas *Aldh1a1* is highly expressed by  $Pten^{fl/fl}; Tsc1^{fl/+}$  and  $p53^{fl/fl}; Tsc1^{fl/+ \text{ or } fl}$  cells.

Furthermore, expression of *Aldh1a3*, *Aldh1a1* and *Il1a* was validated by QRT-PCR assay in 6 additional  $Kras^{G12D}; Tsc1^{fl/+}$  cancer cell lines (Fig. 44a). Western-blot analysis confirmed *Aldh1a3* expression in  $Kras^{G12D}; Tsc1^{fl/+}$  cancer cell lines (Fig. 44b). In addition, *Aldh1a3* expression in vivo was validated by IHC studies: cancer cells in  $Kras^{G12D}; Tsc1^{fl/+}$  mice were strongly stained by *Aldh1a3* antibodies whereas the cystic lesions in  $Pten^{fl/fl}; Tsc1^{fl/+}$  mice were largely negative (Fig. 44c), with the exception of the region with invasive cells (Fig. 44d). Importantly, the same tissue also showed a high activity of Erk signalling, suggesting that *Aldh1a3* expression may be affected by Erk signalling. Taken together, these data suggested that *Aldh1a3* may constitute an important marker that represented the metastatic tumour entity of  $Kras^{G12D}; Tsc1^{fl/+}$  mice.

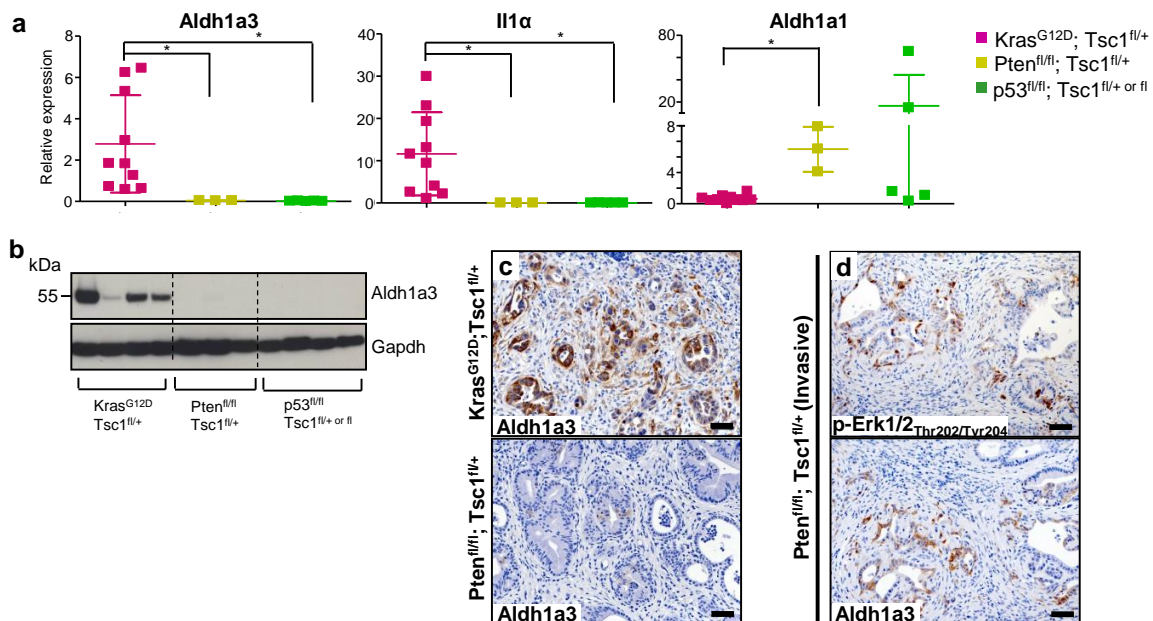


**Figure 44.** (a) QRT-PCR analysis shows mRNA levels of Aldh1a3, Il1 $\alpha$  and Aldh1a1 in different mouse cell lines (normalized to the median expression levels of all cell lines); Data are presented as relative expressions; unpaired t-test, \*:  $p < 0.05$ ; (b) Western-blot analysis shows expression of Aldh1a3 in  $Kras^{G12D}; Tsc1^{fl/+}$  cells, but not in other cell line; one representative blot out of three independent experiments is shown. (c) IHC studies for Aldh1a3 demonstrate positively stained cancer cells in  $Kras^{G12D}; Tsc1^{fl/+}$  mice, but not in cystic lesions of  $Pten^{fl/fl}; Tsc1^{fl/+}$  mice; scale bar: 50  $\mu$ m; (d) IHC studies for p-Erk1/2<sub>Thr202/Tyr204</sub> and Aldh1a3 demonstrate positive stainings in the cystic lesions with invasive features of one  $Pten^{fl/fl}; Tsc1^{fl/+}$  mouse; scale bar: 50  $\mu$ m.

It remains unknown whether ALDH1A3 also labeled a particular subtype of human PDAC. Expression of ALDH1A1 was employed as an internal control. QRT-PCR and Western-blot analysis revealed that 3 out of 8 tested human PDAC cell lines expressed high levels of ALDH1A3 (**Fig. 45a, 45b**). In line with the observations in the mouse cell lines, expression of ALDH1A1 and ALDH1A3 seemed to be mutually exclusive; in the human PDAC cell lines with high levels of ALDH1A3 (Aspc-1, Bxpc-3 and Su86.86), low levels of ALDH1A1 (vice versa) were seen (**Fig. 45a, 45b**). QRT-PCR of bulk normal pancreatic tissues ( $n=10$ ) and PDAC ( $n=20$ ) tissues revealed significant upregulation of ALDH1A3 mRNA expression in PDAC (5 folds; **Fig. 45c**, lower left panel) whereas expression of ALDH1A1 was rather down-regulated (**Fig. 45c**, lower right panel); meanwhile, both TSC1 and TSC2 mRNA expression in these PDACs were significantly down-regulated (**Fig. 45c**, upper panel). The cancer cells in 41% (21/50) of the tested tissues were ALDH1A3-positive ((**Fig. 45d**)). Kaplan-Meier analysis revealed that patients

whose cancer tissues were positive for ALDH1A3 survived significantly shorter after surgical resection than those with ALDH1A3 negativity (median survival: 14.0 vs. 22.8 months, **Fig. 44e**). Although the cancer cells in 47% (22/46) of the human PDAC tissues were strongly positive for ALDH1A1 (**Fig. 44f**), their staining intensities did not correlate with survival (**Fig. 44f**). Notably, further analysis demonstrated that ALDH1A3 expression was associated with the lymphnode (N) status of the patients. Here, 95% (20/21) of the patients with ALDH1A3-positive tumors had lymphatic invasion at the time of diagnosis. In addition, no correlation was found between ALDH1A3 expression and other clinical parameters (**Table 9**). Taken together, these data provide strong evidence that the PDAC entity of *Kras*<sup>G12D</sup>; *Tsc1*<sup>fl/+</sup> mice is represented by the ALDH1A3-positive tumor subtype in humans.

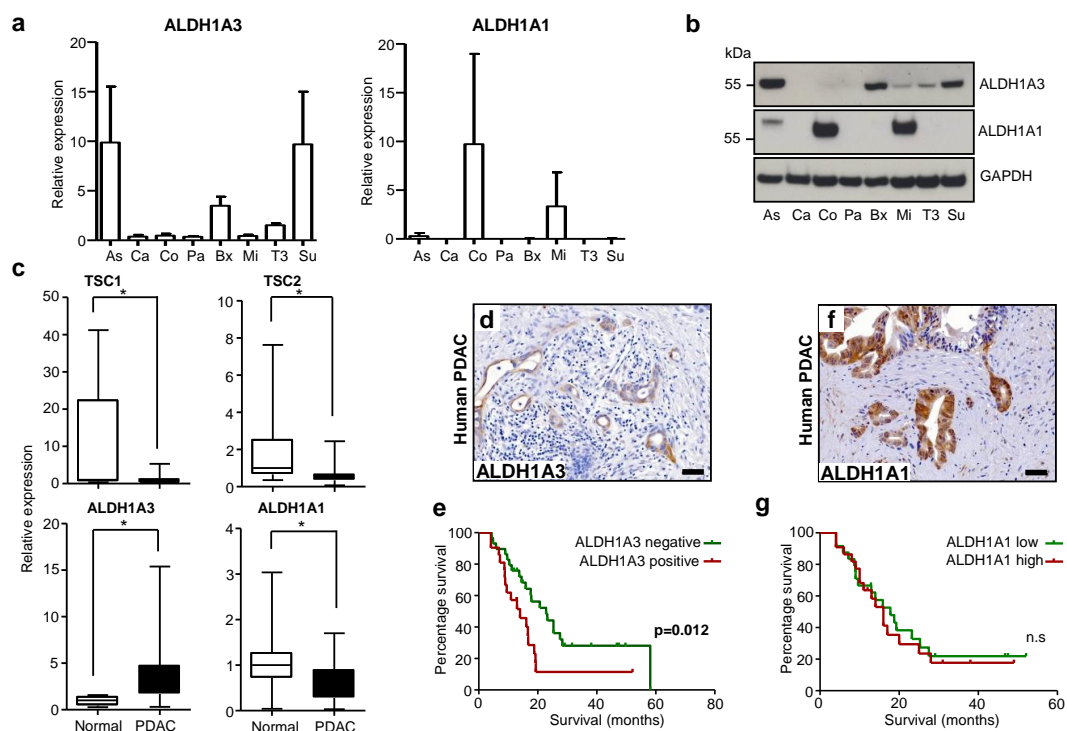


**Figure 45.** (a-b) QRT-PCR and Western-blot analysis show mRNA and protein expression of ALDH1A1 and ALDH1A3 in human PDAC cell lines (Aspc-1 (As), Capan-1 (Ca), Colo357 (Co), Panc-1 (Pa), Bx (Bxpc-3), Mia-PaCa2 (Mi), T3M4 (T3), Su86.86 (Su)); Data are presented as relative expression (normalized to the median expression level of all cell lines); values shown are obtained from at least three independent experiments; One representative blot out of three independent experiments is shown. (c) QRT-PCR data demonstrates mRNA levels of TSC1, TSC2, ALDH1A1 and ALDH1A3 in normal pancreas (n=10) and PDAC tissues (n=20), \*: p<0.05; (d) IHC studies for ALDH1A3 shows positively stained cancer cells; (e) PDAC patients whose cancer tissues are positively stained for ALDH1A3 (n=21) survived significantly shorter than those with ALDH1A3 negativity (n=29) after surgical resection (median survival: 14.0 vs. 22.8 months, logrank test:

p=0.012); (f) IHC studies for ALDH1A1 shows positively stained cancer cells; (g) Kaplan-Meier analysis demonstrates that staining intensities of ALDH1A1 in PDAC cells are not correlated with survival.

**Table 9.** Clinical characteristics and comparison between the two PDAC cohorts.

Variables	PDAC			
	ALDH1A3-negative	ALDH1A3-positive	p-value	In total
Age (years, median)	67.0	66.0	0.73 <sup>1</sup>	-
Gender				
Male	12	13	0.15 <sup>2</sup>	25
Female	17	8	0.25 <sup>3</sup>	25
Size of tumor (T)				
T2	3	2	0.39 <sup>2</sup>	5
T3	21	18	0.41 <sup>3</sup>	39
T4	5	1		6
Lymphnode (N)				
N0	12	1	0.004 <sup>2</sup>	13
N1	17	20	0,002 <sup>3</sup>	37
Metastasis (M)				
M0	27	20	0.75 <sup>2</sup>	47
M1	2	1	1.0 <sup>3</sup>	3
Grade (G)				
G1	5	0	0.11 <sup>2</sup>	5
G2	10	7	0.11 <sup>3</sup>	17
G3	14	14		28
R status				
R0	13	13	0.12 <sup>2</sup>	26
R1	11	8	0.12 <sup>3</sup>	19
unknown	5	0		5
Chemotherapy				
Yes	25	15	0.29 <sup>2</sup>	40
No	4	6		10

1: Mann-U-Whitney-Test; 2: Chi<sup>2</sup>-test; 3: Fisher's exact test



## 5. DISCUSSION

### 5.1. The HNF1A/MIA2 secretory network interacts with the ER stress/UPR system

#### 5.1.1. Common genetic variations and pancreatic cancer risk

The completion of the Human Genome and the International HapMap Projects, together with rapid improvements in genotyping technologies, has rendered GWAS in many disease entities possible (Hardy and Singleton, 2009). Such studies tend to identify common (population frequencies of more than 5%) and low-risk variants (odds ratios of 1.2 to 5.0) for a given disease (Manolio et al., 2008). Recently published GWAS studies have identified a number of loci associated with susceptibility to pancreatic cancer in different populations (Amundadottir et al., 2009; Petersen et al., 2010; Wu et al., 2012). However, in the absence of selective evolutionary pressure, these common variants only cause slight alterations of a gene's expression or a protein's function (Goldstein, 2009; McClellan and King, 2010). Therefore, it has been controversially discussed whether such minor effects add up to an increased cancer risk or whether rather the individual and rare mutations with large effects, which are usually below the detection range of GWAS studies, are responsible for the risk increase. Indeed, recent deep sequencing efforts of drug target genes revealed that many human rare variants potentially also influence human disease risk (Nelson et al., 2012). Nevertheless, genes with common mutations can actually frequently be mapped to core signaling pathways that operate in established pancreatic cancers (Jones et al., 2008), which would suggest that common variants affecting cancer susceptibility may also influence the biological behavior of pancreatic cancer cells. In the current study, a common variant of MIA2, MIA2<sup>I41M</sup>, is associated with high expression levels of ER stress/UPR genes in human PDAC; however, it remains unknown whether the carriers of this variant have an increased or decreased risk for developing PDAC due to the limited number of the analyzed samples.

#### 5.1.2. Common variations of the MIA family and the disease trait of common diseases

Although it is unclear whether variants of HNF1A itself would also influence the biological behavior of pancreatic cancer cells, the MIA2<sup>I41M</sup> variant - a target gene of HNF1A - correlates with the prognosis of PDAC patients. As such, it underscores an important role of the HNF1A/MIA2 secretory axis in pancreatic carcinogenesis. It is important to point out that genetic variations in other members of the MIA family have been repetitively found to be associated with human diseases. For instance, variations within the MIA3 locus have been

demonstrated to be associated with cardiovascular diseases (Kathiresan et al., 2009; Samani et al., 2009; Samani et al., 2007) and a frequent polymorphism in the translation start codon of OTOR is associated with inner-ear dysfunction (Rendtorff et al., 2001). Substitution of mouse Mia2 Phe-91 with Ser in its conserved SH3 domain is associated with a secretory defect of cholesterol in the liver (Pitman et al., 2011). This mutation in mouse Mia2 functionally resembles the human MIA2<sup>L141M</sup> variant because both of them cause secretory defects. These data from human and mouse demonstrate a biological relevance of genetic variations of the MIA family of proteins under different pathological circumstances. Albeit for unknown reasons, it is speculated that more than one third of the human proteins enter the secretory pathway at the ER (Saito et al., 2009). Thus, genetic variations in cargo-recognizing proteins such as MIA2 and MIA3 are hypothesized to have large biological effects because they may alter cargo protein transport efficiency or even the types of cargo proteins. Thereby, the biological impact of these common variations could be amplified through the secreted cargo proteins.

### **5.1.3. The HNF1A/MIA2 axis in hepatic and pancreatic carcinogenesis**

Previously, the HNF1A/MIA2 secretory axis has been demonstrated to have a tumor suppressor function in HCC (Hellerbrand et al., 2008). However, both PDAC and PNET cancer cells widely expressed HNF1A and MIA2 and some cancers even expressed them at a very high level. This observation is in accordance with the data derived from a recent genome characterization, which revealed that MIA2 locates at a genomic region that is amplified in some PDAC cells (Jones et al., 2008). It has also been shown that HNF1A enhances the expression of fibroblast growth factor receptor 4 (FGFR4) in pancreatic cancer cell lines - a growth factor receptor, which is over-expressed in PDAC (Leung et al., 1994; Shah et al., 2002). These data do not support the notion that the HNF1A/MIA2 axis has a tumor suppressor function in pancreatic cancer (as compared to HCC) but rather argue for the opposite function. Indeed, Hnf1a deficiency in mice also induced a paradoxical consequence in the pancreas and liver in terms of carcinogenesis because it impaired large-T-antigen-induced growth and oncogenesis in pancreatic  $\beta$  cells but promoted proliferation of hepatocytes (Servitja et al., 2009). Therefore, the exact function of the HNF1A/MIA2 axis under physiological or pathological circumstances seems to be largely organ- and/or context-dependent.

### **5.1.4. The undefined role of the ER stress/UPR system in pancreatic cancer**

Recently, many genes belonging to the ER stress/UPR system have been demonstrated to be relevant in a variety of tumor entities (Ni and Lee, 2007). For example, BiP, which is a major ER chaperone, affects the metastatic potential of gastric cancer cells and high expression of BiP is associated with a poor prognosis (Lee, 2007; Zhang et al., 2006). Although the role of the ER stress/UPR system in acute pancreatitis has been well characterized (as illustrated in the

introduction), its exact function in pancreatic carcinogenesis remains undefined to date (Kubisch and Logsdon, 2008). In this regard, BiP has recently been identified as a novel tumor marker for pancreatic cancer, which is in line with our observations that half of the PDAC tissues were strongly BiP-positive (Djidja et al., 2009). In addition, the pancreatic cancer cells express high levels of genes belonging to the ER stress/UPR system including proximal signal sensors (PERK, ATF6 and ERN1), the chaperone lectins (Calnexin) and the folding catalysts (PDI). Further studies revealed that ER stress/UPR system actually interacts with the HNF1A/MIA2 secretory axis in determining susceptibility of cancer cells to gemcitabine treatment (see below). Besides, this system has been implicated in the formation of PDAC hypoxia (see second part of discussion).

#### **5.1.5. The interaction between the HNF1A/MIA2 axis and the ER stress/UPR system affects the response to gemcitabine**

At the first glance, it seems difficult to understand why pancreatic cancer cell lines with the MIA2<sup>I141M</sup> variant are highly sensitive to gemcitabine treatment while patients carrying this variant tend to have a more aggressive cancer phenotype (without chemotherapy). However, our data imply that gemcitabine - which is a generally genotoxic substance - preferably eliminates pancreatic cancer cells that are genetically and biologically more aggressive. These findings are consistent with results from a recent study in which PDACs can be classified into three major subtypes: classical, quasi-mesenchymal and exocrine-like, according to their gene expression profiles (Collisson et al., 2011). Among these subtypes, the quasi-mesenchymal subtype is the most aggressive one because patients belonging to this subtype have the worst prognosis. Interestingly however, cell lines with this gene expression signature were highly sensitive towards gemcitabine treatment in vitro. In contrast, cell lines with signatures of the less aggressive, classical subtype, were rather resistant to gemcitabine. These data argue for a distinctive “trade-off” phenomenon, at least in the late stage of PDAC.

The molecular mechanisms responsible for this “trade-off” effect remain largely elusive, not only because the exact gene signature capable of predicting the response to gemcitabine treatment is unclear, but also because the biological impact of the “gemcitabine-sensitivity” signature of pancreatic cancer cells is unknown. In addition to the above-mentioned “quasi-mesenchymal” signature, a recent study uncovered that cell cycle genes were predominantly enriched in primary cancer tissues derived from patients who are clinically responding to gemcitabine treatment (Garrido-Laguna et al., 2011), underscoring the “awkward” fact that cell proliferation is required to mediate the therapeutic effect of gemcitabine; though, proliferation is of course not favorable for the patient’s prognosis. In our study, it has been demonstrated for the first time that high expression of ER stress/UPR genes in pancreatic cancer cells affects the response to gemcitabine treatment.

The MIA2<sup>I141M</sup> caused chronic ER stress which increased expression of many genes of different branches of the UPR (especially the ERN1/XBP1 arm) in order to mitigate the stress increase. Though diverse biological effects of such adaptive responses in the ER have been reported previously (Gupta et al., 2010), the exact impact of this adaptation on the malignant behavior of PDAC is not completely understood. Nevertheless, such an adaptation may increase the ability of cancer cells to cope with ER stress, but simultaneously renders them more susceptible to genotoxic stress. In this case, acquired resistance to natural stress, i.e. ER stress, is traded off with the susceptibility to genotoxic stress (e.g. chemotherapy).

In particular, the current data suggest that the ERN1/XBP1 arm is particularly affected by the MIA2<sup>I141M</sup> variant which further renders the cells more sensitive to gemcitabine. Among the three UPR arms, the ERN1/XBP1 arm widely interacts with different cell death pathways. For example, the cytosolic domain of activated ERN1 binds to TRAF2, which triggers the apoptosis cascade through activation of JNK and ASK1 (Ron and Walter, 2007; Urano et al., 2000; Yoneda et al., 2001). The cytosolic domain of ERN1 physically interacts with the proapoptotic proteins BAX and BAK in coordinating the apoptotic cascade upon ER stress (Hetz et al., 2006). The activated ERN1 directly increases translation of proapoptotic caspase-2 through a specific decay of caspase-2-repressive microRNAs (Upton et al., 2012). Similarly, ERN1 also induces the expression of TXNIP (thioredoxin-interacting protein) by reducing the levels of its destabilizing microRNA, which triggers apoptosis via NLRP3 inflammasome-mediated procaspase-1 cleavage (Lerner et al., 2012). However, it remains unknown which of these mechanisms primarily contributes to increased chemosensitivity conferred by ERN1 expression in pancreatic cell lines.

## **5.2. A central role of the Tsc1-Tsc2 complex and of mTORC1 in pancreatic exocrine malignancy in mice**

### **5.2.1. Activation of feedback signal loops triggered by hyperactive mTORC1 in the pancreas**

Previously, many studies have documented an important role of the TSC1-TSC2 complex and of mTORC1 in the physiology of various organs. For example, a deletion of Tsc1 in hematopoietic stem cells (HSCs) dramatically impaired hematopoiesis and self-renewal of HSCs due to excessive levels of reactive oxygen species (ROS) (Chen et al., 2008). Hyperactive mTORC1 in pancreatic  $\beta$  cells caused by Tsc2 ablation resulted in a progressive reduction in islet mass (Shigeyama et al., 2008). In line, the number of  $\beta$  cells declined and that the mice suffered from diabetes when Tsc1 was pancreas-specifically deleted. In regard to

the exocrine pancreas, the acinar cells are progressively replaced by ductal cells. Currently, there is no evidence that these ductal cells are the result of acinar-to-ductal metaplasia (ADM) and it remains unknown why ductal cells are largely spared from these deleterious effects (Rooman and Real, 2012). Collectively, these data demonstrate that persistent and hyperactivated mTORC1 severely impairs the normal function of the endocrine and exocrine pancreas. However, Tsc1 haploinsufficiency, which does not lead to increased mTORC1 signaling, was tolerant and no significant abnormalities in either endocrine or exocrine pancreas were observed.

As pancreatic acinar and  $\beta$  cells were progressively lost, two negative regulators of mTORC1, p53 and Pten, were induced in pancreatic epithelial cells. Under normal circumstances, p53 and Pten are able to inactivate mTORC1 through a variety of molecular mechanisms, forming two important negative feedback signal loops (see below). The tumor suppressor functions of these two signal loops have been described in many other contexts (Lee et al., 2007a; Mahimainathan et al., 2009; Manning et al., 2005). Therefore, the biological significance of these signal loops in the pancreas was analyzed in this study.

### **5.2.2. Inactivation of the Tsc/mTORC1/Pten signal loop constitutes a major cystic-remodeling force in the adult pancreas**

Previous biochemical studies have established a set of feedback mechanisms responsible for attenuating PI3K/AKT signaling in cells lacking TSC1 or TSC2. These mechanisms complement each other at different levels of signal transduction. Firstly, GRB10 (growth factor receptor-bound protein 10) is phosphorylated and stabilized by the active mTORC1; the stabilized GRB10 inhibits upstream signal inputs of PI3K/AKT at the receptor levels (e.g. insulin or IGF receptors) (Hsu et al., 2011; Yu et al., 2011). Secondly, mTORC1-activated S6K1 phosphorylates insulin receptor substrate (IRS) which either impairs its function as the adaptor protein upstream of PI3K/AKT or targets it for degradation (Harrington et al., 2004; Shah et al., 2004). Lastly, PTEN, which is a putative negative regulator of PI3K/AKT signaling, is induced by active mTORC1 in a HIF-1 $\alpha$ -dependent manner (Mahimainathan et al., 2009; Stambolic et al., 2001). Besides, p53 activated by mTORC1 (see below) also contributes to PTEN expression.

Since PTEN is one of the major tumor suppressors in human PDAC, the biological consequence of inactivating the Tsc/mTORC1/Pten signal loop was analyzed in the pancreas. Inactivation of this loop induced striking remodeling of the exocrine pancreas with small or large cystic lesions. Notably, the cystic lesions were highly immunogenic and triggered strong antitumor immunities. Transplantation of cells lines established from these cystic lesions to T cell-deficient mice invariably initiated invasive PDAC. These data highlight two important facts: 1) dysfunction

of the Tsc/mTORC1/Pten signal loop is a major “cystic-remodeling” force in the adult pancreas; 2) T cell immunity may constitute a last/major tumor suppressive barrier for pancreatic cancers derived from cystic lesions.

The prevalence of pancreatic cystic lesions in the general population is only about 2.4%, as determined by screening studies using magnetic resonance imaging (MRI) (de Jong et al., 2010), however, cystic lesions can be detected in up to 42% of individuals from familial pancreatic cancer (FPC) families (Canto et al., 2012; Potjer et al., 2013). Hence, it is urgent to establish a screening program to identify pre-invasive lesions or early-stage cancers in these high-risk individuals (Loos et al., 2012). In this regard, many image modalities have been proposed but no real progress has been made so far (Canto et al., 2012; Potjer et al., 2013). In the current study, the Tsc/mTORC1/Pten axis was defined as the major signal loop that drives cystic lesion formation in mice. This mouse model can be further exploited for chemopreventive studies in order to search for substances that can delay progression of cystic lesions to invasive carcinomas in the pancreas. Moreover, it also highlights the tumor suppressive function of T cell immunity in maintaining these cystic lesions in the non-invasive state. These findings also raise a critical question: should the cystic lesions themselves or rather the strength of T cell immunity be monitored?

### **5.2.3. Inactivation of the Tsc/mTORC1/p53 signal loop promotes pancreatic malignancy in mice**

The Tsc/mTORC1/p53 signal loop is a delicate feedback system by which cells are able to cope with genotoxic and nutritional stress (Feng et al., 2005). Here, mTORC1 activates p53 by increasing its protein synthesis or its stability, which increases the GAP activity of the Tsc1-Tsc2 complex via AMPK and sestrin 1/2 (Budanov and Karin, 2008; Feng et al., 2007). Hence, the Tsc1-Tsc2 complex constitutes an essential component of the whole signal loop. It has been reported that hyperactivated mTORC1 - caused by loss of Tsc1 or Tsc2 - induced accumulation of p53 and apoptosis in MEFs (mouse embryonic fibroblasts) upon glucose starvation (Lee et al., 2007a). Consistently, the pancreatic acinar cells undergo apoptosis in Tsc1-deficient mice. Additional ablation of p53 eliminated cell death, but simultaneously increased the transformation rate of acinar cells. Certainly, further experiments are required due to the limited number of analyzed compound transgenic mice.

Interestingly, the pancreas of p53<sup>fl/fl</sup>; Tsc1<sup>fl/+</sup> mice was seemingly “normal” except for occasional acinar cells with enlarged nuclei. No putative precursor lesions (e.g. PanINs and AFLs) were seen. However, epithelial cells isolated from these seemingly “normal” pancreases were able to form invasive solid/anaplastic adenocarcinomas in BALB/c nude mice. Furthermore, these tumor-initiating cells exhibited EMT features *in vitro* and *in vivo*. Although EMT features of

p53-deficient pancreatic epithelial cells have previously been described, the exact contribution of Tsc1 haploinsufficiency to the EMT process remains to be defined (Pinho et al., 2011). Importantly, these data strongly argue for the notion that the “normal” pancreas actually contains cells with tumorigenic potential (conferred by p53 deficiency and Tsc1 haploinsufficiency) which can be further expanded in vitro and give rise to tumors in nude mice. Certainly, the possibility that these p53-deficient and Tsc1-haploinsufficient pancreatic epithelial cells tend to acquire key mutations in vitro that allow them to be tumorigenic in nude mice can not be entirely ruled out. Nevertheless, these findings highlight the tumor suppressor function of the Tsc/mTORC1/p53 signal loop in the adult pancreas.

#### **5.2.4. Kras<sup>G12D</sup> and Tsc1 haploinsufficiency initiate necrotic and metastatic PDAC**

One of the major reasons leading to cancer-related death is metastasis. According to recent studies of end stage PDACs, 70% of the patients eventually die of widespread metastasis (Iacobuzio-Donahue et al., 2009). Data from mouse models of PDAC suggest that precancerous cells seem to disseminate into the blood at preneoplastic stages via EMT (Rhim et al., 2012). Furthermore, RNA sequencing of circulating pancreatic cancer cells (CTCs) revealed that WNT signaling may be involved in this process. Furthermore, these CTCs formed non-adherent tumor spheres in culture (Yu et al., 2012) - a feature which is considered to be a property of cancer stem cells (CSCs) or tumor initiating cells (TICs) (Kong et al., 2009). Interestingly, as a crucial driving force for metastasis, hypoxia promoted both EMT features and acquisition of stem cell properties of pancreatic cancer cells (Koong et al., 2000; Olive et al., 2009). In this study, a mouse model of pancreatic cancer driven by Kras<sup>G12D</sup> and Tsc1 haploinsufficiency, which faithfully recapitulates three major metastasis-related biological features: hypoxia, EMT and acquisition of stem cell properties, is described (see discussion 5.3).

Although the tumors developing in Kras<sup>G12D</sup>; Tsc1<sup>fl/+</sup> mice showed large areas of necrosis, the isolated cancer cell lines actually produced high amounts of Vegfa (a potent proangiogenic factor), which is in line with previous studies showing that Tsc1 deficiency induced Vegfa production through activation of mTORC1 (El-Hashemite et al., 2003). Fueled by such high amounts of Vegfa, the initial angiogenic switch can easily be established by these cancer cells at the incipient stage of malignant transformation, facilitating expansion of cancer cells. Eventually, the tumor volume reaches a point where the blood supply is not able to sustain the fast growing tumor body and tissue hypoxia invariably results. However, these cancer cells are not able to further release Vegfa under hypoxic conditions due to hypoxia-induced ER stress. The impaired angiogenic potential under hypoxic conditions further aggravates tissue hypoxia, finally causing tumor metastasis. Certainly, PDAC is an extremely aggressive tumor entity that is

featured by a fast growing tumor (with a facilitated angiogenic switch by high Vegfa secretion), severe tissue hypoxia and early metastasis.

One of the key molecular events is the high levels of Vegfa production driven by Kras<sup>G12D</sup> and Tsc1 haploinsufficiency that renders these cancer cells particularly sensitive to hypoxia-induced ER stress. In general, hypoxia constitutes an important source of ER stress and activates the UPR system to mediate a set of adaptive changes within the solid tumor (Feldman et al., 2005; Romero-Ramirez et al., 2004). However, why protein secretion is impaired and how ER stress is induced by hypoxia is not entirely clear. One of the potential reasons is that oxygen provides the ultimate oxidative potential for disulfide formation, which is essential for the folding of secretory proteins. Vegfa, a primary angiogenic factor, is a typical example: the folding and proper function of Vegfa requires both intramolecular and intersubunit disulfide bonds. Therefore, secretion of Vegfa relies on the maintenance of the oxidative potential of the ER (May et al., 2005). Upon oxygen deprivation, unfolded Vegfa (or other secreted proteins) accumulate in the ER and cause ER stress and UPR. This is especially important for cancer cell lines with high levels of basal Vegfa secretion. Here, the oxygen supply needs to be constantly maintained to support oxidative folding of high-throughput Vegfa secretion. Subtle changes in oxygen supply may disturb proper folding of Vegfa and cause a severe “traffic jam” along the secretory pathway. This partially explains why cancer cells with high levels of basal Vegfa secretion are susceptible to hypoxia-induced ER stress.

Since active mTORC1 is observed in a majority of human PDACs and since more than half of these are positive for the ER stress marker BiP, the above described molecular mechanisms may also contribute to progression of the human disease. Recently, so-called “bioreductive prodrugs” (such as TH-302, a hypoxia-activated prodrug) which only becomes active under hypoxic conditions were designed and tested in clinical trials for treating a variety of malignant diseases including PDAC. Preliminary results from a phase 2 trial in PDAC involving 214 patients have been demonstrated to be promising: the addition of TH-302 to chemotherapy prolonged the average progression-free survival time compared to chemotherapy alone (Moyer, 2012; Wilson and Hay, 2011). The current data suggest that a combination of these prodrugs and substances targeting the ER function may constitute a candidate therapeutic modality for those patients whose cancer entity is similar to the described mouse PDAC (see below).

Notably, these cancer cells are able to overcome hypoxia by deleting the WT allele of Kras, resulting in a Kras<sup>G12D</sup>-LOH. How the Kras<sup>G12D</sup>-LOH reduces basal Vegfa release and how it circumvents hypoxia-induced ER stress is currently unclear. Interestingly, the occurrence of the Kras<sup>G12D</sup>-LOH is accompanied by an acquisition of an anaplastic/dedifferentiated growth pattern - an EMT process. The Kras<sup>G12D</sup>-LOH was initially described in anaplastic/dedifferentiated tumors derived



from mice with  $Kras^{G12D}$  and p16 deficiency (Qiu et al., 2011). In addition, the  $Kras^{G12D}$ -LOH can also be observed in mice with pancreas-specific  $Kras^{G12D}$  expression and Notch2 deficiency in which anaplastic PDAC were reported (personal communication with PD Dr. Jens T. Siveke; Department of Internal Medicine, Technical University of Munich, (Mazur et al., 2010)). How the  $Kras^{G12D}$ -LOH promotes EMT and facilitates the development of anaplastic tumor growth remains to be defined.

Indeed, cancer cells also tend to display EMT features in advanced stages of the disease presumably due to accumulation of genetic/epigenetic alterations (Iacobuzio-Donahue et al., 2009). Using a cohort of patients with invasive PDAC, a recent study systematically analyzed the pathological features of the disease at an early stage (obtained by surgical resection) and at the end stage (obtained by autopsy). Strikingly, this study revealed that the frequency of an undifferentiated morphology (e.g. with anaplastic components) in the end stage of the disease was 16% (12/74) and thus significantly higher than the earlier reported 0.006% in a large surgical series of patients with earlier PDAC stages. In addition, it has been shown that in three out of 74 patients, the anaplastic component represented more than 30% of the tumor mass (Abiatari et al., 2010). Though the  $Kras$ -LOH has been described in human pancreatic cancer cell lines, its occurrence in human PDAC samples has not yet been established. Therefore, whether the  $Kras$ -LOH contributes to anaplastic growth or to EMT of human PDAC requires further investigations.

### **5.3. Molecular subtypes of human PDAC**

As illustrated in the introduction, the molecular subtypes of PDAC are probably defined by many factors including founder mutations, transcriptional profiles and germline mutations. In the current study, a common variant -  $MIA2^{141M}$  - which specifies a subtype of human PDACs featured by high expression of ER stress/UPR genes, is identified. Based on the transcriptome analysis of mouse cell lines with different activation patterns of mTORC1, an ALDH1A3-positive subtype of human PDAC was identified and characterized.

#### **5.3.1. The $MIA2^{141M}$ subtype and chemoresponse**

It has been demonstrated in many other tumor entities that tumors with high expression of ER stress/UPR genes tend to have an unfavorable prognosis (Ni and Lee, 2007). In PDAC, the  $MIA2^{141M}$  variant is associated with increased expression of ER stress/UPR genes, however, patients carrying the  $MIA2^{141M}$  survived longer after tumor resection. Further analysis uncovered that the survival benefit was restricted to those patients who received adjuvant chemotherapy. These findings are important firstly because they define  $MIA2^{141M}$  as an important determinant of chemoresponsiveness in PDAC; secondly, because of a molecular

link between HNF1A, MIA2<sup>I141M</sup> and the ER stress/ERN1 axis; and thirdly, because the cancer cell responsiveness to ER stress is reciprocal to genotoxic stress.

These results will allow substratification of patients into MIA2<sup>WT</sup> and MIA2<sup>I141M</sup> for more individualized adjuvant chemotherapy regimens. And the heterogeneous responses of PDAC towards therapies are also affected by common genetic polymorphisms, as recently described in other entities such as chronic myeloid leukemia and non-small-cell lung cancer (Ng et al., 2012). These findings also hold the promise to develop drugs to manipulate ER stress and thus increase chemosensitivity. In this regard, imexon (a small-molecule agent that binds to glutathione (GSH)) has been shown to inhibit growth of human pancreatic cancer cell lines by causing ER stress (Sheveleva et al., 2012). Besides, induction of ER stress has been shown to sensitize pancreatic cancer cells towards TRAIL-induced cell death (Siegelin, 2012).

### **5.3.2. The ALDH1A3-positive subtype and targeted therapies**

In humans, the ALDH enzymes consist of 19 isoforms that are mainly responsible for aldehyde detoxification (Black and Vasiliou, 2009). A few isoforms (e.g. ALDH1A1 and ALDH1A3) are involved in retinoic acid (RA) signaling, whose function has been particularly linked to the characteristics of cancer stem cells (CSCs) (Marcato et al., 2011a). Previous studies have demonstrated that ALDH1 expression labels pancreatic cancer cells with stem cell features. Expression of ALDH1 is associated with the development of metastasis and negatively impacts overall survivals of PDAC patients (Rasheed et al., 2010). However, it remains unclear which isoform of the ALDH1 family (mainly ALDH1A1 vs. ALDH1A3) contributes to the unfavorable tumor biology of PDAC. Here, a recent study reported that low expression of ALDH1A1 is an unfavorable factor for survival of PDAC patients (Kahlert et al., 2011). However, such a correlation; potentially due to the limited number of analyzed samples, can not be determined by the current study. Interestingly, however, the expression of ALDH1A1 and ALDH1A3 are found to be mutually exclusive in human and mouse cell lines. Furthermore, it is the high expression of ALDH1A3 that correlates with a poor prognosis and lymphatic invasion of human PDACs. Therefore, ALDH1A3 expression marks a tumor entity with a high metastatic potential, which is consistent with the metastatic phenotype of *Kras*<sup>G12D</sup>; *Tsc1*<sup>fl/+</sup> mice. In this case, the tumor entity of *Kras*<sup>G12D</sup>; *Tsc1*<sup>fl/+</sup> mice is represented in humans by ALDH1A3-positive PDACs.

Median survival of patients with ALDH1A3-positive PDACs is only 14 months, which is significantly shorter than the average survival of resected PDAC patients (Kahlert et al., 2011). Therefore, the poor survival of ALDH1A3-positive PDACs contributes significantly to the overall unfavorable prognosis of PDACs. Furthermore, this subset of patients is less likely to respond to the current standard of care. Other therapies (e.g. targeted therapies) should be specifically

exploited for this subtype of PDACs. In this regard, a previous study has demonstrated that blockade of hedgehog signaling by cyclopamine specifically eliminated cells with a high enzymatic activity of ALDH (Feldmann et al., 2007). Furthermore, a combination of a hedgehog inhibitor, an mTOR inhibitor and gemcitabine was effective in eradicating pancreatic cancer cells with stem cells properties (Mueller et al., 2009). Therefore, using an mTOR inhibitor as the backbone, combination therapies targeting the ALDH1A3-positive cancer entity should be exploited.

## 6. SUMMARY

This study demonstrates that the HNF1A/MIA2-mediated secretory pathway crosstalks with the ER stress/UPR system in PDAC. A common MIA2<sup>I141M</sup> variant was identified, which is associated with secretory defects, an increased expression of ER stress/UPR genes and with chemosensitivity to gemcitabine. The Tsc1-Tsc2 complex was shown to play an important role in maintaining the normal physiology of the endocrine and exocrine pancreas. Inactivation of two ancient signal loops, the Tsc/mTORC1/Pten and the Tsc/mTORC1/p53 axis, either significantly impaired organ function by promoting cystic remodeling or increased the transformation. Interaction between the Tsc1-Tsc2 complex and Kras<sup>G12D</sup> induced the development of a highly necrotic and metastatic tumor entity, which is reflected by the ALDH1A3-positive subtype of PDAC in humans.

In addition, the questions raised in the “AIMS OF THIS STUDY” part have been addressed as follows (**Fig. 45**):

Question 1 (Q1): what is the biological and clinical relevance of an interaction between the HNF1A/MIA2-mediated secretory network and the ER stress/UPR system?

Conclusion 1 (C1): HNF1A, MIA2 and components of the ER stress/UPR system are widely expressed in human PDAC tissues and cell lines. A common MIA2<sup>I141M</sup> variant is found to be related with secretory defects and high expression of ER stress/UPR genes (especially the ERN1/XBP1 arm) in human PDAC samples. Further correlation analysis and in vitro characterization uncovered that MIA2<sup>I141M</sup> confers chemosensitivity to gemcitabine, a conventional chemotherapeutic drug for PDAC. These data suggest that the status of ER stress/UPR of PDAC cells affects the response towards conventional chemotherapy, which should be translationally analyzed in preclinical studies.

Question 2 (Q2): what are the functions of the Tsc1-Tsc2 complex in murine pancreatic carcinogenesis specifically driven by Kras<sup>G12D</sup> or by complete Pten loss, or by a combination of both?

Conclusion 2 (C2): Tsc1 haploinsufficiency and Kras<sup>G12D</sup> effectively initiate the formation of murine PADCs featured by hypoxia-induced necrosis, EMT and stem cell properties. A subset of cancer cells acquires a Kras<sup>G12D</sup>-LOH which allows them to forfeit their epithelial phenotypes and to overcome hypoxia-induced necrosis. The Tsc/mTORC1/Pten axis constitutes a negative feedback signal loop that is activated in pancreatic acinar cells with Tsc1 deficiency. Inactivation of this signal loop dramatically remodels the exocrine pancreas with cystic lesions in mice. However, the resulting cystic lesions rarely progress into invasive PDACs due to antitumor T cell immunity. These data define the Tsc/mTORC1/Pten signal loop as the major cystic-remodeling force in the murine pancreas and T cell immunity as the major tumor suppressor.

Question 3 (Q3): what is the role of the Tsc1-Tsc2 complex in murine pancreatic malignancy in the context of p53 loss?

Conclusion 3 (C3): The Tsc/mTORC1/p53 axis is another important feedback signal loop, which is activated in pancreatic acinar cells with Tsc1 deficiency. P53-mediated apoptosis is responsible for the massive cell death in pancreatic acinar cells triggered by Tsc1 deficiency and hyperactivated mTORC1. Inactivation of the signal loop causes acinar cell transformation. Furthermore, the combination of Tsc1 haploinsufficiency and p53 loss do not affect the normal physiology of the pancreas, though, it fosters the development of pre-neoplastic cells showing EMT features in vitro and giving rise to tumors in nude mice. Importantly, these pre-neoplastic cells do not form any known putative precursor lesion of pancreatic cancer. Again, these data underscore the central tumor suppressive role of the Tsc1-Tsc2 complex in pancreatic exocrine malignancy.

Question 4 (Q4): what is the biological significance of the reciprocally regulatory network formed by mTORC1, the ER stress/UPR system and by hypoxic signals in PDAC biology?

Conclusion 4 (C4): Here, the current study demonstrates that pancreatic cancer cells with hyperactivated mTORC1, driven by Kras<sup>G12D</sup> and Tsc1 haploinsufficiency secrete high basal levels of Vegfa. Since disulfide formation is essential for Vegfa secretion, which relies on oxidative folding and oxygen supply in the ER, this disulfide formation renders cancer cells with a high-throughput Vegfa secretion extremely sensitive to hypoxia-induced ER stress. Furthermore, these cancer cells seem to be able to delete the WT Kras allele and thus circumvent “hypersensitivity” to hypoxia-induced ER stress at the price of an acquisition of anaplastic growth. The exact reasons for these observations remain to be defined.

Question 5 (Q5): do the above mentioned signal pathways or biological processes play a role in specifying distinctive molecular subtypes of human PDAC?

Conclusion 5 (C5): The interaction between the MIA2<sup>I141M</sup> variant and the ER stress/UPR system specifies a molecular subtype of human PDAC characterized by high expression of ER stress/UPR genes (especially those of the ERN1/XBP1 arm). This subtype accounts for one third of human PDACs that are more likely to benefit from a gemcitabine-based chemotherapy.

By analyzing expression profiles of a set of murine cell lines (with Tsc1 haploinsufficiency in different contexts), the expressions of Aldh1a1 and Aldh1a3 are mutually exclusive. An aggressive tumor entity with high metastatic potential, EMT and stem cell properties is uniquely marked by Aldh1a3 expression. Consistently, a human ALDH1A3-positive PDAC subtype was correspondingly identified and this subset of patients was shown to have a short postoperative survival and a high lymphatic invasion rate. Furthermore, comprehensive phenotypic characterizations of different pancreatic cancer GEMMs and analysis of expression profiles in the resulting cell lines allowed identification of an ALDH1A3-positive subtype of human PDACs that contributes significantly to the current unfavourable prognosis of PADC. The distinctive tumor biology of this

subset of patients necessitates treatment modalities (e.g. mTOR inhibition-based targeted therapies) other than the current standard of care.

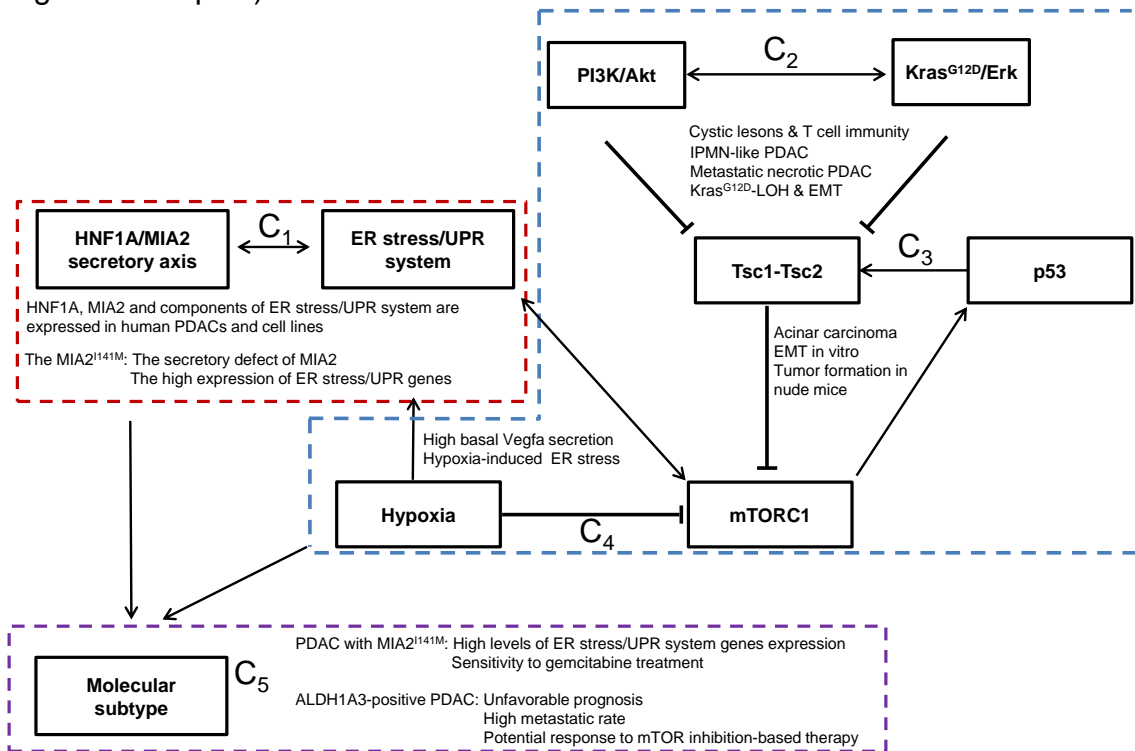


**Figure 45.** Schematic figure illustrating the major findings of this study.

## 7. ABBREVIATIONS

4E-BP1	Eukaryotic translation initiation factor 4E (eIF4E)-binding protein 1
53BP1	Tumor protein p53 binding protein 1
ADM	Acinar-to-ductal metaplasia
AFL	Atypical flat lesion
Aldh1a1	Aldehyde dehydrogenase family 1, subfamily A1
Aldh1a3	Aldehyde dehydrogenase family 1, subfamily A3
AMPK	AMP-activated protein kinase
APS	Ammonium persulfate
ATF6	Activating transcription factor 6
ATM	Ataxia telangiectasia mutated
B220	Protein tyrosine phosphatase, receptor type, C
BiP	Heat shock 70kDa protein 5
Bnip3	BCL2/adenovirus E1B 19kDa interacting protein 3
BRCA2	Breast cancer 2, early onset
BSA	Bovine serum albumin
Caix	Carbonic anhydrase 9
Casp3	Caspase 3
CD3	CD3 antigen, epsilon polypeptide
CD31	platelet/endothelial cell adhesion molecule 1
Cdh17	Cadherin 17
COPII	Coat protein complex-II
Cre	Cre recombinase
CSC	Cancer stem cell
DAPI	4,6-diamidino-2-phenylindole
eIF2 $\alpha$	Eukaryotic translation initiation factor 2 $\alpha$
EMT	Epithelial-to-mesenchymal transition
ER	Endoplasmic reticulum
ERAD	ER-associated degradation
ERAF	ER-assisted folding
ERES	ER exit site
ERK	Extracellular signal-regulated kinase
ERM	Ezrin-radixin-moesin
ERN1	Endoplasmic reticulum to nucleus signaling 1
F4/80	EGF-like module containing, mucin-like, hormone receptor-like sequence 1
FBS	Fetal bovine serum
FDR	False discovery rate
Gabrp	$\gamma$ -aminobutyric acid A receptor, pi
GAP	GTPase Activating Protein
GAPDH	Glyceraldehyde-3-phosphate dehydrogenase

GEF	Guanine-nucleotide exchange factor
GEMM	Genetically engineered mouse model
GRB10	Growth factor receptor-bound protein 10
GSK3	Glycogen synthase kinase 3
GWAS	Genome-wide association study
HCC	Hepatocellular carcinoma
HIF1A	Hypoxia inducible factor 1, $\alpha$ subunit (basic helix-loop-helix transcription factor)
Hk2	Hexokinase 2
HNF1B	HNF1 homeobox B
HRP	Horseradish peroxidase
HSCs	Hematopoietic stem cells
IF	Immunofluorescence
IHC	Immunohistochemistry
IKK2	Inhibitor of kappaB kinase $\beta$
Il1 $\alpha$	Interleukin 1 $\alpha$
IPMN	Intraductal papillary-mucinous neoplasm
KCl	Potassium chloride
KRAS	V-Ki-ras2 Kirsten rat sarcoma viral oncogene homolog
Krt19	Keratin 19
LKB1	Serine/threonine kinase 11
LOH	Loss of heterozygosity
MCN	Mucinous cystic neoplasm
MEF	Mouse embryonic fibroblast
MEK	Mitogen-activated protein kinase kinase
MET	Mesenchymal-to-epithelial transition
MIA2	Melanoma inhibitory activity 2
MODY	Maturity-onset diabetes of the young
mTOR	Mammalian target of rapamycin
MTT	3-(4,5-dimethylthiazole-2-yl)2,5-diphenyltetrazolium bromide
NF- $\kappa$ B	Nuclear factor of kappa light polypeptide gene enhancer in B cells 1
OGTT	Oral glucose tolerance test
p16	Cyclin-dependent kinase inhibitor 2A
p48	Pancreas specific transcription factor, 1a
p53	Tumor protein p53
p62	Sequestosome 1
PALB2	Partner and localizer of BRCA2
PanIN	Pancreatic intraepithelial neoplasia
PARP1	Poly (ADP-ribose) polymerase 1
PBS	Phosphate buffered saline
PCA	Principal component analysis
PDAC	Pancreatic ductal adenocarcinoma



PDI	Pancreas-specific protein disulfide isomerase
Pdx1	Pancreatic and duodenal homeobox 1
PERK	PRKR-like endoplasmic reticulum kinase
PI3K	Phosphatidylinositol-4,5-bisphosphate 3-kinase
PNET	Pancreatic neuroendocrine tumor
PRD domain	Proline-rich domain
Pten	Phosphatase and tensin homolog
REDD1	DNA-damage-inducible transcript 4
ROS	Reactive oxygen species
S6	Ribosomal protein S6
S6K1	S6 kinase 1
SD	Standard deviation
SDS	Laurylsulfate
SH3 domain	SRC Homology 3 Domain
SMAD4	SMAD family member 4
Sox9	SRY-box containing gene 9
TC	Tubular complex
Tns4	Tensin 4
TSC	Tuberous sclerosis
UPR	Unfold-fold protein response
Wfdc2	WAP four-disulfide core domain 2
XBP1	X-box binding protein 1
$\alpha$ -SMA	A-smooth muscle actin

## 8. REFERENCES

- (1993). Identification and characterization of the tuberous sclerosis gene on chromosome 16. *Cell* 75, 1305-1315.
- Abiatari, I., Esposito, I., Oliveira, T. D., Felix, K., Xin, H., Penzel, R., Giese, T., Friess, H., and Kleeff, J. (2010). Moesin-dependent cytoskeleton remodelling is associated with an anaplastic phenotype of pancreatic cancer. *J Cell Mol Med* 14, 1166-1179.
- Aguirre, A. J., Bardeesy, N., Sinha, M., Lopez, L., Tuveson, D. A., Horner, J., Redston, M. S., and DePinho, R. A. (2003). Activated Kras and Ink4a/Arf deficiency cooperate to produce metastatic pancreatic ductal adenocarcinoma. *Genes Dev* 17, 3112-3126.
- Aichler, M., Seiler, C., Tost, M., Siveke, J., Mazur, P. K., Da Silva-Buttkus, P., Bartsch, D. K., Langer, P., Chiblak, S., Durr, A., *et al.* (2012). Origin of pancreatic ductal adenocarcinoma from atypical flat lesions: a comparative study in transgenic mice and human tissues. *J Pathol* 226, 723-734.
- Al-Ghamdi, S., Albasri, A., Cachat, J., Ibrahim, S., Muhammad, B. A., Jackson, D., Nateri, A. S., Kindle, K. B., and Ilyas, M. (2011). Cten is targeted by Kras signalling to regulate cell motility in the colon and pancreas. *PLoS One* 6, e20919.
- Al-Ghamdi, S., Cachat, J., Albasri, A., Ahmed, M., Jackson, D., Zaitoun, A., Guppy, N., Otto, W. R., Alison, M. R., Kindle, K. B., and Ilyas, M. (2013). C-Terminal Tensin-Like Gene Functions as an Oncogene and Promotes Cell Motility in Pancreatic Cancer. *Pancreas* 42, 135-140.
- Amundadottir, L., Kraft, P., Stolzenberg-Solomon, R. Z., Fuchs, C. S., Petersen, G. M., Arslan, A. A., Bueno-de-Mesquita, H. B., Gross, M., Helzlsouer, K., Jacobs, E. J., *et al.* (2009). Genome-wide association study identifies variants in the ABO locus associated with susceptibility to pancreatic cancer. *Nat Genet* 41, 986-990.
- Anelli, T., and Sitia, R. (2008). Protein quality control in the early secretory pathway. *Embo J* 27, 315-327.
- Appenzeller-Herzog, C., and Hall, M. N. (2012). Bidirectional crosstalk between endoplasmic reticulum stress and mTOR signaling. *Trends Cell Biol* 22, 274-282.
- Astrinidis, A., Cash, T. P., Hunter, D. S., Walker, C. L., Chernoff, J., and Henske, E. P. (2002). Tuberin, the tuberous sclerosis complex 2 tumor suppressor gene product, regulates Rho activation, cell adhesion and migration. *Oncogene* 21, 8470-8476.
- Ayala, J. E., Samuel, V. T., Morton, G. J., Obici, S., Croniger, C. M., Shulman, G. I., Wasserman, D. H., and McGuinness, O. P. (2010). Standard operating procedures for describing and performing metabolic tests of glucose homeostasis in mice. *Dis Model Mech* 3, 525-534.
- Bardeesy, N., Aguirre, A. J., Chu, G. C., Cheng, K. H., Lopez, L. V., Hezel, A. F., Feng, B., Brennan, C., Weissleder, R., Mahmood, U., *et al.* (2006a). Both

p16(Ink4a) and the p19(Arf)-p53 pathway constrain progression of pancreatic adenocarcinoma in the mouse. *Proc Natl Acad Sci U S A* 103, 5947-5952.

Bardeesy, N., Cheng, K. H., Berger, J. H., Chu, G. C., Pahler, J., Olson, P., Hezel, A. F., Horner, J., Lauwers, G. Y., Hanahan, D., and DePinho, R. A. (2006b). Smad4 is dispensable for normal pancreas development yet critical in progression and tumor biology of pancreas cancer. *Genes Dev* 20, 3130-3146.

Bayne, L. J., Beatty, G. L., Jhala, N., Clark, C. E., Rhim, A. D., Stanger, B. Z., and Vonderheide, R. H. (2012). Tumor-derived granulocyte-macrophage colony-stimulating factor regulates myeloid inflammation and T cell immunity in pancreatic cancer. *Cancer Cell* 21, 822-835.

Bernardi, R., Guernah, I., Jin, D., Grisendi, S., Alimonti, A., Teruya-Feldstein, J., Cordon-Cardo, C., Simon, M. C., Rafii, S., and Pandolfi, P. P. (2006). PML inhibits HIF-1alpha translation and neoangiogenesis through repression of mTOR. *Nature* 442, 779-785.

Bertout, J. A., Patel, S. A., and Simon, M. C. (2008). The impact of O<sub>2</sub> availability on human cancer. *Nat Rev Cancer* 8, 967-975.

Bi, M., Naczki, C., Koritzinsky, M., Fels, D., Blais, J., Hu, N., Harding, H., Novoa, I., Varia, M., Raleigh, J., *et al.* (2005). ER stress-regulated translation increases tolerance to extreme hypoxia and promotes tumor growth. *Embo J* 24, 3470-3481.

Black, W., and Vasiliou, V. (2009). The aldehyde dehydrogenase gene superfamily resource center. *Hum Genomics* 4, 136-142.

Bosetti, C., Lucenteforte, E., Silverman, D. T., Petersen, G., Bracci, P. M., Ji, B. T., Negri, E., Li, D., Risch, H. A., Olson, S. H., *et al.* (2011). Cigarette smoking and pancreatic cancer: an analysis from the International Pancreatic Cancer Case-Control Consortium (Panc4). *Ann Oncol*.

Bosserhoff, A. K., Moser, M., Scholmerich, J., Buettner, R., and Hellerbrand, C. (2003). Specific expression and regulation of the new melanoma inhibitory activity-related gene MIA2 in hepatocytes. *J Biol Chem* 278, 15225-15231.

Brown, E. J., Albers, M. W., Shin, T. B., Ichikawa, K., Keith, C. T., Lane, W. S., and Schreiber, S. L. (1994). A mammalian protein targeted by G1-arresting rapamycin-receptor complex. *Nature* 369, 756-758.

Budanov, A. V., and Karin, M. (2008). p53 target genes sestrin1 and sestrin2 connect genotoxic stress and mTOR signaling. *Cell* 134, 451-460.

Cafferkey, R., Young, P. R., McLaughlin, M. M., Bergsma, D. J., Koltin, Y., Sathe, G. M., Faucette, L., Eng, W. K., Johnson, R. K., and Livi, G. P. (1993). Dominant missense mutations in a novel yeast protein related to mammalian phosphatidylinositol 3-kinase and VPS34 abrogate rapamycin cytotoxicity. *Mol Cell Biol* 13, 6012-6023.

Canto, M. I., Hruban, R. H., Fishman, E. K., Kamel, I. R., Schulick, R., Zhang, Z., Topazian, M., Takahashi, N., Fletcher, J., Petersen, G., *et al.* (2012). Frequent detection of pancreatic lesions in asymptomatic high-risk individuals. *Gastroenterology* 142, 796-804; quiz e714-795.

Chen, C., Liu, Y., Liu, R., Ikenoue, T., Guan, K. L., and Zheng, P. (2008). TSC-mTOR maintains quiescence and function of hematopoietic stem cells by repressing mitochondrial biogenesis and reactive oxygen species. *J Exp Med* 205, 2397-2408.

Chong-Kopera, H., Inoki, K., Li, Y., Zhu, T., Garcia-Gonzalo, F. R., Rosa, J. L., and Guan, K. L. (2006). TSC1 stabilizes TSC2 by inhibiting the interaction between TSC2 and the HERC1 ubiquitin ligase. *J Biol Chem* 281, 8313-8316.

Collins, M. A., Bednar, F., Zhang, Y., Brisset, J. C., Galban, S., Galban, C. J., Rakshit, S., Flannagan, K. S., Adsay, N. V., and Pasca di Magliano, M. (2012). Oncogenic Kras is required for both the initiation and maintenance of pancreatic cancer in mice. *J Clin Invest* 122, 639-653.

Collisson, E. A., Sadanandam, A., Olson, P., Gibb, W. J., Truitt, M., Gu, S., Cooc, J., Weinkle, J., Kim, G. E., Jakkula, L., *et al.* (2011). Subtypes of pancreatic ductal adenocarcinoma and their differing responses to therapy. *Nat Med* 17, 500-503.

Collisson, E. A., Trejo, C. L., Silva, J. M., Gu, S., Korkola, J. E., Heiser, L. M., Charles, R. P., Rabinovich, B. A., Hann, B., Dankort, D., *et al.* (2012). A central role for RAF-->MEK-->ERK signaling in the genesis of pancreatic ductal adenocarcinoma. *Cancer Discov* 2, 685-693.

Cooke, V. G., LeBleu, V. S., Keskin, D., Khan, Z., O'Connell, J. T., Teng, Y., Duncan, M. B., Xie, L., Maeda, G., Vong, S., *et al.* (2012). Pericyte depletion results in hypoxia-associated epithelial-to-mesenchymal transition and metastasis mediated by met signaling pathway. *Cancer Cell* 21, 66-81.

Cui, Y., Brosnan, J. A., Blackford, A. L., Sur, S., Hruban, R. H., Kinzler, K. W., Vogelstein, B., Maitra, A., Diaz, L. A., Jr., Iacobuzio-Donahue, C. A., and Eshleman, J. R. (2012). Genetically defined subsets of human pancreatic cancer show unique in vitro chemosensitivity. *Clin Cancer Res* 18, 6519-6530.

de Jong, K., Nio, C. Y., Hermans, J. J., Dijkgraaf, M. G., Gouma, D. J., van Eijck, C. H., van Heel, E., Klass, G., Fockens, P., and Bruno, M. J. (2010). High prevalence of pancreatic cysts detected by screening magnetic resonance imaging examinations. *Clin Gastroenterol Hepatol* 8, 806-811.

DeYoung, M. P., Horak, P., Sofer, A., Sgroi, D., and Ellisen, L. W. (2008). Hypoxia regulates TSC1/2-mTOR signaling and tumor suppression through REDD1-mediated 14-3-3 shuttling. *Genes Dev* 22, 239-251.

Djidja, M. C., Claude, E., Snel, M. F., Scriven, P., Francese, S., Carolan, V., and Clench, M. R. (2009). MALDI-ion mobility separation-mass spectrometry imaging of glucose-regulated protein 78 kDa (Grp78) in human formalin-fixed, paraffin-embedded pancreatic adenocarcinoma tissue sections. *J Proteome Res* 8, 4876-4884.

Dong, X., Yang, B., Li, Y., Zhong, C., and Ding, J. (2009). Molecular basis of the acceleration of the GDP-GTP exchange of human ras homolog enriched in brain by human translationally controlled tumor protein. *J Biol Chem* 284, 23754-23764.

El-Hashemite, N., Walker, V., Zhang, H., and Kwiatkowski, D. J. (2003). Loss of Tsc1 or Tsc2 induces vascular endothelial growth factor production through mammalian target of rapamycin. *Cancer Res* 63, 5173-5177.

Elliott, K. S., Zeggini, E., McCarthy, M. I., Gudmundsson, J., Sulem, P., Stacey, S. N., Thorlacius, S., Amundadottir, L., Gronberg, H., Xu, J., *et al.* (2010). Evaluation of association of HNF1B variants with diverse cancers: collaborative analysis of data from 19 genome-wide association studies. *PLoS One* 5, e10858.

Esposito, I., Seiler, C., Bergmann, F., Kleeff, J., Friess, H., and Schirmacher, P. (2007). Hypothetical progression model of pancreatic cancer with origin in the centroacinar-acinar compartment. *Pancreas* 35, 212-217.

Feldman, D. E., Chauhan, V., and Koong, A. C. (2005). The unfolded protein response: a novel component of the hypoxic stress response in tumors. *Mol Cancer Res* 3, 597-605.

Feldmann, G., Dhara, S., Fendrich, V., Bedja, D., Beaty, R., Mullendore, M., Karikari, C., Alvarez, H., Iacobuzio-Donahue, C., Jimeno, A., *et al.* (2007). Blockade of hedgehog signaling inhibits pancreatic cancer invasion and metastases: a new paradigm for combination therapy in solid cancers. *Cancer Res* 67, 2187-2196.

Feng, Z., Hu, W., de Stanchina, E., Teresky, A. K., Jin, S., Lowe, S., and Levine, A. J. (2007). The regulation of AMPK beta1, TSC2, and PTEN expression by p53: stress, cell and tissue specificity, and the role of these gene products in modulating the IGF-1-AKT-mTOR pathways. *Cancer Res* 67, 3043-3053.

Feng, Z., Zhang, H., Levine, A. J., and Jin, S. (2005). The coordinate regulation of the p53 and mTOR pathways in cells. *Proc Natl Acad Sci U S A* 102, 8204-8209.

Galgano, M. T., Hampton, G. M., and Frierson, H. F., Jr. (2006). Comprehensive analysis of HE4 expression in normal and malignant human tissues. *Mod Pathol* 19, 847-853.

Garrido-Laguna, I., Uson, M., Rajeshkumar, N. V., Tan, A. C., de Oliveira, E., Karikari, C., Villaroel, M. C., Salomon, A., Taylor, G., Sharma, R., *et al.* (2011). Tumor engraftment in nude mice and enrichment in stroma-related gene pathways predict poor survival and resistance to gemcitabine in patients with pancreatic cancer. *Clin Cancer Res* 17, 5793-5800.

Goldstein, D. B. (2009). Common genetic variation and human traits. *N Engl J Med* 360, 1696-1698.

Guerra, C., Schuhmacher, A. J., Canamero, M., Grippo, P. J., Verdaguer, L., Perez-Gallego, L., Dubus, P., Sandgren, E. P., and Barbacid, M. (2007). Chronic pancreatitis is essential for induction of pancreatic ductal adenocarcinoma by K-Ras oncogenes in adult mice. *Cancer Cell* 11, 291-302.

Gupta, S., Deepti, A., Deegan, S., Lisbona, F., Hetz, C., and Samali, A. (2010). HSP72 protects cells from ER stress-induced apoptosis via enhancement of IRE1alpha-XBP1 signaling through a physical interaction. *PLoS Biol* 8, e1000410.

Gurkan, C., Stagg, S. M., Lapointe, P., and Balch, W. E. (2006). The COPII cage: unifying principles of vesicle coat assembly. *Nat Rev Mol Cell Biol* 7, 727-738.

Harding, H. P., Zeng, H., Zhang, Y., Jungries, R., Chung, P., Plesken, H., Sabatini, D. D., and Ron, D. (2001). Diabetes mellitus and exocrine pancreatic dysfunction in *perk*<sup>-/-</sup> mice reveals a role for translational control in secretory cell survival. *Mol Cell* 7, 1153-1163.

Hardy, J., and Singleton, A. (2009). Genomewide association studies and human disease. *N Engl J Med* 360, 1759-1768.

Harrington, L. S., Findlay, G. M., Gray, A., Tolkacheva, T., Wigfield, S., Rebholz, H., Barnett, J., Leslie, N. R., Cheng, S., Shepherd, P. R., *et al.* (2004). The TSC1-2 tumor suppressor controls insulin-PI3K signaling via regulation of IRS proteins. *J Cell Biol* 166, 213-223.

Hellerbrand, C., Amann, T., Schlegel, J., Wild, P., Bataille, F., Spruss, T., Hartmann, A., and Bosserhoff, A. K. (2008). The novel gene MIA2 acts as a tumour suppressor in hepatocellular carcinoma. *Gut* 57, 243-251.

Hess, D. A., Humphrey, S. E., Ishibashi, J., Damsz, B., Lee, A. H., Glimcher, L. H., and Konieczny, S. F. (2011). Extensive pancreas regeneration following acinar-specific disruption of *Xbp1* in mice. *Gastroenterology* 141, 1463-1472.

Hetz, C., Bernasconi, P., Fisher, J., Lee, A. H., Bassik, M. C., Antonsson, B., Brandt, G. S., Iwakoshi, N. N., Schinzel, A., Glimcher, L. H., and Korsmeyer, S. J. (2006). Proapoptotic BAX and BAK modulate the unfolded protein response by a direct interaction with IRE1 $\alpha$ . *Science* 312, 572-576.

Hill, R., Calvopina, J. H., Kim, C., Wang, Y., Dawson, D. W., Donahue, T. R., Dry, S., and Wu, H. (2010). PTEN loss accelerates *Kras*G12D-induced pancreatic cancer development. *Cancer Res* 70, 7114-7124.

Hingorani, S. R., Petricoin, E. F., Maitra, A., Rajapakse, V., King, C., Jacobetz, M. A., Ross, S., Conrads, T. P., Veenstra, T. D., Hitt, B. A., *et al.* (2003). Preinvasive and invasive ductal pancreatic cancer and its early detection in the mouse. *Cancer Cell* 4, 437-450.

Hingorani, S. R., Wang, L., Multani, A. S., Combs, C., Deramaudt, T. B., Hruban, R. H., Rustgi, A. K., Chang, S., and Tuveson, D. A. (2005). *Trp53*R172H and *Kras*G12D cooperate to promote chromosomal instability and widely metastatic pancreatic ductal adenocarcinoma in mice. *Cancer Cell* 7, 469-483.

Hiraoka, N., Ino, Y., Sekine, S., Tsuda, H., Shimada, K., Kosuge, T., Zavada, J., Yoshida, M., Yamada, K., Koyama, T., and Kanai, Y. (2010). Tumour necrosis is a postoperative prognostic marker for pancreatic cancer patients with a high interobserver reproducibility in histological evaluation. *Br J Cancer* 103, 1057-1065.

Hruban, R. H., Goggins, M., Parsons, J., and Kern, S. E. (2000). Progression model for pancreatic cancer. *Clin Cancer Res* 6, 2969-2972.

Hsu, P. P., Kang, S. A., Rameseder, J., Zhang, Y., Ottina, K. A., Lim, D., Peterson, T. R., Choi, Y., Gray, N. S., Yaffe, M. B., *et al.* (2011). The mTOR-regulated phosphoproteome reveals a mechanism of mTORC1-mediated inhibition of growth factor signaling. *Science* 332, 1317-1322.

Hsu, Y. C., Chern, J. J., Cai, Y., Liu, M., and Choi, K. W. (2007). *Drosophila* TCTP is essential for growth and proliferation through regulation of dRheb GTPase. *Nature* 445, 785-788.

Huang, J., and Manning, B. D. (2008). The TSC1-TSC2 complex: a molecular switchboard controlling cell growth. *Biochem J* 412, 179-190.

Iacobuzio-Donahue, C. A. (2012). Genetic evolution of pancreatic cancer: lessons learnt from the pancreatic cancer genome sequencing project. *Gut* 61, 1085-1094.

Iacobuzio-Donahue, C. A., Fu, B., Yachida, S., Luo, M., Abe, H., Henderson, C. M., Vilardell, F., Wang, Z., Keller, J. W., Banerjee, P., *et al.* (2009). DPC4 gene status of the primary carcinoma correlates with patterns of failure in patients with pancreatic cancer. *J Clin Oncol* 27, 1806-1813.

Iacobuzio-Donahue, C. A., Velculescu, V. E., Wolfgang, C. L., and Hruban, R. H. (2012). Genetic basis of pancreas cancer development and progression: insights from whole-exome and whole-genome sequencing. *Clin Cancer Res* 18, 4257-4265.

Inoki, K., Li, Y., Xu, T., and Guan, K. L. (2003a). Rheb GTPase is a direct target of TSC2 GAP activity and regulates mTOR signaling. *Genes Dev* 17, 1829-1834.

Inoki, K., Li, Y., Zhu, T., Wu, J., and Guan, K. L. (2002). TSC2 is phosphorylated and inhibited by Akt and suppresses mTOR signalling. *Nat Cell Biol* 4, 648-657.

Inoki, K., Ouyang, H., Zhu, T., Lindvall, C., Wang, Y., Zhang, X., Yang, Q., Bennett, C., Harada, Y., Stankunas, K., *et al.* (2006). TSC2 integrates Wnt and energy signals via a coordinated phosphorylation by AMPK and GSK3 to regulate cell growth. *Cell* 126, 955-968.

Inoki, K., Zhu, T., and Guan, K. L. (2003b). TSC2 mediates cellular energy response to control cell growth and survival. *Cell* 115, 577-590.

Iwawaki, T., Akai, R., and Kohno, K. (2010). IRE1alpha disruption causes histological abnormality of exocrine tissues, increase of blood glucose level, and decrease of serum immunoglobulin level. *PLoS One* 5, e13052.

Jones, S., Hruban, R. H., Kamiyama, M., Borges, M., Zhang, X., Parsons, D. W., Lin, J. C., Palmisano, E., Brune, K., Jaffee, E. M., *et al.* (2009). Exomic sequencing identifies PALB2 as a pancreatic cancer susceptibility gene. *Science* 324, 217.

Jones, S., Zhang, X., Parsons, D. W., Lin, J. C., Leary, R. J., Angenendt, P., Mankoo, P., Carter, H., Kamiyama, H., Jimeno, A., *et al.* (2008). Core signaling pathways in human pancreatic cancers revealed by global genomic analyses. *Science* 321, 1801-1806.

Kahlert, C., Bergmann, F., Beck, J., Welsch, T., Mogler, C., Herpel, E., Dutta, S., Niemietz, T., Koch, M., and Weitz, J. (2011). Low expression of aldehyde dehydrogenase 1A1 (ALDH1A1) is a prognostic marker for poor survival in pancreatic cancer. *BMC Cancer* 11, 275.

Kandt, R. S., Haines, J. L., Smith, M., Northrup, H., Gardner, R. J., Short, M. P., Dumars, K., Roach, E. S., Steingold, S., Wall, S., and *et al.* (1992). Linkage of an

important gene locus for tuberous sclerosis to a chromosome 16 marker for polycystic kidney disease. *Nat Genet* 2, 37-41.

Kathiresan, S., Voight, B. F., Purcell, S., Musunuru, K., Ardissino, D., Mannucci, P. M., Anand, S., Engert, J. C., Samani, N. J., Schunkert, H., *et al.* (2009). Genome-wide association of early-onset myocardial infarction with single nucleotide polymorphisms and copy number variants. *Nat Genet* 41, 334-341.

Kennedy, A. L., Morton, J. P., Manoharan, I., Nelson, D. M., Jamieson, N. B., Pawlikowski, J. S., McBryan, T., Doyle, B., McKay, C., Oien, K. A., *et al.* (2011). Activation of the PIK3CA/AKT pathway suppresses senescence induced by an activated RAS oncogene to promote tumorigenesis. *Mol Cell* 42, 36-49.

Kitada, T., Seki, S., Sakaguchi, H., Sawada, T., Hirakawa, K., and Wakasa, K. (2003). Clinicopathological significance of hypoxia-inducible factor-1alpha expression in human pancreatic carcinoma. *Histopathology* 43, 550-555.

Kleeff, J., Ishiwata, T., Maruyama, H., Friess, H., Truong, P., Buchler, M. W., Falb, D., and Korc, M. (1999). The TGF-beta signaling inhibitor Smad7 enhances tumorigenicity in pancreatic cancer. *Oncogene* 18, 5363-5372.

Kong, B., Michalski, C. W., Erkan, M., Friess, H., and Kleeff, J. (2011). From tissue turnover to the cell of origin for pancreatic cancer. *Nat Rev Gastroenterol Hepatol* 8, 467-472.

Kong, B., Michalski, C. W., and Kleeff, J. (2009). Tumor initiating cells in pancreatic cancer: A critical view. *World J Stem Cells* 1, 8-10.

Koong, A. C., Mehta, V. K., Le, Q. T., Fisher, G. A., Terris, D. J., Brown, J. M., Bastidas, A. J., and Vierra, M. (2000). Pancreatic tumors show high levels of hypoxia. *Int J Radiat Oncol Biol Phys* 48, 919-922.

Koumenis, C., Naczki, C., Koritzinsky, M., Rastani, S., Diehl, A., Sonenberg, N., Koromilas, A., and Wouters, B. G. (2002). Regulation of protein synthesis by hypoxia via activation of the endoplasmic reticulum kinase PERK and phosphorylation of the translation initiation factor eIF2alpha. *Mol Cell Biol* 22, 7405-7416.

Kubisch, C. H., and Logsdon, C. D. (2008). Endoplasmic reticulum stress and the pancreatic acinar cell. *Expert Rev Gastroenterol Hepatol* 2, 249-260.

Kunz, J., Henriquez, R., Schneider, U., Deuter-Reinhard, M., Movva, N. R., and Hall, M. N. (1993). Target of rapamycin in yeast, TOR2, is an essential phosphatidylinositol kinase homolog required for G1 progression. *Cell* 73, 585-596.

Kwiatkowski, D. J., Zhang, H., Bandura, J. L., Heiberger, K. M., Glogauer, M., el-Hashemite, N., and Onda, H. (2002). A mouse model of TSC1 reveals sex-dependent lethality from liver hemangiomas, and up-regulation of p70S6 kinase activity in Tsc1 null cells. *Hum Mol Genet* 11, 525-534.

Lamb, R. F., Roy, C., Diefenbach, T. J., Vinters, H. V., Johnson, M. W., Jay, D. G., and Hall, A. (2000). The TSC1 tumour suppressor hamartin regulates cell adhesion through ERM proteins and the GTPase Rho. *Nat Cell Biol* 2, 281-287.



Laplante, M., and Sabatini, D. M. (2012). mTOR signaling in growth control and disease. *Cell* 149, 274-293.

Lee, A. H., Chu, G. C., Iwakoshi, N. N., and Glimcher, L. H. (2005). XBP-1 is required for biogenesis of cellular secretory machinery of exocrine glands. *Embo J* 24, 4368-4380.

Lee, A. S. (2007). GRP78 induction in cancer: therapeutic and prognostic implications. *Cancer Res* 67, 3496-3499.

Lee, C. H., Inoki, K., Karbowniczek, M., Petroulakis, E., Sonenberg, N., Henske, E. P., and Guan, K. L. (2007a). Constitutive mTOR activation in TSC mutants sensitizes cells to energy starvation and genomic damage via p53. *Embo J* 26, 4812-4823.

Lee, D. F., Kuo, H. P., Chen, C. T., Hsu, J. M., Chou, C. K., Wei, Y., Sun, H. L., Li, L. Y., Ping, B., Huang, W. C., *et al.* (2007b). IKK beta suppression of TSC1 links inflammation and tumor angiogenesis via the mTOR pathway. *Cell* 130, 440-455.

Leibowitz, G., Cerasi, E., and Ketzinel-Gilad, M. (2008). The role of mTOR in the adaptation and failure of beta-cells in type 2 diabetes. *Diabetes Obes Metab* 10 Suppl 4, 157-169.

Lerner, A. G., Upton, J. P., Praveen, P. V., Ghosh, R., Nakagawa, Y., Igbaria, A., Shen, S., Nguyen, V., Backes, B. J., Heiman, M., *et al.* (2012). IRE1alpha induces thioredoxin-interacting protein to activate the NLRP3 inflammasome and promote programmed cell death under irremediable ER stress. *Cell Metab* 16, 250-264.

Lesche, R., Groszer, M., Gao, J., Wang, Y., Messing, A., Sun, H., Liu, X., and Wu, H. (2002). Cre/loxP-mediated inactivation of the murine Pten tumor suppressor gene. *Genesis* 32, 148-149.

Leung, H. Y., Gullick, W. J., and Lemoine, N. R. (1994). Expression and functional activity of fibroblast growth factors and their receptors in human pancreatic cancer. *Int J Cancer* 59, 667-675.

Li, D., Duell, E. J., Yu, K., Risch, H. A., Olson, S. H., Kooperberg, C., Wolpin, B. M., Jiao, L., Dong, X., Wheeler, B., *et al.* (2012). Pathway Analysis of Genome-wide Association Study Data Highlights Pancreatic Development Genes as Susceptibility Factors for Pancreatic Cancer. *Carcinogenesis*.

Li, Y., Wang, Y., Kim, E., Beemiller, P., Wang, C. Y., Swanson, J., You, M., and Guan, K. L. (2007). Bnip3 mediates the hypoxia-induced inhibition on mammalian target of rapamycin by interacting with Rheb. *J Biol Chem* 282, 35803-35813.

Ling, J., Kang, Y., Zhao, R., Xia, Q., Lee, D. F., Chang, Z., Li, J., Peng, B., Fleming, J. B., Wang, H., *et al.* (2012). KrasG12D-induced IKK2/beta/NF-kappaB activation by IL-1alpha and p62 feedforward loops is required for development of pancreatic ductal adenocarcinoma. *Cancer Cell* 21, 105-120.

Loos, M., Michalski, C. W., and Kleeff, J. (2012). Asymptomatic pancreatic lesions: new insights and clinical implications. *World J Gastroenterol* 18, 4474-4477.

Lugea, A., Tischler, D., Nguyen, J., Gong, J., Gukovsky, I., French, S. W., Gorelick, F. S., and Pandolfi, S. J. (2011). Adaptive unfolded protein response attenuates alcohol-induced pancreatic damage. *Gastroenterology* *140*, 987-997.

Ma, L., Chen, Z., Erdjument-Bromage, H., Tempst, P., and Pandolfi, P. P. (2005). Phosphorylation and functional inactivation of TSC2 by Erk implications for tuberous sclerosis and cancer pathogenesis. *Cell* *121*, 179-193.

Ma, L., Teruya-Feldstein, J., Bonner, P., Bernardi, R., Franz, D. N., Witte, D., Cordon-Cardo, C., and Pandolfi, P. P. (2007). Identification of S664 TSC2 phosphorylation as a marker for extracellular signal-regulated kinase mediated mTOR activation in tuberous sclerosis and human cancer. *Cancer Res* *67*, 7106-7112.

Mahimainathan, L., Ghosh-Choudhury, N., Venkatesan, B., Das, F., Mandal, C. C., Dey, N., Habib, S. L., Kasinath, B. S., Abboud, H. E., and Ghosh Choudhury, G. (2009). TSC2 deficiency increases PTEN via HIF1alpha. *J Biol Chem* *284*, 27790-27798.

Maitra, A., Adsay, N. V., Argani, P., Iacobuzio-Donahue, C., De Marzo, A., Cameron, J. L., Yeo, C. J., and Hruban, R. H. (2003). Multicomponent analysis of the pancreatic adenocarcinoma progression model using a pancreatic intraepithelial neoplasia tissue microarray. *Mod Pathol* *16*, 902-912.

Malhotra, J. D., and Kaufman, R. J. (2007). Endoplasmic reticulum stress and oxidative stress: a vicious cycle or a double-edged sword? *Antioxid Redox Signal* *9*, 2277-2293.

Maniati, E., Bossard, M., Cook, N., Candido, J. B., Emami-Shahri, N., Nedospasov, S. A., Balkwill, F. R., Tuveson, D. A., and Hagemann, T. (2011). Crosstalk between the canonical NF-kappaB and Notch signaling pathways inhibits Ppargamma expression and promotes pancreatic cancer progression in mice. *J Clin Invest* *121*, 4685-4699.

Manning, B. D., Logsdon, M. N., Lipovsky, A. I., Abbott, D., Kwiatkowski, D. J., and Cantley, L. C. (2005). Feedback inhibition of Akt signaling limits the growth of tumors lacking Tsc2. *Genes Dev* *19*, 1773-1778.

Manolio, T. A., Brooks, L. D., and Collins, F. S. (2008). A HapMap harvest of insights into the genetics of common disease. *J Clin Invest* *118*, 1590-1605.

Marcato, P., Dean, C. A., Giacomantonio, C. A., and Lee, P. W. (2011a). Aldehyde dehydrogenase: its role as a cancer stem cell marker comes down to the specific isoform. *Cell Cycle* *10*, 1378-1384.

Marcato, P., Dean, C. A., Pan, D., Araslanova, R., Gillis, M., Joshi, M., Helyer, L., Pan, L., Leidal, A., Gujar, S., *et al.* (2011b). Aldehyde dehydrogenase activity of breast cancer stem cells is primarily due to isoform ALDH1A3 and its expression is predictive of metastasis. *Stem Cells* *29*, 32-45.

Marino, S., Vooijs, M., van Der Gulden, H., Jonkers, J., and Berns, A. (2000). Induction of medulloblastomas in p53-null mutant mice by somatic inactivation of Rb in the external granular layer cells of the cerebellum. *Genes Dev* *14*, 994-1004.

May, D., Itin, A., Gal, O., Kalinski, H., Feinstein, E., and Keshet, E. (2005). Ero1-L alpha plays a key role in a HIF-1-mediated pathway to improve disulfide bond formation and VEGF secretion under hypoxia: implication for cancer. *Oncogene* 24, 1011-1020.

Mazur, P. K., Einwachter, H., Lee, M., Sipos, B., Nakhai, H., Rad, R., Zimber-Strobl, U., Strobl, L. J., Radtke, F., Kloppel, G., *et al.* (2010). Notch2 is required for progression of pancreatic intraepithelial neoplasia and development of pancreatic ductal adenocarcinoma. *Proc Natl Acad Sci U S A* 107, 13438-13443.

McClellan, J., and King, M. C. (2010). Genetic heterogeneity in human disease. *Cell* 141, 210-217.

Melisi, D., Niu, J., Chang, Z., Xia, Q., Peng, B., Ishiyama, S., Evans, D. B., and Chiao, P. J. (2009). Secreted interleukin-1alpha induces a metastatic phenotype in pancreatic cancer by sustaining a constitutive activation of nuclear factor-kappaB. *Mol Cancer Res* 7, 624-633.

Molero, X., Vaquero, E. C., Flandez, M., Gonzalez, A. M., Ortiz, M. A., Cibrian-Uhalte, E., Servitja, J. M., Merlos, A., Juanpere, N., Massumi, M., *et al.* (2012). Gene expression dynamics after murine pancreatitis unveils novel roles for Hnf1alpha in acinar cell homeostasis. *Gut* 61, 1187-1196.

Morton, J. P., Jamieson, N. B., Karim, S. A., Athineos, D., Ridgway, R. A., Nixon, C., McKay, C. J., Carter, R., Brunton, V. G., Frame, M. C., *et al.* (2010). LKB1 haploinsufficiency cooperates with Kras to promote pancreatic cancer through suppression of p21-dependent growth arrest. *Gastroenterology* 139, 586-597, 597 e581-586.

Moyer, M. W. (2012). Targeting hypoxia brings breath of fresh air to cancer therapy. *Nat Med* 18, 636-637.

Mueller, M. T., Hermann, P. C., Witthauer, J., Rubio-Viqueira, B., Leicht, S. F., Huber, S., Ellwart, J. W., Mustafa, M., Bartenstein, P., D'Haese, J. G., *et al.* (2009). Combined targeted treatment to eliminate tumorigenic cancer stem cells in human pancreatic cancer. *Gastroenterology* 137, 1102-1113.

Nellist, M., Verhaaf, B., Goedbloed, M. A., Reuser, A. J., van den Ouweland, A. M., and Halley, D. J. (2001). TSC2 missense mutations inhibit tuberin phosphorylation and prevent formation of the tuberin-hamartin complex. *Hum Mol Genet* 10, 2889-2898.

Nelson, M. R., Wegmann, D., Ehm, M. G., Kessner, D., St Jean, P., Verzilli, C., Shen, J., Tang, Z., Bacanu, S. A., Fraser, D., *et al.* (2012). An abundance of rare functional variants in 202 drug target genes sequenced in 14,002 people. *Science* 337, 100-104.

Neoptolemos, J. P., Stocken, D. D., Friess, H., Bassi, C., Dunn, J. A., Hickey, H., Beger, H., Fernandez-Cruz, L., Dervenis, C., Lacaine, F., *et al.* (2004). A randomized trial of chemoradiotherapy and chemotherapy after resection of pancreatic cancer. *N Engl J Med* 350, 1200-1210.

Ng, K. P., Hillmer, A. M., Chuah, C. T., Juan, W. C., Ko, T. K., Teo, A. S., Ariyaratne, P. N., Takahashi, N., Sawada, K., Fei, Y., *et al.* (2012). A common BIM deletion polymorphism mediates intrinsic resistance and inferior responses to tyrosine kinase inhibitors in cancer. *Nat Med* 18, 521-528.

Ni, M., and Lee, A. S. (2007). ER chaperones in mammalian development and human diseases. *FEBS Lett* 581, 3641-3651.

Niizeki, H., Kobayashi, M., Horiuchi, I., Akakura, N., Chen, J., Wang, J., Hamada, J. I., Seth, P., Katoh, H., Watanabe, H., *et al.* (2002). Hypoxia enhances the expression of autocrine motility factor and the motility of human pancreatic cancer cells. *Br J Cancer* 86, 1914-1919.

Niu, J., Li, Z., Peng, B., and Chiao, P. J. (2004). Identification of an autoregulatory feedback pathway involving interleukin-1alpha in induction of constitutive NF-kappaB activation in pancreatic cancer cells. *J Biol Chem* 279, 16452-16462.

Olive, K. P., Jacobetz, M. A., Davidson, C. J., Gopinathan, A., McIntyre, D., Honess, D., Madhu, B., Goldgraben, M. A., Caldwell, M. E., Allard, D., *et al.* (2009). Inhibition of Hedgehog signaling enhances delivery of chemotherapy in a mouse model of pancreatic cancer. *Science* 324, 1457-1461.

Oprins, A., Rabouille, C., Posthuma, G., Klumperman, J., Geuze, H. J., and Slot, J. W. (2001). The ER to Golgi interface is the major concentration site of secretory proteins in the exocrine pancreatic cell. *Traffic* 2, 831-838.

Orban, P. C., Chui, D., and Marth, J. D. (1992). Tissue- and site-specific DNA recombination in transgenic mice. *Proc Natl Acad Sci U S A* 89, 6861-6865.

Ozcan, U., Ozcan, L., Yilmaz, E., Duvel, K., Sahin, M., Manning, B. D., and Hotamisligil, G. S. (2008). Loss of the tuberous sclerosis complex tumor suppressors triggers the unfolded protein response to regulate insulin signaling and apoptosis. *Mol Cell* 29, 541-551.

Panarelli, N. C., Yantiss, R. K., Yeh, M. M., Liu, Y., and Chen, Y. T. (2012). Tissue-specific cadherin CDH17 is a useful marker of gastrointestinal adenocarcinomas with higher sensitivity than CDX2. *Am J Clin Pathol* 138, 211-222.

Penchev, V. R., Rasheed, Z. A., Maitra, A., and Matsui, W. (2012). Heterogeneity and targeting of pancreatic cancer stem cells. *Clin Cancer Res* 18, 4277-4284.

Petersen, G. M., Amundadottir, L., Fuchs, C. S., Kraft, P., Stolzenberg-Solomon, R. Z., Jacobs, K. B., Arslan, A. A., Bueno-de-Mesquita, H. B., Gallinger, S., Gross, M., *et al.* (2010). A genome-wide association study identifies pancreatic cancer susceptibility loci on chromosomes 13q22.1, 1q32.1 and 5p15.33. *Nat Genet* 42, 224-228.

Petersen, G. M., de Andrade, M., Goggins, M., Hruban, R. H., Bondy, M., Korczak, J. F., Gallinger, S., Lynch, H. T., Syngal, S., Rabe, K. G., *et al.* (2006). Pancreatic cancer genetic epidemiology consortium. *Cancer Epidemiol Biomarkers Prev* 15, 704-710.

Pierce, B. L., and Ahsan, H. (2011). Genome-wide "pleiotropy scan" identifies HNF1A region as a novel pancreatic cancer susceptibility locus. *Cancer Res* 71, 4352-4358.

Pinho, A. V., Rومان, I., and Real, F. X. (2011). p53-dependent regulation of growth, epithelial-mesenchymal transition and stemness in normal pancreatic epithelial cells. *Cell Cycle* 10, 1312-1321.

Pitman, J. L., Bonnet, D. J., Curtiss, L. K., and Gekakis, N. (2011). Reduced cholesterol and triglycerides in mice with a mutation in Mia2, a liver protein that localizes to ER exit sites. *J Lipid Res* 52, 1775-1786.

Plank, T. L., Yeung, R. S., and Henske, E. P. (1998). Hamartin, the product of the tuberous sclerosis 1 (TSC1) gene, interacts with tuberin and appears to be localized to cytoplasmic vesicles. *Cancer Res* 58, 4766-4770.

Pontoglio, M., Sreenan, S., Roe, M., Pugh, W., Ostrega, D., Doyen, A., Pick, A. J., Baldwin, A., Velho, G., Froguel, P., *et al.* (1998). Defective insulin secretion in hepatocyte nuclear factor 1alpha-deficient mice. *J Clin Invest* 101, 2215-2222.

Pore, N., Jiang, Z., Shu, H. K., Bernhard, E., Kao, G. D., and Maity, A. (2006). Akt1 activation can augment hypoxia-inducible factor-1alpha expression by increasing protein translation through a mammalian target of rapamycin-independent pathway. *Mol Cancer Res* 4, 471-479.

Potjer, T. P., Schot, I., Langer, P., Heverhagen, J. T., Wasser, M. N., Slater, E. P., Kloppel, G., Morreau, H. M., Bonsing, B. A., de Vos Tot Nederveen Cappel, W. H., *et al.* (2013). Variation in Precursor Lesions of Pancreatic Cancer among High-Risk Groups. *Clin Cancer Res* 19, 442-449.

Potter, C. J., Pedraza, L. G., and Xu, T. (2002). Akt regulates growth by directly phosphorylating Tsc2. *Nat Cell Biol* 4, 658-665.

Pylayeva-Gupta, Y., Lee, K. E., Hajdu, C. H., Miller, G., and Bar-Sagi, D. (2012). Oncogenic Kras-induced GM-CSF production promotes the development of pancreatic neoplasia. *Cancer Cell* 21, 836-847.

Qiu, W., Sahin, F., Iacobuzio-Donahue, C. A., Garcia-Carracedo, D., Wang, W. M., Kuo, C. Y., Chen, D., Arking, D. E., Lowy, A. M., Hruban, R. H., *et al.* (2011). Disruption of p16 and activation of Kras in pancreas increase ductal adenocarcinoma formation and metastasis in vivo. *Oncotarget* 2, 862-873.

Rasheed, Z. A., Yang, J., Wang, Q., Kowalski, J., Freed, I., Murter, C., Hong, S. M., Koorstra, J. B., Rajeshkumar, N. V., He, X., *et al.* (2010). Prognostic significance of tumorigenic cells with mesenchymal features in pancreatic adenocarcinoma. *J Natl Cancer Inst* 102, 340-351.

Rehmann, H., Bruning, M., Berghaus, C., Schwarten, M., Kohler, K., Stocker, H., Stoll, R., Zwartkuis, F. J., and Wittinghofer, A. (2008). Biochemical characterisation of TCTP questions its function as a guanine nucleotide exchange factor for Rheb. *FEBS Lett* 582, 3005-3010.

Rendtorff, N. D., Frodin, M., Attie-Bitach, T., Vekemans, M., and Tommerup, N. (2001). Identification and characterization of an inner ear-expressed human

melanoma inhibitory activity (MIA)-like gene (MIAL) with a frequent polymorphism that abolishes translation. *Genomics* 71, 40-52.

Rhim, A. D., Mirek, E. T., Aiello, N. M., Maitra, A., Bailey, J. M., McAllister, F., Reichert, M., Beatty, G. L., Rustgi, A. K., Vonderheide, R. H., *et al.* (2012). EMT and dissemination precede pancreatic tumor formation. *Cell* 148, 349-361.

Roberts, N. J., Jiao, Y., Yu, J., Kopelovich, L., Petersen, G. M., Bondy, M. L., Gallinger, S., Schwartz, A. G., Syngal, S., Cote, M. L., *et al.* (2012). ATM mutations in patients with hereditary pancreatic cancer. *Cancer Discov* 2, 41-46.

Romero-Ramirez, L., Cao, H., Nelson, D., Hammond, E., Lee, A. H., Yoshida, H., Mori, K., Glimcher, L. H., Denko, N. C., Giaccia, A. J., *et al.* (2004). XBP1 is essential for survival under hypoxic conditions and is required for tumor growth. *Cancer Res* 64, 5943-5947.

Ron, D., and Walter, P. (2007). Signal integration in the endoplasmic reticulum unfolded protein response. *Nat Rev Mol Cell Biol* 8, 519-529.

Rooman, I., and Real, F. X. (2012). Pancreatic ductal adenocarcinoma and acinar cells: a matter of differentiation and development? *Gut* 61, 449-458.

Roux, P. P., Ballif, B. A., Anjum, R., Gygi, S. P., and Blenis, J. (2004). Tumor-promoting phorbol esters and activated Ras inactivate the tuberous sclerosis tumor suppressor complex via p90 ribosomal S6 kinase. *Proc Natl Acad Sci U S A* 101, 13489-13494.

Rutkowski, D. T., and Hegde, R. S. (2010). Regulation of basal cellular physiology by the homeostatic unfolded protein response. *J Cell Biol* 189, 783-794.

Saito, K., Chen, M., Bard, F., Chen, S., Zhou, H., Woodley, D., Polischuk, R., Schekman, R., and Malhotra, V. (2009). TANGO1 facilitates cargo loading at endoplasmic reticulum exit sites. *Cell* 136, 891-902.

Samani, N. J., Deloukas, P., Erdmann, J., Hengstenberg, C., Kuulasmaa, K., McGinnis, R., Schunkert, H., Soranzo, N., Thompson, J., Tiret, L., and Ziegler, A. (2009). Large scale association analysis of novel genetic loci for coronary artery disease. *Arterioscler Thromb Vasc Biol* 29, 774-780.

Samani, N. J., Erdmann, J., Hall, A. S., Hengstenberg, C., Mangino, M., Mayer, B., Dixon, R. J., Meitinger, T., Braund, P., Wichmann, H. E., *et al.* (2007). Genomewide association analysis of coronary artery disease. *N Engl J Med* 357, 443-453.

Sauer, B. (1987). Functional expression of the cre-lox site-specific recombination system in the yeast *Saccharomyces cerevisiae*. *Mol Cell Biol* 7, 2087-2096.

Sauer, B., and Henderson, N. (1988). Site-specific DNA recombination in mammalian cells by the Cre recombinase of bacteriophage P1. *Proc Natl Acad Sci U S A* 85, 5166-5170.

Schneider, G., Siveke, J. T., Eckel, F., and Schmid, R. M. (2005). Pancreatic cancer: basic and clinical aspects. *Gastroenterology* 128, 1606-1625.

Semenza, G. L. (2012). Hypoxia-inducible factors in physiology and medicine. *Cell* 148, 399-408.

Servitja, J. M., Pignatelli, M., Maestro, M. A., Cardalda, C., Boj, S. F., Lozano, J., Blanco, E., Lafuente, A., McCarthy, M. I., Sumoy, L., *et al.* (2009). Hnf1alpha (MODY3) controls tissue-specific transcriptional programs and exerts opposed effects on cell growth in pancreatic islets and liver. *Mol Cell Biol* 29, 2945-2959.

Shackelford, D. B., and Shaw, R. J. (2009). The LKB1-AMPK pathway: metabolism and growth control in tumour suppression. *Nat Rev Cancer* 9, 563-575.

Shah, O. J., Wang, Z., and Hunter, T. (2004). Inappropriate activation of the TSC/Rheb/mTOR/S6K cassette induces IRS1/2 depletion, insulin resistance, and cell survival deficiencies. *Curr Biol* 14, 1650-1656.

Shah, R. N., Ibbitt, J. C., Alitalo, K., and Hurst, H. C. (2002). FGFR4 overexpression in pancreatic cancer is mediated by an intronic enhancer activated by HNF1alpha. *Oncogene* 21, 8251-8261.

Shaw, R. J., and Cantley, L. C. (2006). Ras, PI(3)K and mTOR signalling controls tumour cell growth. *Nature* 441, 424-430.

Shaw, R. J., Kosmatka, M., Bardeesy, N., Hurley, R. L., Witters, L. A., DePinho, R. A., and Cantley, L. C. (2004). The tumor suppressor LKB1 kinase directly activates AMP-activated kinase and regulates apoptosis in response to energy stress. *Proc Natl Acad Sci U S A* 101, 3329-3335.

Sheveleva, E. V., Landowski, T. H., Samulitis, B. K., Bartholomeusz, G., Powis, G., and Dorr, R. T. (2012). Imexon induces an oxidative endoplasmic reticulum stress response in pancreatic cancer cells. *Mol Cancer Res* 10, 392-400.

Shibaji, T., Nagao, M., Ikeda, N., Kanehiro, H., Hisanaga, M., Ko, S., Fukumoto, A., and Nakajima, Y. (2003). Prognostic significance of HIF-1 alpha overexpression in human pancreatic cancer. *Anticancer Res* 23, 4721-4727.

Shigeyama, Y., Kobayashi, T., Kido, Y., Hashimoto, N., Asahara, S., Matsuda, T., Takeda, A., Inoue, T., Shibutani, Y., Koyanagi, M., *et al.* (2008). Biphasic response of pancreatic beta-cell mass to ablation of tuberous sclerosis complex 2 in mice. *Mol Cell Biol* 28, 2971-2979.

Siegel, R., Ward, E., Brawley, O., and Jemal, A. (2011). Cancer statistics, 2011: the impact of eliminating socioeconomic and racial disparities on premature cancer deaths. *CA Cancer J Clin* 61, 212-236.

Siegelin, M. D. (2012). Utilization of the cellular stress response to sensitize cancer cells to TRAIL-mediated apoptosis. *Expert Opin Ther Targets* 16, 801-817.

Slater, E. P., Langer, P., Niemczyk, E., Strauch, K., Butler, J., Habbe, N., Neoptolemos, J. P., Greenhalf, W., and Bartsch, D. K. (2010). PALB2 mutations in European familial pancreatic cancer families. *Clin Genet* 78, 490-494.

Sofer, A., Lei, K., Johannessen, C. M., and Ellisen, L. W. (2005). Regulation of mTOR and cell growth in response to energy stress by REDD1. *Mol Cell Biol* 25, 5834-5845.

Stambolic, V., MacPherson, D., Sas, D., Lin, Y., Snow, B., Jang, Y., Benchimol, S., and Mak, T. W. (2001). Regulation of PTEN transcription by p53. *Mol Cell* 8, 317-325.

Stanger, B. Z., Stiles, B., Lauwers, G. Y., Bardeesy, N., Mendoza, M., Wang, Y., Greenwood, A., Cheng, K. H., McLaughlin, M., Brown, D., *et al.* (2005). Pten constrains centroacinar cell expansion and malignant transformation in the pancreas. *Cancer Cell* 8, 185-195.

Stevens, R. J., Roddam, A. W., and Beral, V. (2007). Pancreatic cancer in type 1 and young-onset diabetes: systematic review and meta-analysis. *Br J Cancer* 96, 507-509.

Strobel, O., Rosow, D. E., Rakhlin, E. Y., Lauwers, G. Y., Trainor, A. G., Alsina, J., Fernandez-Del Castillo, C., Warshaw, A. L., and Thayer, S. P. (2010). Pancreatic duct glands are distinct ductal compartments that react to chronic injury and mediate Shh-induced metaplasia. *Gastroenterology* 138, 1166-1177.

Su, G. H., Hruban, R. H., Bansal, R. K., Bova, G. S., Tang, D. J., Shekher, M. C., Westerman, A. M., Entius, M. M., Goggins, M., Yeo, C. J., and Kern, S. E. (1999). Germline and somatic mutations of the STK11/LKB1 Peutz-Jeghers gene in pancreatic and biliary cancers. *Am J Pathol* 154, 1835-1840.

Su, M. C., Yuan, R. H., Lin, C. Y., and Jeng, Y. M. (2008). Cadherin-17 is a useful diagnostic marker for adenocarcinomas of the digestive system. *Mod Pathol* 21, 1379-1386.

Takehara, A., Hosokawa, M., Eguchi, H., Ohigashi, H., Ishikawa, O., Nakamura, Y., and Nakagawa, H. (2007). Gamma-aminobutyric acid (GABA) stimulates pancreatic cancer growth through overexpressing GABAA receptor pi subunit. *Cancer Res* 67, 9704-9712.

Tezel, E., Nagasaka, T., Nomoto, S., Sugimoto, H., and Nakao, A. (2000). Neuroendocrine-like differentiation in patients with pancreatic carcinoma. *Cancer* 89, 2230-2236.

Ting, D. T., Lipson, D., Paul, S., Brannigan, B. W., Akhavanfard, S., Coffman, E. J., Contino, G., Deshpande, V., Iafrate, A. J., Letovsky, S., *et al.* (2011). Aberrant overexpression of satellite repeats in pancreatic and other epithelial cancers. *Science* 331, 593-596.

Um, S. H., Frigerio, F., Watanabe, M., Picard, F., Joaquin, M., Sticker, M., Fumagalli, S., Allegrini, P. R., Kozma, S. C., Auwerx, J., and Thomas, G. (2004). Absence of S6K1 protects against age- and diet-induced obesity while enhancing insulin sensitivity. *Nature* 431, 200-205.

Upton, J. P., Wang, L., Han, D., Wang, E. S., Huskey, N. E., Lim, L., Truitt, M., McManus, M. T., Ruggero, D., Goga, A., *et al.* (2012). IRE1alpha cleaves select microRNAs during ER stress to derepress translation of proapoptotic Caspase-2. *Science* 338, 818-822.

Urano, F., Wang, X., Bertolotti, A., Zhang, Y., Chung, P., Harding, H. P., and Ron, D. (2000). Coupling of stress in the ER to activation of JNK protein kinases by transmembrane protein kinase IRE1. *Science* 287, 664-666.

van Slegtenhorst, M., de Hoogt, R., Hermans, C., Nellist, M., Janssen, B., Verhoef, S., Lindhout, D., van den Ouweland, A., Halley, D., Young, J., *et al.*



(1997). Identification of the tuberous sclerosis gene TSC1 on chromosome 9q34. *Science* 277, 805-808.

van Slegtenhorst, M., Nellist, M., Nagelkerken, B., Cheadle, J., Snell, R., van den Ouweland, A., Reuser, A., Sampson, J., Halley, D., and van der Sluijs, P. (1998). Interaction between hamartin and tuberin, the TSC1 and TSC2 gene products. *Hum Mol Genet* 7, 1053-1057.

Villarroel, M. C., Rajeshkumar, N. V., Garrido-Laguna, I., De Jesus-Acosta, A., Jones, S., Maitra, A., Hruban, R. H., Eshleman, J. R., Klein, A., Laheru, D., *et al.* (2011). Personalizing cancer treatment in the age of global genomic analyses: PALB2 gene mutations and the response to DNA damaging agents in pancreatic cancer. *Mol Cancer Ther* 10, 3-8.

Vincent, A., Herman, J., Schulick, R., Hruban, R. H., and Goggins, M. (2011). Pancreatic cancer. *Lancet* 378, 607-620.

Wienecke, R., Konig, A., and DeClue, J. E. (1995). Identification of tuberin, the tuberous sclerosis-2 product. Tuberin possesses specific Rap1GAP activity. *J Biol Chem* 270, 16409-16414.

Wilson, D. G., Phamluong, K., Li, L., Sun, M., Cao, T. C., Liu, P. S., Modrusan, Z., Sandoval, W. N., Rangell, L., Carano, R. A., *et al.* (2011). Global defects in collagen secretion in a Mia3/TANGO1 knockout mouse. *J Cell Biol* 193, 935-951.

Wilson, W. R., and Hay, M. P. (2011). Targeting hypoxia in cancer therapy. *Nat Rev Cancer* 11, 393-410.

Wiseman, R. L., Powers, E. T., Buxbaum, J. N., Kelly, J. W., and Balch, W. E. (2007). An adaptable standard for protein export from the endoplasmic reticulum. *Cell* 131, 809-821.

Wolff, N. C., Vega-Rubin-de-Celis, S., Xie, X. J., Castrillon, D. H., Kabbani, W., and Brugarolas, J. (2011). Cell-type-dependent regulation of mTORC1 by REDD1 and the tumor suppressors TSC1/TSC2 and LKB1 in response to hypoxia. *Mol Cell Biol* 31, 1870-1884.

Wouters, B. G., and Koritzinsky, M. (2008). Hypoxia signalling through mTOR and the unfolded protein response in cancer. *Nat Rev Cancer* 8, 851-864.

Wu, C., Miao, X., Huang, L., Che, X., Jiang, G., Yu, D., Yang, X., Cao, G., Hu, Z., Zhou, Y., *et al.* (2012). Genome-wide association study identifies five loci associated with susceptibility to pancreatic cancer in Chinese populations. *Nat Genet* 44, 62-66.

Xiao, G. H., Shoarinejad, F., Jin, F., Golemis, E. A., and Yeung, R. S. (1997). The tuberous sclerosis 2 gene product, tuberin, functions as a Rab5 GTPase activating protein (GAP) in modulating endocytosis. *J Biol Chem* 272, 6097-6100.

Yachida, S., White, C. M., Naito, Y., Zhong, Y., Brosnan, J. A., Macgregor-Das, A. M., Morgan, R. A., Saunders, T., Laheru, D. A., Herman, J. M., *et al.* (2012). Clinical significance of the genetic landscape of pancreatic cancer and implications for identification of potential long-term survivors. *Clin Cancer Res* 18, 6339-6347.

Yamagata, K., Furuta, H., Oda, N., Kaisaki, P. J., Menzel, S., Cox, N. J., Fajans, S. S., Signorini, S., Stoffel, M., and Bell, G. I. (1996). Mutations in the hepatocyte nuclear factor-4alpha gene in maturity-onset diabetes of the young (MODY1). *Nature* 384, 458-460.

Ying, H., Elpek, K. G., Vinjamoori, A., Zimmerman, S. M., Chu, G. C., Yan, H., Fletcher-Sananikone, E., Zhang, H., Liu, Y., Wang, W., *et al.* (2011). PTEN is a major tumor suppressor in pancreatic ductal adenocarcinoma and regulates an NF-kappaB-cytokine network. *Cancer Discov* 1, 158-169.

Yoneda, T., Imaizumi, K., Oono, K., Yui, D., Gomi, F., Katayama, T., and Tohyama, M. (2001). Activation of caspase-12, an endoplasmic reticulum (ER) resident caspase, through tumor necrosis factor receptor-associated factor 2-dependent mechanism in response to the ER stress. *J Biol Chem* 276, 13935-13940.

Yu, M., Ting, D. T., Stott, S. L., Wittner, B. S., Oszolak, F., Paul, S., Ciciliano, J. C., Smas, M. E., Winokur, D., Gilman, A. J., *et al.* (2012). RNA sequencing of pancreatic circulating tumour cells implicates WNT signalling in metastasis. *Nature* 487, 510-513.

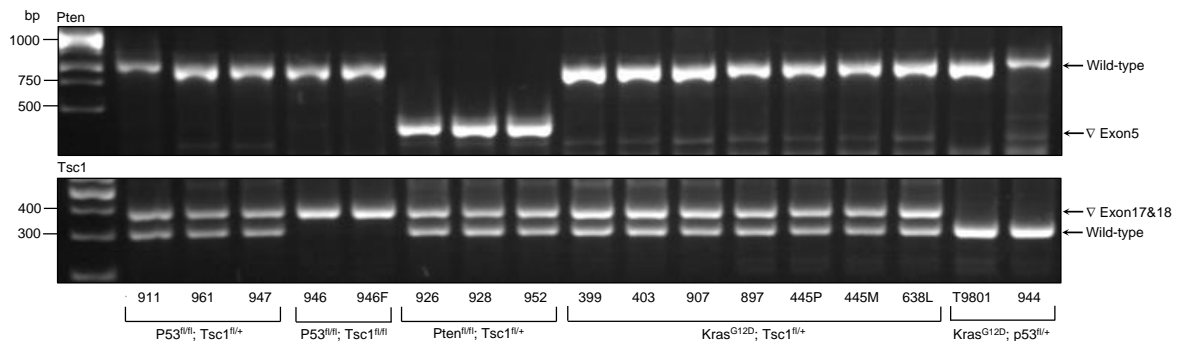
Yu, Y., Yoon, S. O., Poulogiannis, G., Yang, Q., Ma, X. M., Villen, J., Kubica, N., Hoffman, G. R., Cantley, L. C., Gygi, S. P., and Blenis, J. (2011). Phosphoproteomic analysis identifies Grb10 as an mTORC1 substrate that negatively regulates insulin signaling. *Science* 332, 1322-1326.

Zhang, H., Bosch-Marce, M., Shimoda, L. A., Tan, Y. S., Baek, J. H., Wesley, J. B., Gonzalez, F. J., and Semenza, G. L. (2008). Mitochondrial autophagy is an HIF-1-dependent adaptive metabolic response to hypoxia. *J Biol Chem* 283, 10892-10903.

Zhang, J., Jiang, Y., Jia, Z., Li, Q., Gong, W., Wang, L., Wei, D., Yao, J., Fang, S., and Xie, K. (2006). Association of elevated GRP78 expression with increased lymph node metastasis and poor prognosis in patients with gastric cancer. *Clin Exp Metastasis* 23, 401-410.

Zhang, P., McGrath, B., Li, S., Frank, A., Zambito, F., Reinert, J., Gannon, M., Ma, K., McNaughton, K., and Cavener, D. R. (2002). The PERK eukaryotic initiation factor 2 alpha kinase is required for the development of the skeletal system, postnatal growth, and the function and viability of the pancreas. *Mol Cell Biol* 22, 3864-3874.

## 9. SUPPLEMENTARY DATA



**Supplementary Figure 1.** PCR analysis demonstrates the genotyping results of mouse cell lines

**Supplementary Table 1.** The top-100 differentially expressed genes

Gene symbol	**FDR	*Pten <sup>fl/fl</sup> ; Tsc1 <sup>fl/+</sup>	*p53 <sup>fl/fl</sup> ; Tsc1 <sup>fl/+ or fl</sup>	*Kras <sup>G12D</sup> ; Tsc1 <sup>fl/+</sup>
Trp53	2.062E-17	11.94	8.32	12.21
Hspb8	7.800E-13	10.40	11.59	7.17
Fam84a	1.531E-12	7.71	7.30	10.78
Aldh1a3	1.531E-12	8.26	8.37	12.08
Eml2	3.285E-12	9.39	8.81	10.40
Cadps	4.956E-12	9.64	6.88	6.98
1700007K13Rik	4.956E-12	9.60	6.69	7.66
Ano3	8.957E-12	8.97	5.25	6.18
Unc13a	9.341E-12	8.19	7.99	9.35
Wfdc2	9.341E-12	12.37	7.95	12.75
Psrc1	9.851E-12	10.84	8.65	10.20
Tns4	9.851E-12	7.28	7.91	12.79
Arhgap28	1.117E-11	6.89	8.86	6.35
Ltf	1.117E-11	9.32	6.44	6.75
Cdh17	1.177E-11	10.78	6.74	12.53
Dock4	1.177E-11	10.41	8.49	10.78
Trp53inp2	2.146E-11	11.66	11.89	10.78
Atp2b4	2.809E-11	10.21	9.61	7.20
Dhh	2.851E-11	7.61	7.51	9.66
Slc9a9	2.851E-11	8.81	8.19	6.67
Tnfrsf22	2.902E-11	10.40	10.35	12.15
Pitpnc1	2.902E-11	10.18	8.86	10.76
Glrp1	2.902E-11	7.17	7.63	10.57
9030617O03Rik	3.162E-11	10.39	7.74	10.23

Paox	3.162E-11	8.69	9.01	10.32
Eif5a2	3.428E-11	9.36	9.86	8.36
D0H4S114	3.859E-11	10.80	12.46	8.35
Polk	4.521E-11	10.49	9.37	10.72
Mum111	4.521E-11	7.10	9.46	6.82
Esyt2	5.151E-11	10.98	10.55	11.77
Spink4	5.732E-11	11.79	7.42	8.31
Pi4k2b	5.885E-11	9.39	9.51	10.75
Il1a	6.492E-11	5.49	5.30	10.28
4933426M11Rik	6.863E-11	12.17	10.83	11.59
Noxo1	6.916E-11	9.55	7.69	8.11
Map3k2	7.516E-11	10.13	9.75	10.89
Fndc3a	7.746E-11	11.29	10.66	11.85
Gm1943	1.133E-10	11.22	11.71	10.75
Eya1	1.267E-10	6.91	9.84	7.00
Ccng1	1.317E-10	13.39	12.28	13.18
Exoc4	1.389E-10	11.69	10.55	11.11
Pkn3	1.438E-10	7.61	7.67	9.45
Rnf169	1.472E-10	11.09	9.57	10.47
Sgms2	1.556E-10	10.35	10.25	12.05
Pgcp	1.704E-10	11.63	11.05	9.46
Sesn3	1.784E-10	12.08	11.77	10.46
Zfp277	1.957E-10	10.18	9.57	10.64
Pim3	1.981E-10	9.75	10.23	10.78
Tgfb2	2.109E-10	10.96	11.29	7.66
Pkia	2.109E-10	9.29	9.90	7.70
Rps6ka5	2.208E-10	7.87	7.20	8.76
Slc12a2	3.165E-10	12.54	11.47	12.94
Samd12	3.613E-10	10.39	7.60	9.59
Grb10	3.613E-10	9.65	11.36	6.96
Maf	3.667E-10	8.98	10.33	8.79
Zfp521	3.838E-10	8.05	9.97	6.81
Prkg2	4.090E-10	6.35	7.00	9.50
Gnai1	4.101E-10	10.80	10.99	7.71
Fgfr2	4.276E-10	11.10	9.29	6.97
Hsd17b2	5.429E-10	8.89	6.24	6.26
Phlda3	5.429E-10	11.79	10.67	11.38
Fam73a	5.429E-10	9.24	8.92	10.36
Tnfaip2	5.651E-10	11.85	9.51	12.34
Masp1	5.651E-10	11.17	11.49	8.85
Abcb1a	6.105E-10	9.03	8.22	10.63

Tnfrsf10b	6.105E-10	11.72	10.75	11.95
Myo7a	6.233E-10	10.20	9.93	8.90
Galnt3	6.233E-10	10.09	8.83	11.29
9130017N09Rik	6.701E-10	10.36	8.10	10.29
Zmat3	6.701E-10	10.68	8.85	9.90
Pbp2	6.701E-10	7.05	7.08	9.71
Fas	7.848E-10	9.33	9.30	7.37
Dcxr	8.182E-10	10.50	9.09	10.00
Dcaf5	8.182E-10	10.57	9.74	10.52
Elovl4	8.182E-10	7.70	9.20	7.22
Irak1bp1	8.182E-10	8.87	9.57	7.86
Cxcl12	8.182E-10	9.55	11.57	7.33
Edn1	8.234E-10	8.39	9.68	6.86
Dgka	9.184E-10	11.18	9.53	11.27
Cryab	9.184E-10	12.08	12.33	9.47
Scn3b	9.310E-10	7.53	6.53	6.41
6530418L21Rik	9.423E-10	7.83	6.76	7.28
Pkhd1	9.423E-10	10.00	10.23	8.06
Hook2	9.644E-10	8.81	8.22	9.24
Mgat5	9.645E-10	10.01	9.10	11.12
Spry4	1.084E-09	9.04	8.91	10.93
Pik3r3	1.095E-09	10.05	10.25	7.39
Uchl1	1.096E-09	8.19	10.58	7.97
Erc5	1.273E-09	10.27	9.21	9.67
Krt7	1.298E-09	11.56	9.49	12.72
Dusp14	1.429E-09	9.71	11.05	9.94
Pld1	1.429E-09	11.80	9.70	10.24
Fam115c	1.546E-09	8.85	9.01	6.98
Ndufb9	1.546E-09	12.14	12.59	11.71
D4Bwg0951e	1.598E-09	12.82	12.33	11.26
Nuak1	1.717E-09	10.63	11.44	8.98
Plac8	1.733E-09	11.27	10.82	12.82
Doc2b	1.740E-09	7.85	9.45	7.45
Exd2	1.765E-09	9.66	8.89	10.07
Trappc6a	1.765E-09	10.05	9.57	10.43

\*: Mean expression; \*\*FDR: false discovery rate

## 10. CURRICULUM VITAE

**Family Name:** Kong  
**First Name:** Bo  
**Date of birth:** 10.21.1981  
**Gender:** Male  
**Marital Status:** Single  
**Nationality:** Chinese  
**Present Address:** Pfälzer-Wald-Straße 1, 81539 München  
**Tel:** 089 4140 6193, 017631188151

**E-mail:** kongbo81@hotmail.com

### Education and Work Experience:

04. 2009 - PhD - Medical Life Science and Technology  
TECHNISCHE UNIVERSITÄT MÜNCHEN

09. 2007- Research fellow, Medical thesis research, TECHNISCHE  
03. 2009 UNIVERSITÄT MÜNCHEN

09. 2004- Master of Surgical Science  
07. 2007 Southeast University, China

09. 1999- Bachelor of Medicine  
07. 2004 Southeast University, China

**Dr. med. dissertation 2011:** “AZGP1 is a tumor suppressor in pancreatic cancer inducing mesenchymal-to-epithelial transdifferentiation by inhibiting TGFβ-mediated ERK signaling”, summa cum laude

### Published Papers:

- **Kong B**, Michalski CW, Hong X, et al., Oncogene. 2010; 29:5146-58.
- **Kong B**, Michalski CW, Erkan M, et al., Nat Rev Gastroenterol Hepatol. 2011;8:467-72.
- Regel I, **Kong B**, Raulefs S, et al., Langenbecks Arch Surg. 2012;397:507-12.

- De Oliveira T, Abiatari I, Raulefs S, et al., Mol Cancer. 2012;11:19
- Erkan M, Reiser-Erkan C, Michalski CW, et al., Curr Mol Med. 2012;12:288-303.
- **Kong B**, Michalski CW, Friess H, Kleeff J. Exp Oncol. 2010;32:186-9.
- Samkharadze T, Erkan M, Reiser-Erkan C, et al., Am J Gastroenterol. 2011;106:968-80.
- Herner A, Sauliunaite D, Michalski CW, et al., Int J Cancer. 2011, epub.
- **Kong B**, Michalski CW, Kleeff J. World J Stem Cells. 2009;1:8-10.
- Ketterer K, **Kong B**, Frank D, et al., Cancer Lett. 2009;277:72-81.
- Hong X, Michalski CW, **Kong B**, et al., J Surg Oncol. 2010;101:564-9.
- Jiang X, Abiatari I, **Kong B**, et al., Pancreatology. 2009;9:165-72.
- Abiatari I, Gillen S, DeOliveira T, et al., Int J Oncol. 2009;35:1111-6.

## 11. ACKNOWLEDGEMENTS

I am grateful to the executive committee of the Medical Life Science and Technology PhD program who gave me the opportunity to carry out my dissertation within the framework of the PhD program at the Technische Universität München. The research work was performed between 04.2009 and 02.2013.

I would like to thank my supervisor Prof. Jörg Kleeff for his scientific supervision, instruction, advice and support.

I would like to thank PD Dr. Christoph W. Michalski who co-supervised the project and provided enormous support for this PhD study.

I would like to thank Prof. Irene Esposito and Dr. Anna Melissa Schlitter who provided expertise in pathological evaluation and who provided tissue samples of esophageal cancer.

I would like to thank Prof. Jörg Kleeff, PD Dr. Christoph W. Michalski and Prof. Irene Esposito for discussing, reading and correcting the final dissertation.

I would like to thank Prof. Bernhard Holzmann for the discussion of the dissertation research and his helpful advice.

I would like to thank Prof. Helmut Friess who provided general support for this project.

I would like to thank Weiwei Wu for her enormous technical support and for maintenance of the mouse tissue archive.

I would like to thank Tao Chen who provided expertise in mouse surgery.

I would like to thank Wilhelm Schönherr, Weiwei Wu, Chengjia Qian and Tao Chen who performed the necropsy examinations for some transgenic mice.

I would like to thank Carsten Jäger who coordinated tissue collection, maintained the patient database and analyzed the clinical data for this project.

I would like to thank Ivane Abiatari who collected tissues and maintained the tissue bank for this project.

I would like to thank Manja Thorwirth, Nadja Maeritz and Carmen Marthen who genotyped the transgenic mice and who organized mouse husbandry.

I would like to thank Dr. Ulrich Nitsche and PD Dr. Klaus-Peter Janssen who provided genomic DNAs of colon cancer samples, clinical data and HEK293 cells.



I would like to thank PD Dr. Jens T. Siveke who provided the p48<sup>Cre</sup> mouse line and some of the mouse cancer cell lines.

I would like to thank Dr. Ivonne Regel who drafted the “Tierversuchantrag” for this project.

I would like to thank Dr. Martin Irmeler and Dr. Johannes Beckers who performed the microarray experiments.

I would like to thank Philipp Bruns and Prof. Fabian J. Theis who helped analyzing the array data for the project.

I would like to thank Dr. Susanne Raulefs for her effort in organizing the lab and for her scientific discussion.

I would like to thank Nora Behler who provided expertise in performing immunofluorescence experiments.

I would like to thank PD Dr. Mert Erkan for frequent and fruitful scientific discussions.

I would like to thank Dr. Nataliya Valkovska who provided help in establishing the immune cell staining protocols.

I would like to thank my colleagues of the pancreas research group, Dr. Xin Hong, Dr. Sylvia Streit, Tiago De Oliveira, Danguole Sauliunaite, Dr. Tamar Samkharadze, Dr. Simon Rieder, Daniela Stangel, Sina Fritzsche, Georg Leinenkugel and Simone Hausmann for their kind support during my work.

I would like to thank all those patients and organ donors who donated tissues and organs for this research.

I am indebted to the Scholarship Council of the Ministry of Education of China and the Commission for Clinical Research of the TU Munich (KKF) for funding parts of this study.

Finally, I would like also thank my fiancée Huang Beili and my parents for their continuous support.